I. LATENT HEAT OF VAPORIZATION OF PROPANE

II. PARTIAL AND TOTAL HEATS OF VAPORIZATION FOR THE N-PROPANE/N-DECANE MIXTURE

Thesis by

Norman Lewis Helgeson

In Partial Fulfillment of the Requirements

For the Degree of

Doctor of Philosophy

California Institute of Technology

Pasadena, California

1973

(Submitted June 23, 1972)

ACKNOWLEDGEMENTS

First, I would like to thank the California Institute of Technology for its generous financial support throughout my residence at Caltech. In addition to Institute Fellowships, I was supported at various times by the Fellowship of Standard Oil of California, a National Science Foundation Engineering Traineeship, and Institute Research Assistantships.

The initial phase of my graduate work was supervised by Professor B. H. Sage to whom I am grateful for his patience and encouragement. I am also indebted to Professor Sage for permission to continue with experimental measurements using apparatus which he had previously developed. Professor C. J. Pings supervised the major portion of this thesis and it was he who fell heir to many of the problems associated with its development and completion. I would like to express my appreciation for his personal interest and support throughout the course of the investigation, and also for providing an environment which permitted considerable freedom of endeavor.

Numerous other people have been helpful in one way or another: Hollis Reamer supplied valuable assistance with the operational characteristics of the experimental apparatus, George Griffith was always available and more than helpful with any problems associated with equipment repair, and Ray Reed, Henry Smith and Chic Nakawatase contributed at various times during the experimental phase of the project.

I would especially like to acknowledge the encouragement and continuing patience of my wife, Ann, who has been through it all.

for ann, john, katherine, and . . .

ABSTRACT

Experimental measurements are reported for total and partial heats-of-vaporization for the n-propane/n-decane system. Results are given for the 100, 130 and 160°F. isotherms and cover the entire composition range. It is shown that the temperature and concentration gradients which develop within the system during the vaporization process may, in some cases, cause a significant (~0.4%) deviation in the calculated results. A method is provided for introducing a correction for this effect. Based on the partial heat-of-vaporization of n-propane, heats-of-mixing for the liquid solution are calculated. The results are in qualitative agreement with predictions from theories for n-alkane liquid mixtures.

TABLE OF CONTENTS

ACKNOWLEDGEMENTS ii

ABSTRACT iv

LIST OF TABLES vii

LIST OF FIGURES ix

I LATENT HEAT OF VAPORIZATION OF PROPANE 1

II PARTIAL AND TOTAL HEATS OF VAPORIZATION FOR THE N-PROPANE/N-DECANE MIXTURE 5

INTRODUCTION 6

THERMODYNAMIC RELATIONS 9

EQUIPMENT AND EXPERIMENTAL PROCEDURES 12

CALCULATIONS AND RESULTS 17

SUMMARY 22

REFERENCES 24

NOMENCLATURE 26

APPENDICES

I THERMODYNAMIC DEVELOPMENT 42

EQUILIBRIUM CASE 44

IRREVERSIBLE EFFECTS AT LIQUID-VAPOR INTERFACE 51

THERMODYNAMIC METHOD FOR CALCULATING ΔH^M 58

II EXPERIMENTAL EQUIPMENT 67

TEMPERATURE RECORDING INSTRUMENTS 67

PRESSURE RECORDING INSTRUMENTS 68

SUMMARY OF EXPERIMENTAL MEASUREMENTS 74

CALORIMETER VOLUME 74

APPENDICES, Continued

III CALIBRATION OF PRESSURE GAGE 80

DESCRIPTION OF PRESSURE GAGE 80

CALIBRATION PROCEDURES AND RESULTS 82

COMPARISON WITH STAINLESS STEEL BOURDON TUBE 85

IV CALORIMETER TEMPERATURE MEASUREMENTS 92

REPORTABLE TEMPERATURE OF VAPORIZATION 93

ZERO HEAT TRANSFER 96

CALORIMETER TEMPERATURE GRADIENTS 98

SUMMARY 104

V ANALYTICAL REPRESENTATION OF HEATS-OF-MIXING 110

VI HEAT TRANSFER AND AGITATOR CALIBRATION 115

HEAT TRANSFER CALIBRATION 116

AGITATOR CALIBRATION 120

VII TABULAR SUMMARY OF EXPERIMENTAL RESULTS 129

PROPOSITION I 136

PROPOSITION II 160

PROPOSITION III 168

LIST OF TABLES

Table	Title	Page
	PART I	
I	Experimental results for latent heat at vaporization of propane	3
II	Comparison of results from several investigators	3
III	Critically chosen values of some properties of propane	4
	PART II	
1	Comparison of total change due to non-equilibrium effects and the sum of changes due to mass and pressure drop effects	28
APPENDICES		
II-1	Results of experimental determination of calorimeter volume	76
III-1	Calibration constants of Texas Instrument Pressure Gage	86
VI-1	Results of measurements for determining calorimeter heat transfer correction	125
VII-1	Estimated uncertainty of experimental measurements	130
VII-2	Summary of test results	131
VII-3	Calculations of heat-of-mixing from heat-of-vaporization data	135

Table	Title	Page
	PROPOSITION II	
1	Sensitivity of flame ionization detector to several hydrocarbon species	166

LIST OF FIGURES

Figure	Title	Page
	PART I	
1.	Latent heat of vaporization for propane.	3
2.	Residual latent heat of vaporization.	3
	PART II	
1.	Measured pressure drop as a function of flow rate for n-propane/n-decane system.	29
2.	Development of pseudo-steady-state pressure profile.	30
3.	Functional schematic of calorimeter and associated equipment.	31
4.	Calorimeter temperature, pressure and energy addition profiles for experimental test.	32
5.	Definition of thermodynamic states for heat-of-vaporization calculations.	33
6.	Summary of calculated results for total heats-of-vaporization (non-equilibrium calculation).	34
7.	Residual heats-of-vaporization (non-equilibrium calculation).	35
8.	Comparison of heat-of-vaporization results for non-equilibrium and equilibrium calculations.	36
9.	Residual partial enthalpy of vaporization of n-propane.	37
10.	Thermodynamic cycle for calculating partial enthalpy of liquid n-propane.	38

Figure	Title	Page
11.	Calculated partial enthalpies of n-propane and n-decane.	39
12.	Calculated heats-of-mixing for n-propane/ n-decane liquid mixtures.	40
13.	Liquid phase heats-of-mixing as predicted by corresponding states correlation.	41
APPENDICES		
I-1.	Pressure, temperature and composition changes for vaporization processes in multicomponent systems.	63
I-2.	Interaction of thermodynamic system with surroundings.	64
I-3.	Schematic representation (A) and experimentally measured (B) temperature profile through vapor-liquid interface during vaporization.	65
I-4.	Thermodynamic states through which material passes upon vaporization.	66
II-1.	Scale drawing of calorimeter.	77
II-2.	Pressure measuring system.	78
II-3.	Schematic summary of experimental measurements.	79
III-1.	Schematic diagram of Texas Instrument Pressure Guage, Model 141.	88
III-2.	Apparatus for calibration of pressure gage.	89
III-3.	Results of calibration for Texas Instrument Gage.	90
III-4.	Comparison of calibration results for quartz and stainless steel helical coils.	91
IV-1.	Scale drawing showing location of temperature sensing devices used with calorimeter.	106

Figure	Title	Page
IV-2.	Apparent temperature profile of calorimeter for equilibrium conditions.	107
IV-3.	Time response of thermocouples to energy pulse from electrical heater.	108
IV-4.	Time response of differential thermocouples (DTT, DTW) to initiation of vapor flow experimental (A) and analytical (B).	109
V-1.	Heats-of-mixing at 20°C. for n-alkane liquid mixtures.	114
VI-1.	Physical (A) and analytical (B) models for heat transfer to the calorimeter wall.	126
VI-2.	Calculated temperature profile of calorimeter wall.	127
VI-3.	Liquid flow field within calorimeter.	128
	PROPOSITION I	
1.	History of hot spot development.	150
2.	Coordinate systems for heat conduction analysis.	151
3.	Calculated temperature profile and regression rate for 100 ampere current.	152
4.	Longitudinal temperature equilibration following current interruption.	153
5.	Effect of radial dissipation on lower surface temperature after current interruption.	154
6.	Calculated temperature profiles through .050" (.127 cm.) titanium skin material for erosion rate (U_s) of 3 cm/sec.	155
7.	Conceptual development of hot-spot and burn-through ignition mechanisms.	156

Figure	Title	Page
8.	Thermal ignition delay as function of wall temperature.	157
9.	Estimated temperature histories of inner surface of fuel tank.	158
10.	Illustration of conditions for non-ignition, hot-spot ignition and ignition due to burn-through.	159
	PROPOSITION II	
1.	Flow schematic of sampling and analysis system.	167
	PROPOSITION III	
1.	Comparison of actual and model fuel tank venting.	176
2.	Illustrative(fuel/air) composition profiles in ullage as a function of time for variable v_f/v_s.	177
3.	Ullage fuel/air composition profiles for several fuel temperatures (test time 1 hour).	178

PART I

LATENT HEAT OF VAPORIZATION OF PROPANE*

* Part I was published as a paper by N.L. Helgeson and B.H. Sage "Latent Heat of Vaporization of Propane," J. Chem. Eng. Data, 12 (1967), 47.

Reprinted from JOURNAL OF CHEMICAL & ENGINEERING DATA, Vol. 12, No. 1, January 1967, Page 47

2838

Latent Heat of Vaporization of Propane

N. L. HELGESON and B. H. SAGE
Chemical Engineering Laboratory, California Institute of Technology, Pasadena, Calif.

Calorimetric measurements of the latent heat of vaporization of propane were made in the temperature interval between 100° and 135° F. A critical review of the available calorimetric and volumetric data was made and an analytical expression developed by regression analysis, to describe the latent heat of vaporization for propane from 0° F. to the critical state with a standard error of estimate of 1.5 B.t.u. per pound.

THE latent heat of vaporization of propane has been the subject of a number of investigations. The early work of Dana *et al.* (*3*) was followed by some additional calorimetric measurements of the latent heat of vaporization of this hydrocarbon (*6*). The volumetric behavior of the compound and the vapor pressure have been studied by several investigators (*1*, *2*, *5*, *8*, *9*). There existed discrepancies of the order of 5 B.t.u. per pound between the latent heat of vaporization as estimated at 80° F. from the two calorimetric investigations (*3*, *6*), and from the more recent volumetric measurements (*1*, *2*, *5*) and the calorimetric data at a temperature of 100° F.

As a result of this discrepancy, calorimetric measurements were made of the latent heat of vaporization of propane. The technique and equipment employed have been described (*4*, *7*) and differ materially from the apparatus used earlier (*6*). The temperatures were measured with a platinum resistance thermometer which was compared recently with the indications of a similar instrument calibrated by the National Bureau of Standards. The temperature within the calorimeter was known within 0.01° F. of the international platinum scale. Temperature differences were established within 0.002° F. The experimental results are set forth in Table I. The measurements were not carried above 135° F. because the large volumetric corrections necessary in the calorimetric measurements made use of the Clapeyron equation based upon volumetric and vapor pressure measurements a preferable approach. The calorimeter is not arranged to permit measurements below 100° F. Direct comparison of the present calorimetric measurements with the data mentioned earlier is presented in Figure 1. In this figure, where data were obtained at nearly the same temperature, a single average value was depicted.

The following analytical expression was used to describe the latent heat of vaporization of propane in the temperature interval between 40° and 206.26° F.:

$$l = A(T_c - T)^{1/3} + B(T_c - T)^{2/3} + C(T_c - T) \quad (1)$$

The application of least square regression methods yielded the following coefficients: $A = 21.771$; $B = 1.8935$; and $C = -0.10836$, with a standard deviation, σ, of 1.5 B.t.u. per pound from the experimental values depicted in Figure 1. The critical temperature employed was 665.95° R., based on Beattie's (*2*) measurements.

To illustrate the quantitative nature of the disagreement of the several sets of data, residual values of the latent heat of vaporization have been calculated, using Equation 1 as a reference value. The residual latent heat of vaporization is defined as

$$l = l_r - l_e \quad (2)$$

and is shown as a function of temperature for each of the experimental points employed in obtaining the points shown in Figure 2. The range of temperatures, the standard error of estimate, and average error are reported in Table II for each set of data from the values obtained from Equation 1.

As can be seen from Figure 2, the data of Dana *et al.* (*3*) yield values of at least 5 B.t.u. per pound above the current data when extrapolated to 100° F. The earlier

Table I. Experimental Results for Latent Heat of Vaporization of Propane

Temperature, ° F.	Pressure, p.s.i.a.	Energy Added: Electrically, B.t.u.	Energy Added: By Agitation, B.t.u.	Energy Added: By Conduction & Radiation, B.t.u.	Weight of Material Withdrawn, Lb.	Super Heat of Liquid, ° F.	dP''/dT, p.s.i./° F.	Specific Volume Bubble Point, Cu. Ft./Lb.	Volumetric Term,[a] B.t.u./Lb.	Latent Heat of Vaporization, B.t.u./Lb.
100	188.7	3.8687	0.0680	−0.0010	0.027627	0.06	2.4378	0.03390	8.560	133.96
100	188.7	3.2311	0.0664	−0.0105	0.023286	0.09	2.4378	0.03390	8.560	132.68
100	188.7	2.7045	0.0529	−0.0032	0.019465	0.06	2.4378	0.03390	8.560	133.00
100	188.7	3.1647	0.0647	−0.0073	0.022758	0.07	2.4378	0.03390	8.560	133.09
120	242.7	4.0332	0.0472	−0.0037	0.030399	0.07	2.9483	0.03547	11.220	122.95
120	242.7	4.7240	0.0579	0.0053	0.035754	0.06	2.9483	0.03547	11.220	122.74
130	273.5	3.1396	0.0471	−0.0006	0.024587	0.05	3.2215	0.03637	12.788	116.85
130	273.5	3.3003	0.0536	0.0000	0.025834	0.06	3.2215	0.03637	12.788	117.09
130	273.5	3.4455	0.0512	−0.0012	0.026955	0.04	3.2215	0.03637	12.788	116.93
135	289.9	3.2296	0.0438	0.0062	0.025749	0.06	3.3640	0.03686	13.644	113.79
135	289.9	3.8423	0.0521	0.0031	0.030766	0.06	3.3640	0.03686	13.644	113.10
135	289.9	5.3429	0.0705	−0.0079	0.042737	0.07	3.3640	0.03686	13.644	112.91
135	289.9	3.7124	0.0530	0.0041	0.029658	0.06	3.3640	0.03686	13.644	113.52
135	289.9	3.6679	0.0897	0.0130	0.029750	0.04	3.3640	0.03686	13.644	113.14

[a] $V_l T(dP''/dT)$.

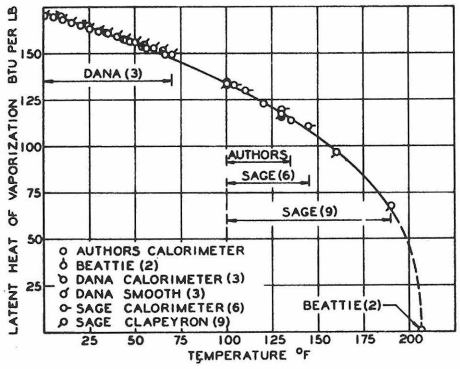

Figure 1. Latent heat of vaporization for propane

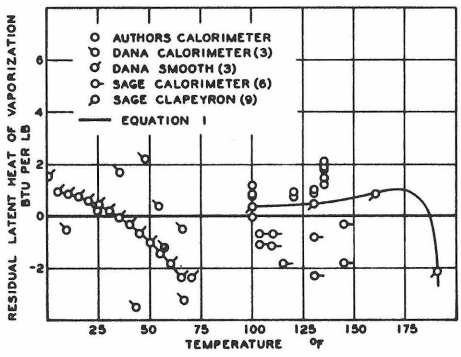

Figure 2. Residual latent heat of vaporization

calorimetric measurements of Sage (*6*) are lower than those extrapolated from the data of Dana but are higher by at least 2 B.t.u. per pound than the current calorimetric data. The volumetric measurements of Sage *et al.* (*9*) utilizing the Clapeyron equation give average agreement within 0.35 B.t.u. per pound with the current calorimetric data, in the temperature interval between 100° and 130° F. However, the agreement is less satisfactory at 135° F.

Table II. Comparison of Results from Several Investigators

Source	Number of Points: Used	Number of Points: Rejected[a]	Temp., ° F.: Min.	Temp., ° F.: Max.	Deviation, B.t.u./Lb.: Average[b]	Deviation, B.t.u./Lb.: Standard[c]
Authors	14	0	100	135	1.12	1.23
Dana (*3*)[d]	15	0	0	70	1.07	1.26
Sage (*6*)	16	7	103	167	1.43	1.53
Sage (*9*)[e]	4	0	100	190	0.98	1.21
Over-all	49	7	0	190	1.16	1.45

[a] Data points rejected when deviation of experimental values exceeds 2σ.

[b] Average deviation defined by:

$$s = \sum_{1}^{N} | l_r - l_e | /N.$$

[c] Standard deviation defined by:

$$\sigma = \left[\sum_{1}^{N} (l_r - l_e)^2/N \right]^{1/2}.$$

[d] Smoothed.

[e] Volumetric data from (*9*).

Table III presents values of the vapor pressure, the slope of the vapor pressure curve, and the specific volume of the coexisting gas and liquid phases as a function of temperature, based upon the volumetric and phase measurements of Sage *et al.* (*5, 9*) and Beattie (*1*) at a temperature above 135° F. Also included are values of the latent heat of vaporization. At temperatures below 135° and above 70° F., the current and the earlier (*6*) calorimetric data were employed to establish the latent heat of vaporization, and to evaluate the specific volume of the coexisting gas phase by use of the Clapeyron equation. At temperatures above 135° F., the Clapeyron equation was applied to the volumetric data of Sage *et al.* (*5, 9*) and Beattie (*1, 2*) to yield the appropriate values of the latent heat of vaporization. At temperatures below 70° F., the data of Dana *et al.* (*3*) were employed.

Table III. Critically Chosen Values of Some Properties of Propane

Temp., °F.	Vapor Pressure, p.s.i.a.	dP''/dT, P.S.I./°F.	Specific Volume, Cu. Ft./Lb. Dew point	Specific Volume, Cu. Ft./Lb. Bubble point	Latent Heat of Vaporization, B.t.u./Lb.
40	79.0	1.288	1.3627	0.03055	158.7
50	92.8	1.451	1.1638	0.03100	155.0
60	107.8	1.626	0.9983	0.03150	151.2
70	125.0	1.814	0.8596	0.03202	147.2
80	144.1	2.016	0.7428	0.03261	143.0
90	165.3	2.231	0.6437	0.03322	138.5
100	188.7	2.461	0.5592	0.03388	133.9
110	214.5	2.705	0.4868	0.03465	128.9
120	242.7	2.964	0.4244	0.03547	123.6
130	273.5	3.238	0.3702	0.03638	118.0
140	307.3	3.527	0.3230	0.03740	111.8
150	344.0	3.832	0.2814	0.03855	105.0
160	383.8	4.153	0.2446	0.03994	97.4
170	426.9	4.490	0.2115	0.04177	88.8
180	473.6	4.843	0.1811	0.04411	78.6
190	524.8	5.213	0.1514	0.04683	65.6

ACKNOWLEDGMENT

The experimental work reported was carried out with the financial support of the Standard Oil Company of California, which made available a fellowship to Norman L. Helgeson. Virginia M. Berry contributed to the calculation of the experimental results and B. Lawson Miller to the preparation of the manuscript.

NOMENCLATURE

A, B, C = coefficients for Equation 1
d = differential operator
l = latent heat of vaporization, B.t.u./lb.
l = residual latent heat of vaporization, B.t.u./lb.
N = number of points
P'' = vapor pressure, p.s.i.a.
s = average deviation expressed in B.t.u./lb. and defined in Table II
T = absolute temperature, ° R.
V = specific volume, cu.ft./lb.
σ = standard deviation expressed in B.t.u./lb. and defined in Table II
Σ = summation operator

Subscripts

b = bubble point
c = critical
d = dew point
e = experimental
r = reference

LITERATURE CITED

(1) Beattie, J. A., Kay, W. C., Kaminsky, J., *J. Am. Chem. Soc.* **59,** 1589 (1937).
(2) Beattie, J. A., Poffenberger, Noland, Hadlock, Canfield, *J. Chem. Phys.* **3,** 96 (1935).
(3) Dana, L. I., Jenkins, A. C., Burdick, J. N., Timm, R. C., *Refrig. Eng.* **12,** 387 (1926).
(4) McKay, R. A., Sage, B. H., J. CHEM. ENG. DATA **5,** 21 (1960).
(5) Reamer, H. H., Sage, B. H., Lacey, W. N., *Ind. Eng. Chem.* **41,** 482 (1949).
(6) Sage, B. H., Evans, H. D., Lacey, W. N., *Ibid.*, **31,** 763 (1939).
(7) Sage, B. H., Hough, E. W., *Anal. Chem.* **22,** 1304 (1950).
(8) Sage, B. H., Schaafsma, J. G., Lacey, W. N., *Ind. Eng. Chem.* **26,** 1218 (1934).
(9) Sage, B. H., Lacey, W. N., "Thermodynamic Properties of the Lighter Paraffin Hydrocarbons and Nitrogen," American Petroleum Institute, New York, 1950.

RECEIVED for review June 20, 1966. Accepted October 10, 1966. This paper was accepted as a contribution to this Journal by R. L. Pigford, Editor of *Ind. Eng. Chem. Fundamentals.*

PART II

PARTIAL AND TOTAL HEATS OF VAPORIZATION FOR N-PROPANE/N-DECANE MIXTURE

INTRODUCTION

Chemical engineers are always interested in increasing the scope and improving the accuracy of the thermodynamic data which characterize the materials with which they work. Determination of the enthalpy change on vaporization for both pure components and for mixtures is useful in that this information is often necessary before the energy requirements of industrial processes can be determined. The primary purpose of this paper is to present the results of measurements for the enthalpy change which occurs for the isothermal vaporization of an n-propane/n-decane mixture. Measurements are reported for the 100, 130 and 160^{o}F. isotherms for the composition range of 0.0 - 0.60 weight fraction (0.0 - 0.95 mole fraction) n-propane. A constant volume isothermal calorimeter was used for the experimental measurements. The secondary objectives are to evaluate the effects which temperature and concentration gradients within the calorimeter have on the calculated results and also to report heats-of-mixing for the n-propane/n-decane liquid solutions.

Heats-of-vaporization are available in standard tables along with other properties which describe pure materials. Similar information for mixtures, however, has become available only in the last several years. Much of this has been related to the properties of the light hydrocarbon gases (e.g. methane and n-propane (1)) because of the large industrial interest which has centered on these materials. Additional enthalpy data have been reported by Lenoir (2, 3, 4) and co-workers

for a number of binary systems and also several ternaries. The components of the latter mixtures ranged from n-pentane to n-hexadecane and included several unsaturated hydrocarbons and cyclo-paraffins as well. All of the above measurements were made using a flow calorimeter. Huisman (5) reported heats-of-vaporization measurements for the n-butane/n-decane system using a constant-volume isothermal calorimeter.

The absence, until recently, of a significant amount of data describing heats-of-vaporization of mixtures is understandable. The problem is difficult to define as several effects are involved and it is not easy to isolate one factor from another. This problem has been circumvented, for the most part, in the measurements reported for flow calorimeters as only total enthalpy changes have been reported. The problem of determining a partial enthalpy change upon vaporization and its relationship to other available thermodynamic data has not been dealt with. Huisman reported a partial enthalpy of vaporization but he did not evaluate the irreversible effects present within the liquid phase nor did he attempt to relate his results to liquid solution theory.

In the investigation reported below the irreversible effects and partial quantities are both evaluated. Concentration gradients may not be an important factor in many mixtures, however for wide-boiling mixtures where one component is preferentially evaporated, irreversible effects should not be neglected. The experimental measurements reported below are such that the effect of both temperature and concentration gradients could be determined. A large amount of volumetric, phase equilibrium and calormetric data for this system was already available

and this permitted calculating a heat-of-mixing of the pure liquid components. The latter is compared to results of a corresponding states theory for mixtures of n-alkanes (6).

THERMODYNAMIC RELATIONS

For a single component system the enthalpy change upon vaporization may be calculated from (7)

$$H_g - H_\ell = \frac{q}{\Delta m_a} \frac{V_g - V_\ell}{V_\ell} + C_{p,g}(T_\ell - T_g)$$

for a constant volume calorimeter. q is the thermal energy added to the calorimeter and includes the effects of electrical energy addition, agitation and a small correction for heat leak. Δm_a is the amount of sample passing from the calorimeter and the ratio $(V_g - V_\ell)/V_\ell$ is a correction for the amount of material which is evaporated but which stays within the calorimeter. The importance of accurate volumetric information to the calculation of heats-of-vaporization is apparent in this relation.

The second term in the equation accounts for a small temperature gradient (0.2 - 0.3°F.) which develops at the interface in the liquid phase (or sub-cooling of the vapor). It is a small effect and is often neglected in calculations for determining the latent heat-of-vaporization for pure materials.

For a binary system Huisman (8) has shown that the total heat-of-vaporization may be calculated from

$$\sum_{k=1}^{2}\{(\bar{H}_{k,g}-\bar{H}_{k,\ell})y_k\}^* = \left[\frac{1}{\Delta m_a-\Delta m_{k,g}/y_k}\right] \times \left[-q-\left\{m_g T\left(\frac{\partial V_g}{\partial T}\right)_{P,y} + m_\ell T\left(\frac{\partial V_\ell}{\partial T}\right)_{P,x}\right\}^* \Delta P + (\bar{H}_{j,g}-\bar{H}_{j,\ell})(\Delta m_{j,g}-\frac{1-y_k}{y_k}\Delta m_{k,g})\right] \quad (2)$$

and

$$\Delta m_{k,g} = \Delta\left(y_k \frac{V-\underline{m}V_\ell}{V_g-V_\ell}\right) \quad (3)$$

These equations assume that a uniform temperature and pressure exists within the calorimeter and that each phase is maintained at a uniform concentration. Whereas the neglect of temperature and concentration gradients may be justified when pure materials are involved (Equation (1) above), irreversible effects which are present in the liquid phase of a mixture may not be negligible. The calorimeter pressure drop which occurs on initiation of vapor flow as a result of temperature and concentration gradients for the n-propane/n-decane system is shown in Figure 1. The pressure drop increases with flow rate and is more than an order of magnitude greater than that which is observed when a pure component is vaporized. The large increase is the result of concentration gradients which, for the binary, develop at the liquid interface. The development of this pseudo-steady-state pressure profile is illustrated in Figure 2.

The importance of volumetric data to heats-of-vaporization calculations for a single component system was described above and a similar statement may be made with regard to mixtures. In the

latter case $\Delta m_{k,g}$, which is a first order correction to the amount of material passing from the calorimeter (see Equation (2)), is calculated from a material balance which is dependent on available volumetric data of the liquid and vapor phases (see Equation (3)). ($\Delta m_{k,g}$ represents the accumulation of component k (n-propane) in the vapor phase between the beginning and the end of an experimental test.) From the equation-of-state it can be seen that, at constant temperature, the amount of material in the vapor phase is proportional to (P/Z). An increase in pressure results in a decrease in Z so that the material balance becomes quite sensitive to errors is the calorimeter pressure. Large changes in the calorimeter pressure must then have a significant effect on the quantity $m_{k,g}$ and possibly on the quantity $\Delta m_{k,g}$. In order to evaluate this effect precisely(±0.05 psi)experimentally measured pressures were required. An accuracy of ±0.5 psia was estimated to be adequate. The deviation of the calorimeter from an equilibrium condition may also affect other terms in Equation (2). This is discussed further below, along with the experimental results.

In spite of the non-equilibrium which exists between the bulk liquid and bulk vapor phases, it may be assumed that the vaporization process itself occurs under conditions of equilibrium (9). Thus the thermodynamic quantity, the heat-of-vaporization is obtained.

Because of the considerable difference in volatility of n-propane and n-decane it is possible to rearrange Equation (2) so that a partial enthalpy of vaporization for n-propane may be calculated (8). This partial enthalpy-of-vaporization can then be used to calculate a heat-of-mixing for the high-pressure n-propane/n-decane liquid system.

EQUIPMENT AND EXPERIMENTAL PROCEDURES

The calorimeter and most of the associated equipment have been discussed in ample detail previously (7). Only a review of some of the major features of the equipment and a discussion of improvements in instrumentation are offered here. The calorimeter, itself, is an elongated sphere (4.5 inch diameter) fabricated of stainless steel, the halves of which are joined by a cylindrical section one inch in length and of the same diameter as the sphere. It has a total internal volume (including approximately 20 cc nuisance volume) of 1,256 cc. Sample enters through a steel tube which passes up through the bottom of the vacuum jacket and is attached to the base of the lower half of the calorimeter. The calorimeter pressure is measured through this same line (see Figure 3).

The primary energy source is an electrical resistance heater immersed in the liquid phase and the material which is evaporated passes from the calorimeter through small (1/16 inch diameter) steel tubing which terminates at an orifice block. The rate of vaporization is controlled by the use of either one or a combination of up to three interchangeable orifice plates through which critical flow is maintained. The vapor then passes to a chilled sample bomb where it is collected and later weighed. During vaporization the action of an agitator causes the liquid phase to circulate and maintains the liquid phase at a near uniform temperature and concentration.

The absolute temperature at which an experimental test was

conducted was determined from measurements with a platinum resistance thermometer which was immersed in the oil bath surrounding the vacuum jacket. Once a test was underway, however, temperature changes of the calorimeter were monitored with a second platinum resistance thermometer mounted within the calorimeter thermometer well. The output of the latter thermometer was fed through an amplifier to either a null detector or to a strip chart recorder. With this procedure it was possible to not only monitor calorimeter temperature changes of $<0.001^{o}F$, but also to obtain an immediate visual display of the rate-of-change of the calorimeter temperature. The latter information was important so that appropriate action could be taken to maintain the calorimeter at a nearly constant temperature throughout an experimental test.

The determination of the calorimeter pressure was a critical part of the measurements reported and several factors were involved in selecting an instrument by which values of acceptable accuracy and precision could be obtained. Absolute pressures were used, in conjuntion with a material balance, to determine the composition of both the liquid and the vapor phases within the calorimeter. They were also used to determine the specific volume of the vapor phase which was used in the evaluation of the enthalpy change upon vaporization (see Equations (2,3)) and to evaluate the concentration gradients which developed in the liquid phase during a test. The pressure decreased continuously during an experimental test so that dynamic rather than static pressure measurements were required. Also, in order to establish a pressure-time profile, it was necessary that several pressure measurements be taken over the relatively short period of each experimental

test. Therefore, both the time response of the instrument to pressure changes and the ease of making the individual measurements were important considerations. The accuracy and precision required for these measurements were discussed above.

These various requirements were satisfied by a commercially available pressure gauge (Texas Instruments Precision Pressure Gage Model 141). A fused quartz bourdon tube designed for a pressure range of 0-500 psig was used as the pressure sensitive element. The gauge was calibrated for pressure changes relative to atmospheric using a Hart Pressure Balance (dead-weight tester) as the primary standard. The quoted accuracy and precision of the latter were 1:10,000, and 1:20,000, respectively. Pressure steps supplied by this standard resulted in readings on the Texas Instruments (TI) Pressure Gage which were reproducible to within the precision of the pressure standard. The gauge was calibrated for both increasing and decreasing pressure steps with identical results. To determine the absolute pressure of the system corrections for the atmospheric pressure and for liquid head were added to the relative pressure changes measured with the TI gauge.

The materials used were research grade(reported 99.9 percent purity) n-propane and n-decane purchased from Phillips Petroleum Co. Gas chromatograph and mass spectograph analyses of the n-decane and a vapor-pressure test of the n-propane confirmed these results. The n-propane was deaerated and the n-decane was dried over sodium and also dearated before loading into the calorimeter.

The liquid phase volumetric operating limits were set at 550 and 1090. cc. to maintain the immersion heater under the

liquid surface at all times and also to prevent carry-over of liquid droplets by the vapor stream. During a series of experimental tests the amount of n-decane retained in the calorimeter remained nearly constant as only a small amount vaporized along with the n-propane. Therefore, in order to cover the complete composition range and still maintain the liquid contents of the calorimeter within the operating limits several calorimeter loadings were required.

The temperature and pressure operating limits were (100-400°F) and (0-300 psi), respectively. The latter limit prevented measurements from being made at high n-propane concentrations on the 160°F isotherm. There was also a low concentration limit for the fraction n-propane contained in the liquid phase. A concentration gradient developed in the sample loading tube during an experimental test so that under conditions of rapid calorimeter pressure changes, bubbles apparently formed in the loading tube. These bubbles then rose through the sampling tube into the calorimeter bomb and caused an exchange of material between the calorimeter system and the sampling tube. This phenomenon was observable as temperature and pressure perturbations from steady, mean values and was of consequence only at small (<.05 weight) fractions n-propane.

Temperature, pressure and energy profiles for a test are shown in Figure 4. The vaporization process was specified as isothermal and the temperature profile remained almost constant after an initial period of adjustment. Temperature excursions were rarely greater than $\pm$ 0.010°F from the starting temperature and were often within $\pm$.005°F. The temperature profile shown is actually more erratic than that usually obtained so that the response of the calorimeter temperature to changes in the rate of

electrical addition could be illustrated. In the calculations the assumption was made that the starting and stopping temperatures of individual tests were identical so that it was possible to neglect the thermal capacity of the calorimeter. Therefore, the calorimeter was allowed to run for 10-15 minutes under apparently steady conditions prior to the start of the actual test to allow transient temperature gradients within the calorimeter walls to dissipate.

The effect that the changing calorimeter pressure had on the mass flow rate from the calorimeter is evident from the energy profile. The energy requirement continued to decrease with pressure as temperature was maintained constant. At low fractions n-propane the mass flux changed rapidly with time and several current adjustments were often necessary in order to maintain the isothermal nature of the tests. These frequent adjustments introduced a small additional uncertainty into the experimental results. The measured pressure returned to an equilibrium value when the mass flow was stopped.

CALCULATIONS AND RESULTS

The enthalpy change upon vaporization of the n-propane/n-decane mixture was determined from calculations using Equations (2) and (3). Initially, a series of thermodynamic states was defined which corresponded to specific operating points of an experimental test (see Figure 5). The definition of these states served as the basis of a calorimeter material balance and also for the evaluation of several of the energy terms.

States 2 and 7 refer to the equilibrium conditions which existed in the calorimeter prior to the start of the vapor flow and after the vapor flow had stopped at the end of a test. The pressure of State 3 was determined by linear extrapolation of the measured pressure history back to time zero (see Figure 2) and assumes that the pressure changed instantaneously when mass flow was inititated. As a finite amount of time ($\sim$200 seconds) was required for the calorimeter to reach a pseudo-steady operating condition (with respect to pressure), State 3 does not represent an actual thermodynamic condition. However, it serves to identify the steady-state pressure which would have existed within the calorimeter at time zero if vapor had been flowing. Therefore, the pressure difference between States 2 and 3 may be taken to represent the pressure drop which occurs due to temperature and concentration gradients at the vapor-liquid interface. The difference in pressure between States 6 and 7 provides a similar measure of the gradients which existed during the latter part of the test.

States 4 and 5 define the thermodynamic end-points of the ex-

periment and the interval (t_6-t_5) is the shut-down time. The dotted lines connecting States 2 and 7 represent the assumed path of the calorimeter pressure if irreversible effects are ignored. States 4' and 5', therefore, are the end-points of a test for the case where equilibrium is assumed to exist throughout the calorimeter.

A computer program was written with which this sequence of thermodynamic states could be calculated, and an option of following either the solid or broken lines (i.e., either equilibrium or non-equilibrium conditions) was provided. In this way the quantitative effects of temperature and concentration gradients at the interface were evaluated. The only difference in the two procedures was that for the equilibrium case the material balance was made assuming that the calorimeter pressure was in equilibrium with the bulk liquid phase while for the non-equilibrium calculations experimentally measured pressures were used.

The change in the energy of the fluid phases due to calorimeter pressure changes was evaluated with available volumetric data (10,11). Average thermodynamic values of States 4 and 5 were used for evaluating the temperature derivatives of the specific values and also for determining the amount of material contained within each phase. The partial enthalpy change upon vaporization of n-decane was estimated from

$$(\bar{H}_{j,g} - \bar{H}_{j,\ell}) = \Delta E_v^\circ + P(\bar{V}_{j,g} - \bar{V}_{j,\ell})$$

which assumes that the change in internal energy upon vaporization is independent of composition of the liquid phase. Vapor phase volumes, $\bar{V}_{j,g}$, were obtained from binary compressibility data (11). Some error was associated with the evaluation of these two terms, however, their contribution to the total energy was small so that the error involved in their calculation was also small.

The total amount of material present within the calorimeter was determined from a knowledge of the initial material charged and also from subsequent measured withdrawals. The component balance was known from direct measurements for only the first test in a series. For succeeding tests knowledge of the phase compositions depended upon material balance calculations. The calculated results, however, could be compared to the liquid composition which corresponded to the measured calorimeter pressures. The material balance calculations were iterative and a value of $m_{k.g}$ was assumed to start them. Iterations were continued until the assumed and calculated values of the vapor-phase mass agreed to within 0.1 mg.

The calculated results for a total of 51 tests at 100, 130 and 160°F are shown in Figure 6. The non-equilibrium calculation procedure was used. Results for pure n-propane and n-decane were available from previous measurements (12,13,14) and values for the heat-of-vaporization for the pure materials are joined by a straight line. Two additional measurements for the heat-of-vaporization of pure n-decane at 160°F are shown in Figure 6. The agreement with literature values was within 0.2 percent.

A more critical evaluation of the data can be obtained if re-

sidual values of the heat-of-vaporization are calculated and convenient reference functions for this purpose are indicated by the straight lines shown in Figure 6. Residual values of the experimental data points can then be calculated from

$$\Delta H_{RES} = \Delta H_{REF} - \Delta H_{EXP}$$

and are shown plotted as a function of composition in Figure 7. The solid line drawn through the data points represents a least-squares fit of the data to a cubic equation, and the dashed line is an extrapolation of this fit. The results show that to within a small correction the enthalpy change upon vaporization is a linear function of the weight fraction of the liquid phase composition. The root-mean-square deviation of the experimental data points from the curve fits are 0.43, 0.35 and 0.15 Btu/lb respectively for the 100, 130, and 160°F isotherms.

A comparison of calculated results which were obtained assuming that (a.) non-equilibrium and (b.) equilibrium conditions existed within the calorimeter is shown in Figure 8. The resulting data fit is displaced downward 0.25 Btu/lb for the equilibrium calculation and the root-mean-square deviation of the data increased from 0.15 to 0.33 Btu/lb. A further comparison of these two calculational procedures is shown in Table 1. The percentage change in the calculated heat-of-vaporization is almost completely accounted for by the mass change ($\Delta m_{k.g}$) and pressure drop effects. In many of the tests the percentage change in the heat-of vaporization is negligible while in others it is as much as three times as great as the root-mean-square deviation.

In Figure 9 the partial enthalpy change upon vaporization for n-propane at 160°F is compared to the total heat-of-vaporization results given above. Because of the low volatility of the n-decane only a small change is apparent. The partial enthalpy-of-vaporization can then be used to calculate a liquid phase heats-of-mixing. The partial enthalpy of n-propane in liquid solution is determined by calculating around a thermodynamic cycle. The measurements reported above are for step B. Values for the heat-of-vaporization of the pure component (step E) are available in the literature (13) and volumetric and calorimetric data for calculating the enthalpy changes as a function of pressure (steps A and D) are also available. Thus, the partial enthalpy change of n-propane upon mixing of the liquid phase components can be determined by difference. That of n-decane can be calculated from the Gibbs-Duhem equation (see Figure 11). These two partial quantities are then combined to yield liquid phase heats-of-mixing as shown in Figure 12.

Hijman and Holleman have presented a corresponding states development for liquid mixtures of the n-alkanes and the resulting correlation for heats-of-mixing is based upon data taken for materials which ranged in chain length from 6 to 62. Therefore, although these results may not be strictly applicable to the present situation it is of interest to compare the heats-of-mixing reported here to those values which may be predicted by the corresponding states correlation of Hijman. For the n-propane/n-decane system the predicted values of the heat-of-mixing as a function of temperature are shown in Figure 13. For comparison to the data the correlation curve for 160°F is also shown on Figure 12.

SUMMARY

Total heats-of-vaporization data have been presented for the n-propane/n-decane binary liquid system. The results showed a small, but consistent deviation from a reference function determined as the liquid-phase, weight-fraction average of the heats-of-vaporization of the pure components.

The effect of temperature and concentration gradients which developed in the liquid phase was evaluated. It was shown that these gradients, which may lead to pressure changes of several psi within the calorimeter, can introduce significant errors into the calculated results. The error, however, can be reduced to a negligible level if experimental pressure measurements of sufficient accuracy are obtained. In contrast to most heats-of-vaporization measurements where it is normally assumed that the process proceeds under near-equilibrium conditions, in the present case an equilibrium quantity was evaluated from a process where significant deviations from equilibrium occurred.

Heats-of-mixing were calculated for the 100, 130 and 160°F isotherms for liquid solution of n-propane and n-decane. Calculated as they were, the heats-of-mixing are probably not of sufficient accuracy to be helpful in evaluating conditions of phase equilibrium. However, the results may be useful in helping to evaluate theoretical developments for liquid n-alkane mixtures. There are heats-of-mixing data available in the literature for n-alkane system where the components have fewer than five carbon atoms. One system for which data are available is

the methane/n-propane system (3θ, but these data were obtained for a temperature of 100°F and heats-of-mixing were positive. Heats-of-mixing for the present system are strongly negative and represent solutions having a different reduced state.

A more detailed discussion of several portions of this paper is presented in the Appendices which follow. The Appendices are:

I. Thermodynamic Development

II. Experimental Equipment

III. Calibration of Pressure Guage

IV. Calorimeter Temperature Measurements

V. Analytical Representation of Heats-of-Mixing

VI. Heat Transfer and Agitator Calibration

VII. Tabular Summary of Experimental Data

REFERENCES

1. Yesavage, V.F., D.L. Katz, and J.E. Powers, J. Chem. Eng. Data, 14 (1969), 197.

2. Lenoir, J.M., D.R. Robinson, and H.G. Hipkin, J. Chem. Eng. Data, 15 (1970), 26.

3. Lenoir, J.M., H.G. Hipkin, J. Chem. Eng. Data, 15 (1970), 368.

4. Lenoir, J.M., George K. Kuravila, and H.G. Hipkin, J. Chem. Eng. Data, 16 (1971), 271.

5. Huisman, J. and B.H. Sage, J. Chem. Eng. Data, 10 (1965), 250.

6. Hijman, J., and Th. Holleman, Advances in Chemical Physics, XVI, I. Prigogine and S.A. Rice, Eds., Interscience (1969), 223.

7. McKay, R.A., Ph.D. Thesis, California Institute of Technology (1959).

8. Huisman, J., Ph.D. Thesis, California Institute of Technology (1964).

9. Schrage, R.W., Interphase Mass Transfer, Columbia University Press (1953).

10. Sage, Bruce H. and William N. Lacey, Thermodynamic Properties of the Lighter Paraffin Hydrocarbons and Nitrogen, API 37 (1950).

11. Reamer, H.H., and B.H. Sage, J. Chem. Eng. Data, 11 (1966), 17.

12. Yesavage, V.F., Ph.D. Thesis, University of Michigan (1968).

13. Helgeson, N.L., and B.H. Sage, J. Chem. Eng. Data, 12 (1967), 47.

14. Couch, H.T., William Kozicki, and B.H. Sage, J. Chem. Eng. Data, 8 (1963), 346.

15. McKay, R.A. and B.H. Sage, Supplementary Material for Manuscript 5143.1, Chemical Engineering Laboratory, California Institute of Technoloby (1959).

16. Groeber, H., S. Erk, and U. Grigull, Fundamentals of Heat Transfer, McGraw-Hill (1961), 360.

17. Jakob, Max, Mechanical Engineering, 58 (1936), 643.

18. Florschuetz, L.W. and B.T. Chao, ASME J. Heat Transfer (1965), 209.

19. Chao, B.T. and D.D. Wittkee, ASME J. Heat Transfer (1967), 17.

20. Pruger, W.Z., Phys., 115 (1940), 202.

21. Rowlinson, J.F., Liquids and Liquid Mixtures, 1st Ed., Academic Press (1959).

22. Sage, B.H., and E.W. Hough, Anal. Chem., 22 (1950), 1304.

23. Wu, S.Y., Ph.D. Thesis, California Institute of Technology (1972).

24. Carslaw, H.C., and J.C. Jaeger, Conduction of Heat in Solids, 2nd Ed., Oxford University Press (1959).

25. Groeber, H., op. cit., 49.

26. Bronstad, J.N., and J. Kofoed, Kgl. Danske Videnskab. Selskab. Mat. Fys. Medd., 22 (1946) 1.

27. Hijman, J., Molecular Physics, 1 (1958), 307.

28, McGlashan, M.L., Molecular Physics, 4 (1961), 87.

29. Hijman, J. and Th. Holleman, Molecular Physics, 4 (1961), 91.

30. McGlashan, M.L. and K.W. Morcom, Trans Faraday Society, 57 (1961), 907.

31. Holleman, Th., Physica, 29 (1963), 585.

32. Flory, P.J., R.A. Orwall, and A. Vrij, J. Amer. Chem. Soc., 86 (1964), 3507.

33. Holleman. Th. and J. Hijman, Physica, 28 (1962), 604.

34. Bird, R.B., W.E. Stewart and E.N. Lightfoot, Transport Phenomena, John Wiley and Sons (1960).

35. Bird, R.B., op. cit., 91.

36. Cutler, A.J.B., and J.A. Morrison, Trans. Faraday Soc., 61 (1965), 429.

37. Mickley,H.S., T.K. Sherwood, and G.E. Reed, Applied Mathematics in Chemical Engineering, McGraw-Hill (1957), 59.

NOMENCLATURE

C	Heat Capacity
E	Specific Internal Energy
H	Specific Enthalpy
k	Thermal Conductivity
m	Mass of Material in System
n	Number Carbon Atoms in Molecular Species
p	Pressure
q	Energy Added to Thermodynamic System in Form of Heat
r	Bubble Radius
R	Universal Gas Constant
T	Temperature
V	Specific Volume
w	Energy added to Thermodynamic System as Pressure-Volume Work
x	Liquid Phase Composition
y	Vapor-Phase Composition
y	Ratio of Absolute Temperatures in Heat-Of-Mixing Correlation
Z	Compressibility Factor
$\alpha, \lambda, \mu, u, A_1, A_2, A_3$	Parameters Used in Heat-Of-Mixing Correlation
σ	Surface Tension

Superscripts

M	Denotes Effect Associated With Mixing Process

o	Denotes Pure Component
*	Denotes Average Quantity
—	Denotes Partial Thermodynamic Quantity

Subscripts

a	Refers to Material Transferred Across Boundary of Thermodynamic System
ag	Agitator Energy Addition
b	Bubble Conditions
c	Refers to Calorimeter Bomb Itself
e	Electrical Energy Addition
g	Vapor Phase
ht	Energy Addition Due to Heat Transfer
i	Interfacial Conditions
j	Any Component Other Than k
k	Component k Which May Be Any Component From 1 to n
ℓ	Liquid Phase
n	Total Number of Components Present
s	System Quantity
vp	Vapor Pressure
—	Denotes Total System Quantity

TABLE 1

COMPARISON OF TOTAL CHANGE DUE TO NON-EQUILIBRIUM EFFECTS
AND THE SUM OF CHANGES DUE TO MASS AND PRESSURE DROP EFFECTS

RUN	$(\Delta H_V)_{EQ}$ (BTU/LBM)	$(\Delta H_V)_{NEQ}$ (BTU/LBM)	$\Delta(\Delta H_V)$ (BTU/LBM)	TOTAL INCREASE (%)	MASS AND P.D. INCREASE (%)
603	136.38	136.61	0.23	0.17	0.15
604	130.61	130.82	0.21	0.16	0.16
605	132.35	132.56	0.21	0.16	0.17
608	136.70	136.70	0.00	0.00	0.00
609	137.92	137.78	-0.14	- .10	-0.08
610	138.80	138.68	-0.12	-0.09	-0.07
613	141.98	139.23	-2.75	-1.97	-1.78
614	130.36	130.57	0.21	0.16	0.17
616	134.15	134.38	0.23	0.17	0.16
617	136.77	136.88	0.11	0.08	0.08
618	140.84	140.43	-0.41	-0.29	-0.28
663	118.04	118.05	0.01	0.01	0.01
664	120.09	120.01	-0.08	-0.07	-0.08
665	122.54	122.38	-0.16	-0.13	-0.16
666	124.87	124.46	-0.41	-0.33	-0.33
667	127.02	126.53	-0.49	-0.39	-0.42

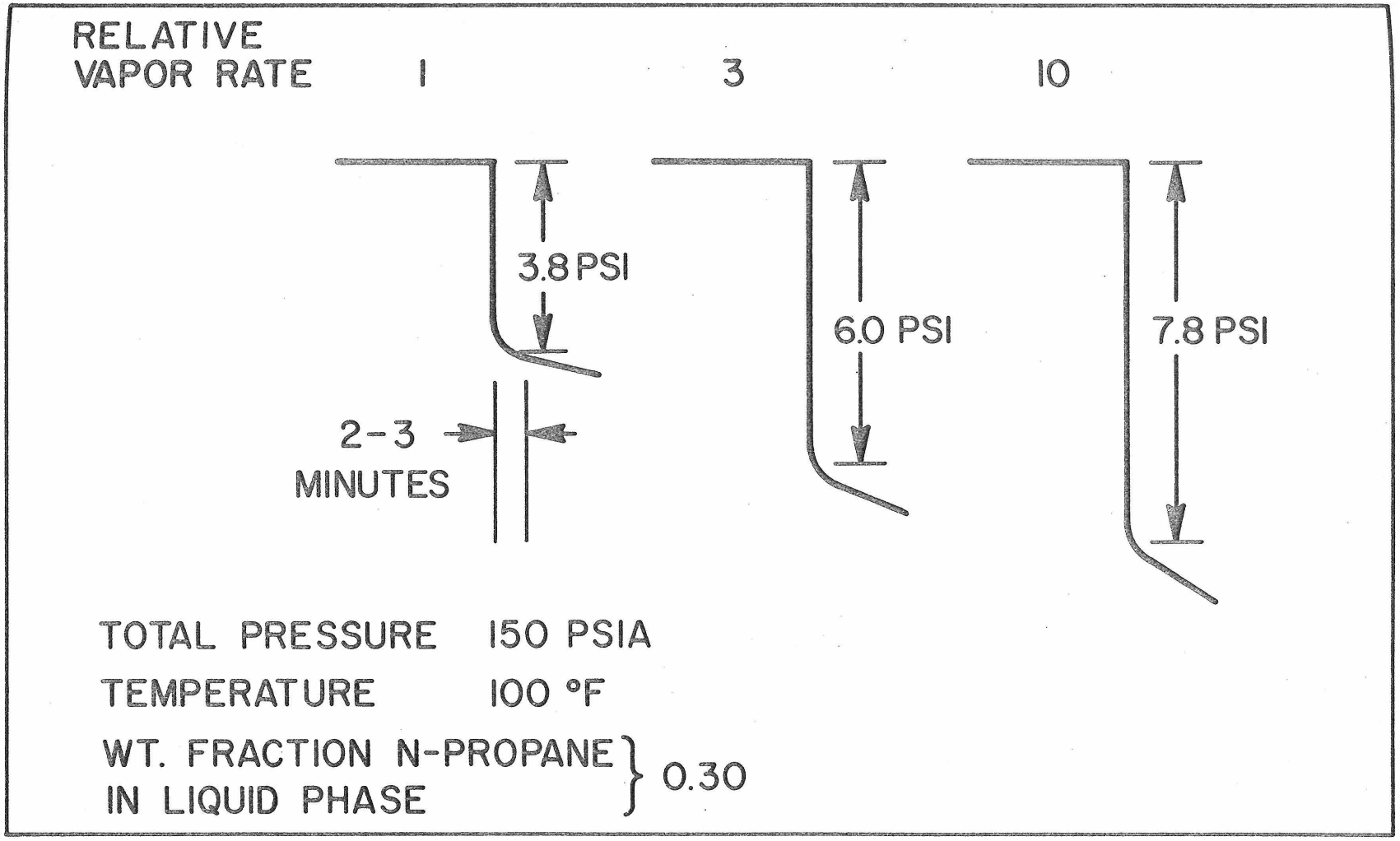

FIGURE 1. MEASURED PRESSURE DROP AS A FUNCTION OF FLOW RATE FOR N-PROPANE/N-DECANE SYSTEM.

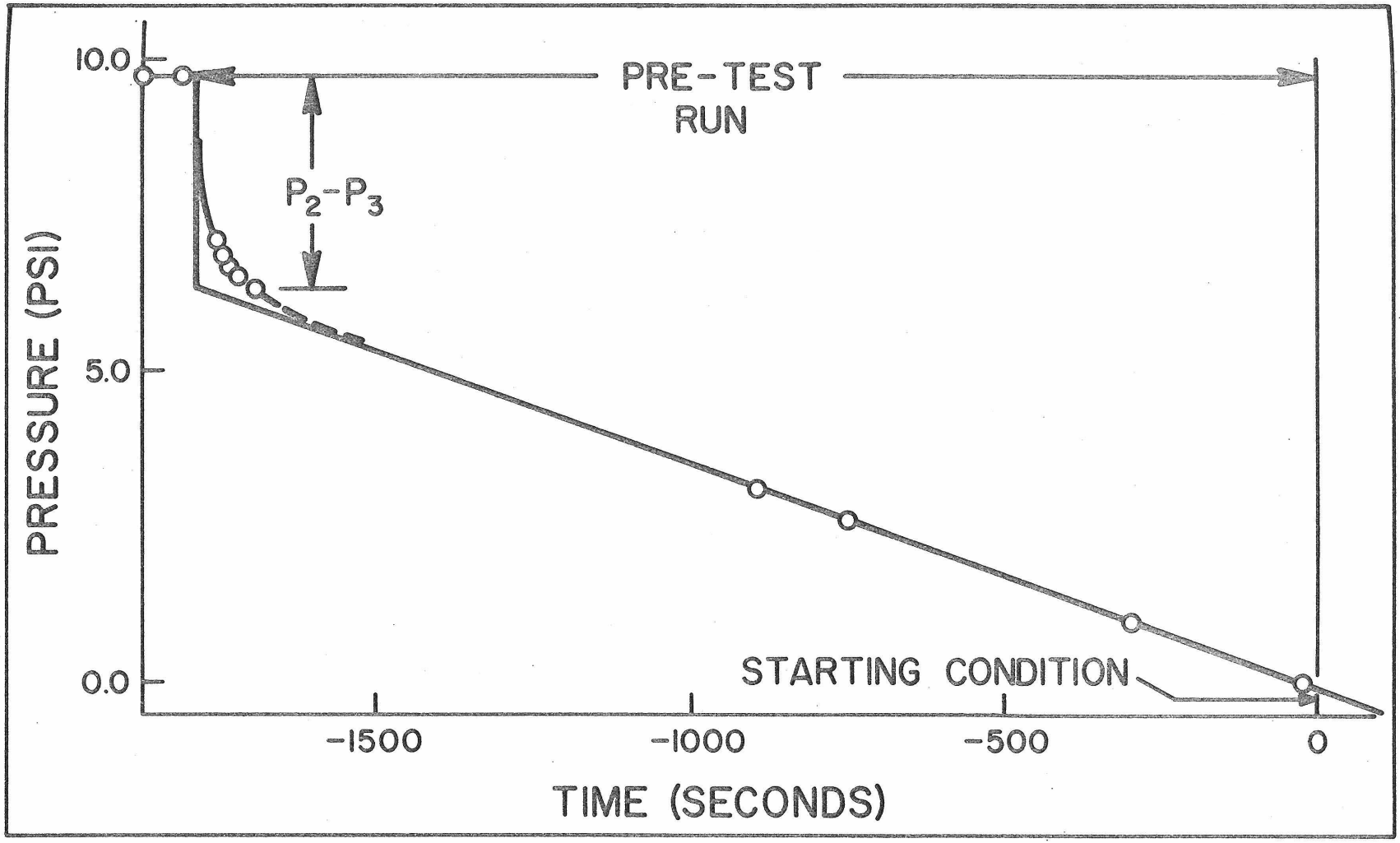

FIGURE 2. DEVELOPMENT OF PSEUDO-STEADY-STATE PRESSURE PROFILE.

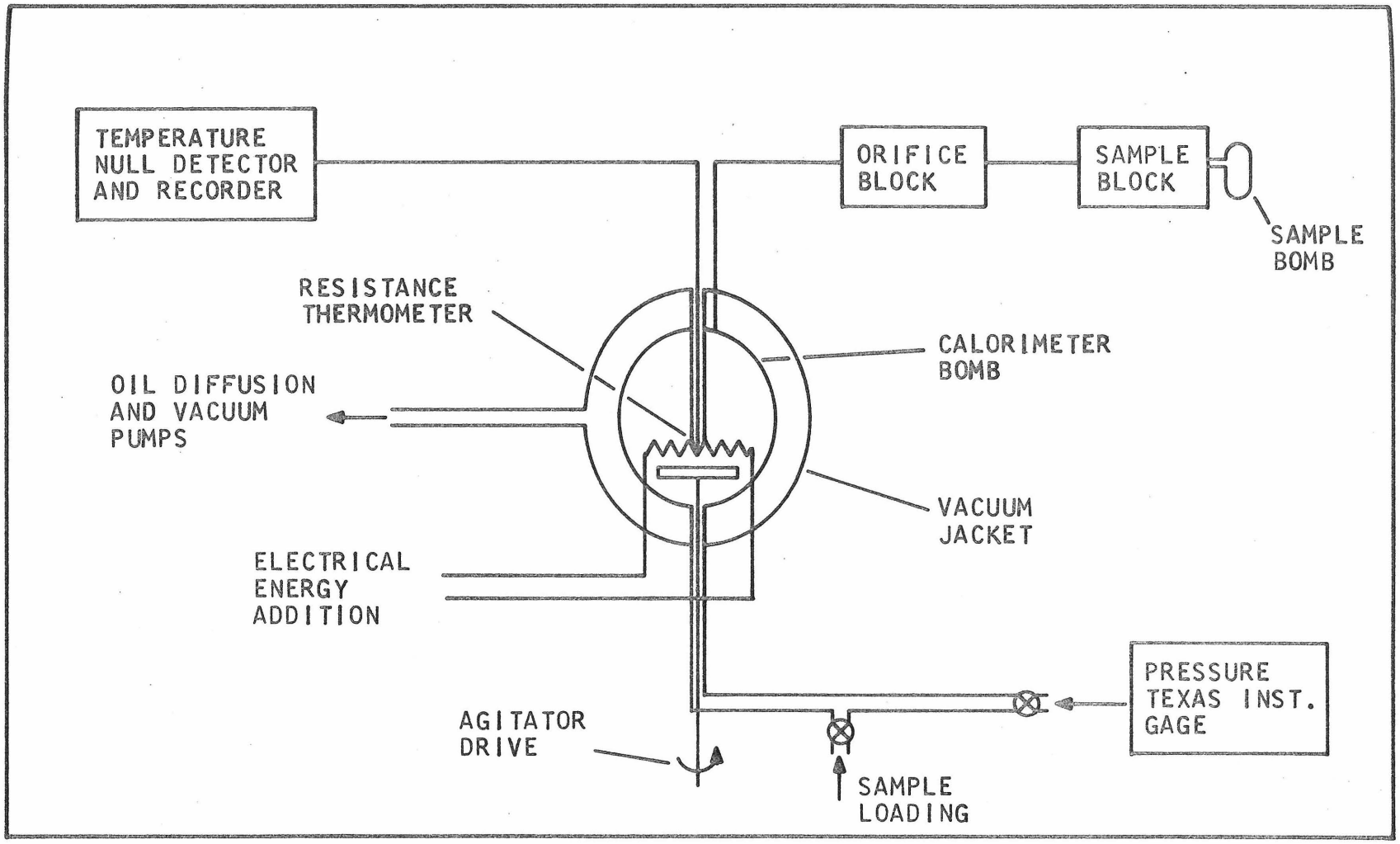

FIGURE 3. FUNCTIONAL SCHEMATIC OF CALORIMETER AND ASSOCIATED EQUIPMENT.

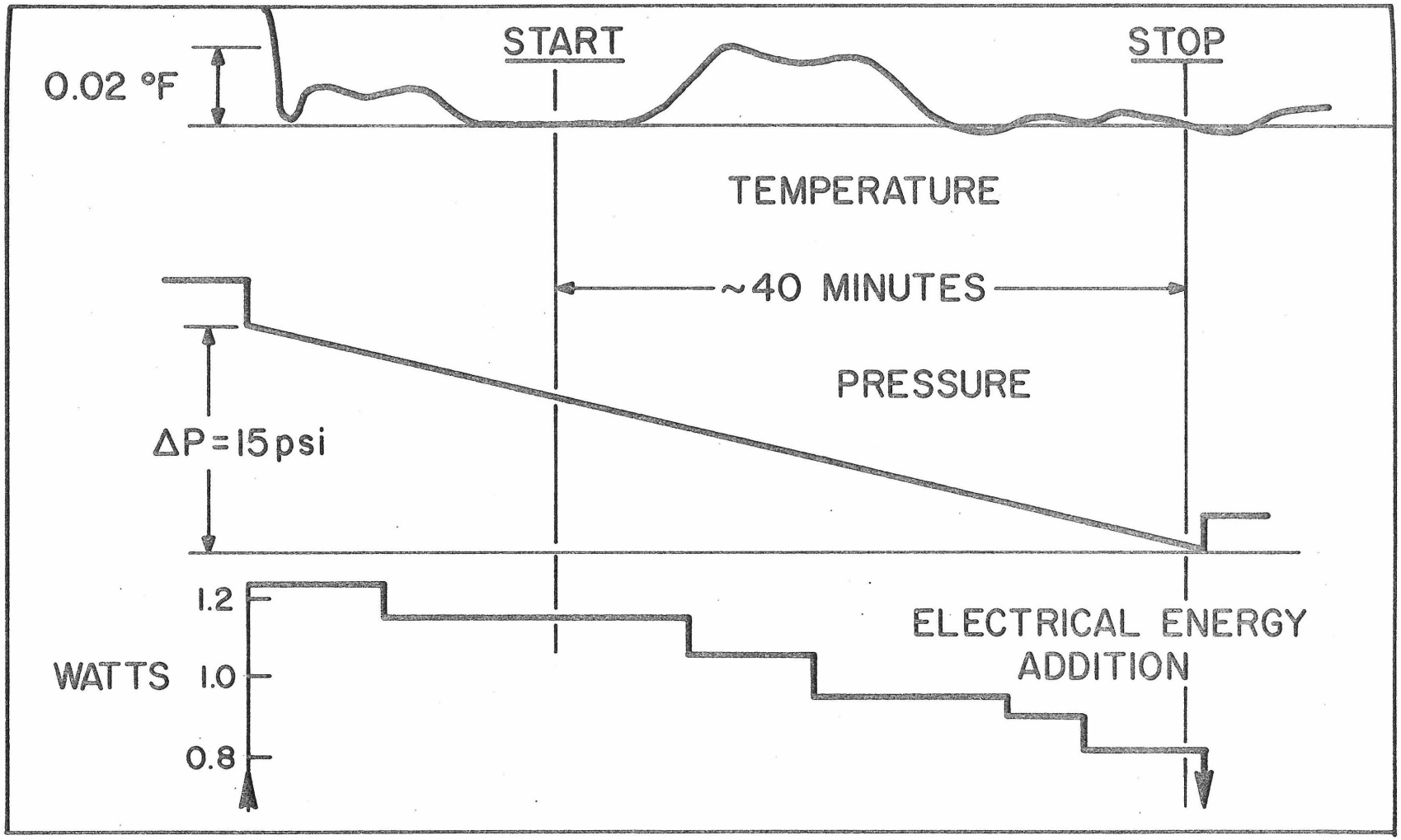

FIGURE 4. CALORIMETER TEMPERATURE, PRESSURE AND ENERGY ADDITION PROFILES FOR EXPERIMENTAL TEST.

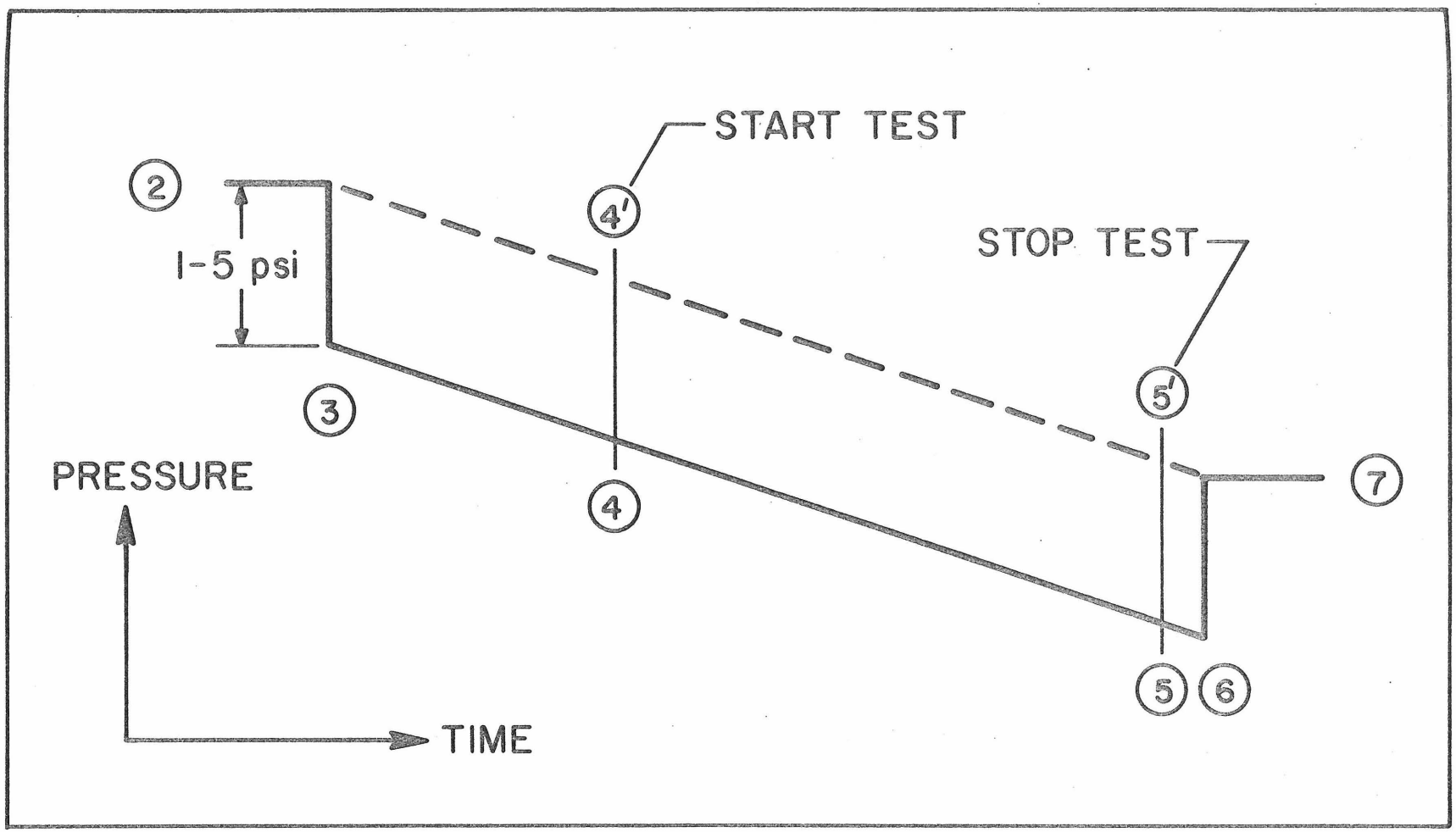

FIGURE 5. DEFINITION OF THERMODYNAMIC STATES FOR HEAT-OF-VAPORIZATION CALCULATIONS.

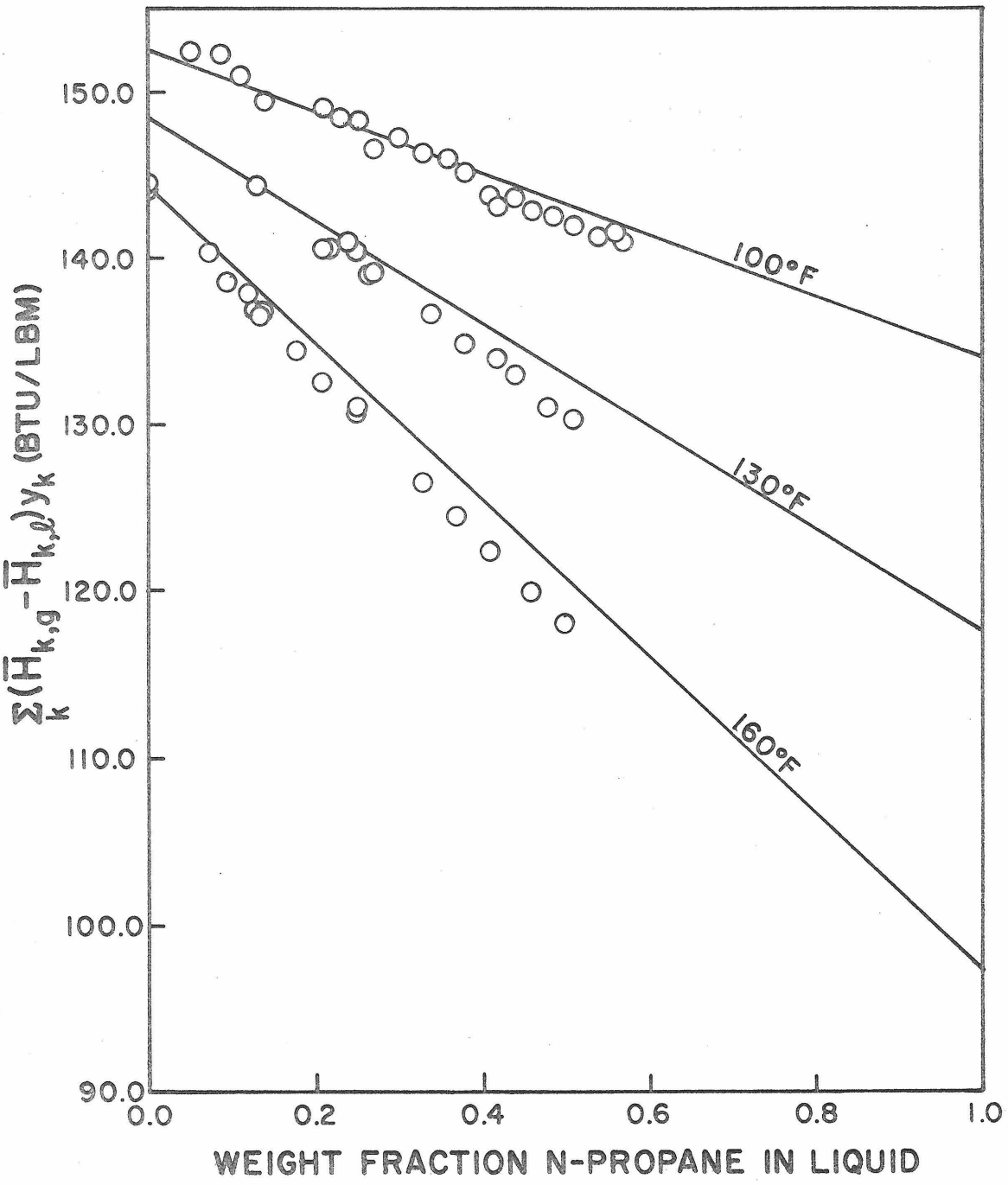

FIGURE 6. SUMMARY OF CALCULATED RESULTS FOR TOTAL HEATS-OF-VAPORIZATION (NON-EQUILIBRIUM CALCULATION).

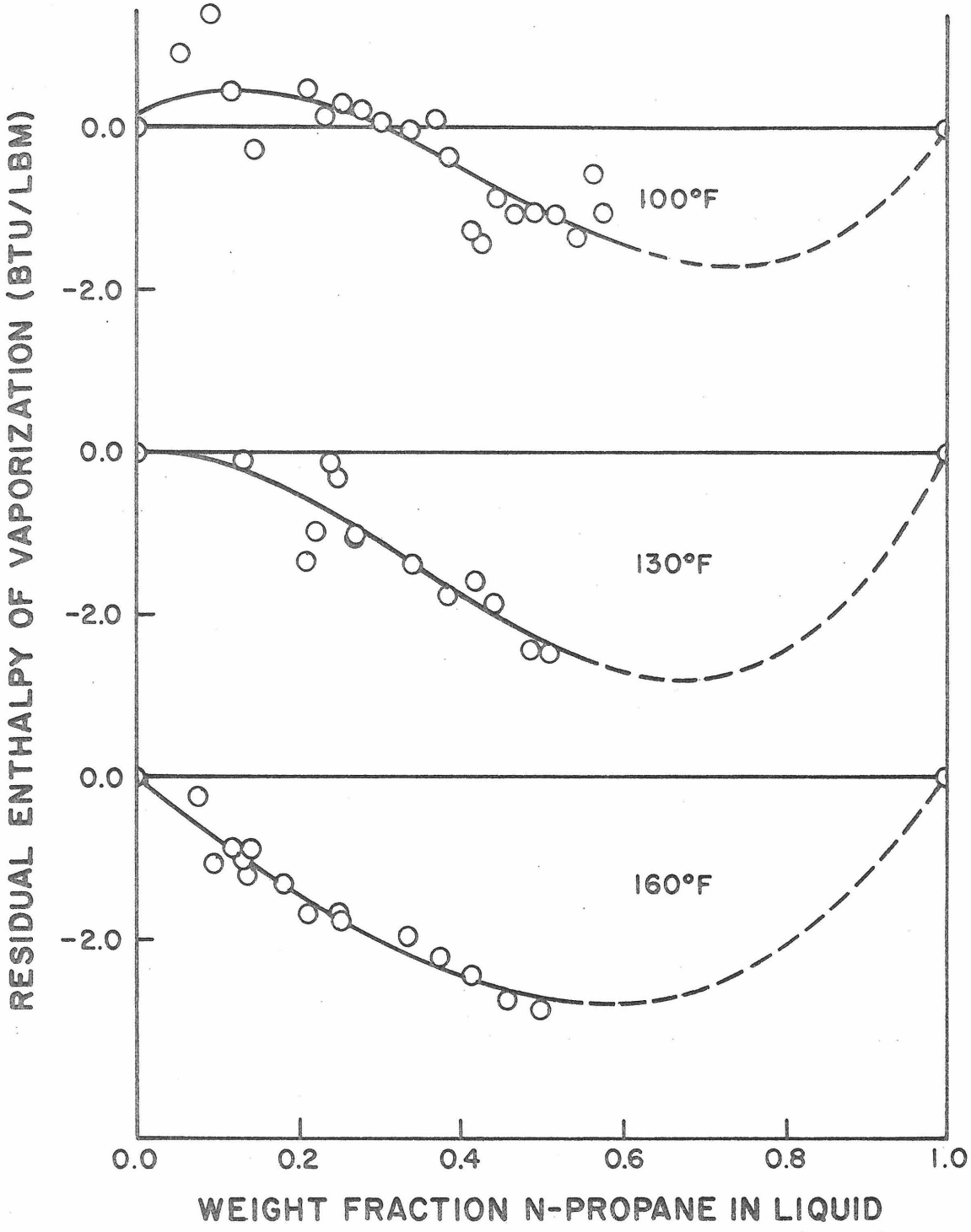

FIGURE 7. RESIDUAL HEATS-OF-VAPORIZATION (NON-EQUILIBRIUM CALCULATION)

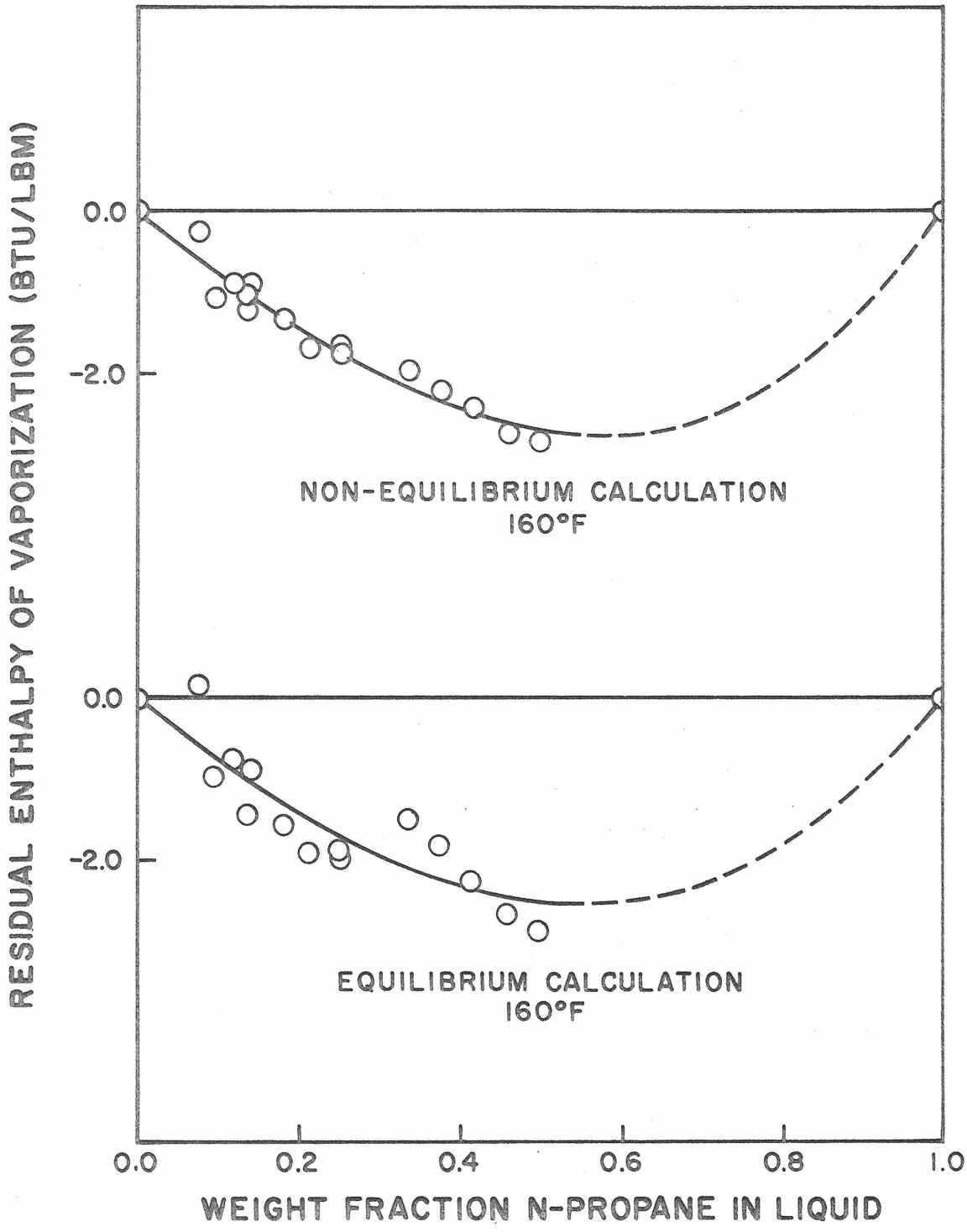

FIGURE 8. COMPARISON OF HEAT-OF-VAPORIZATION RESULTS FOR NON-EQUILIBRIUM AND EQUILIBRIUM CALCULATIONS.

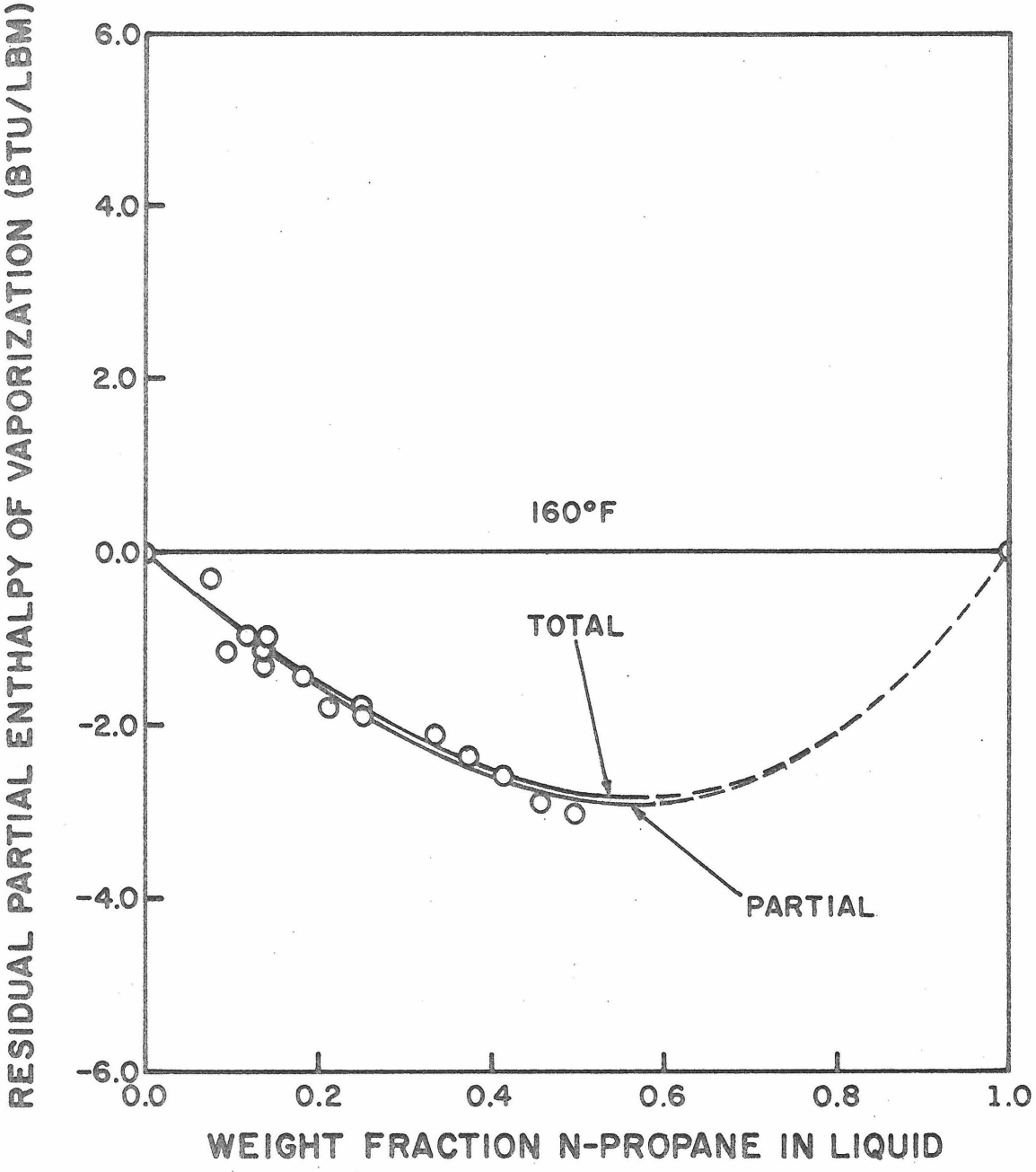

FIGURE 9. RESIDUAL PARTIAL ENTHALPY OF VAPORIZATION OF N-PROPANE.

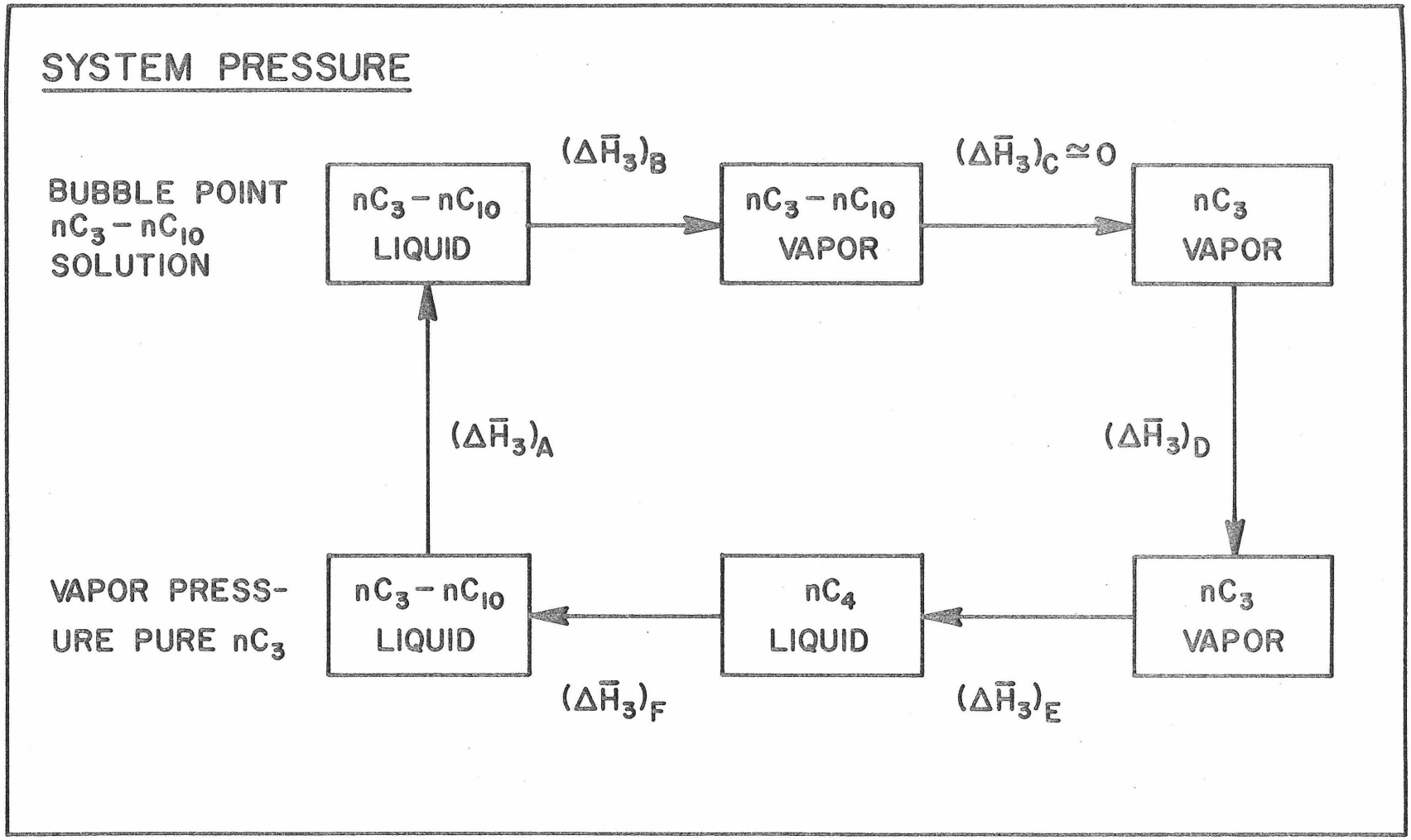

FIGURE 10. THERMODYNAMIC CYCLE FOR CALCULATING PARTIAL ENTHALPY OF LIQUID N-PROPANE.

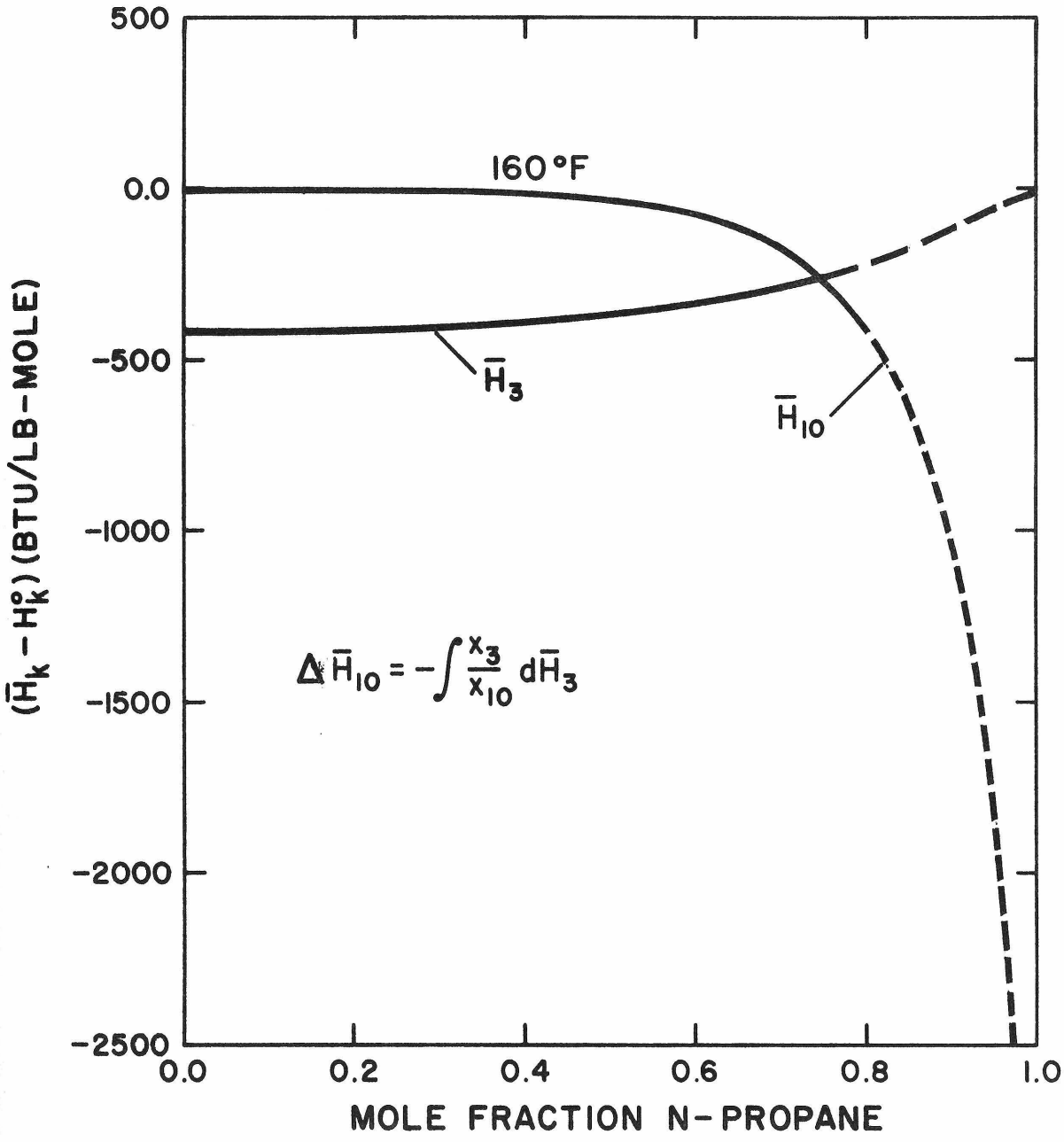

FIGURE 11. CALCULATED PARTIAL ENTHALPIES OF N-PROPANE AND N-DECANE.

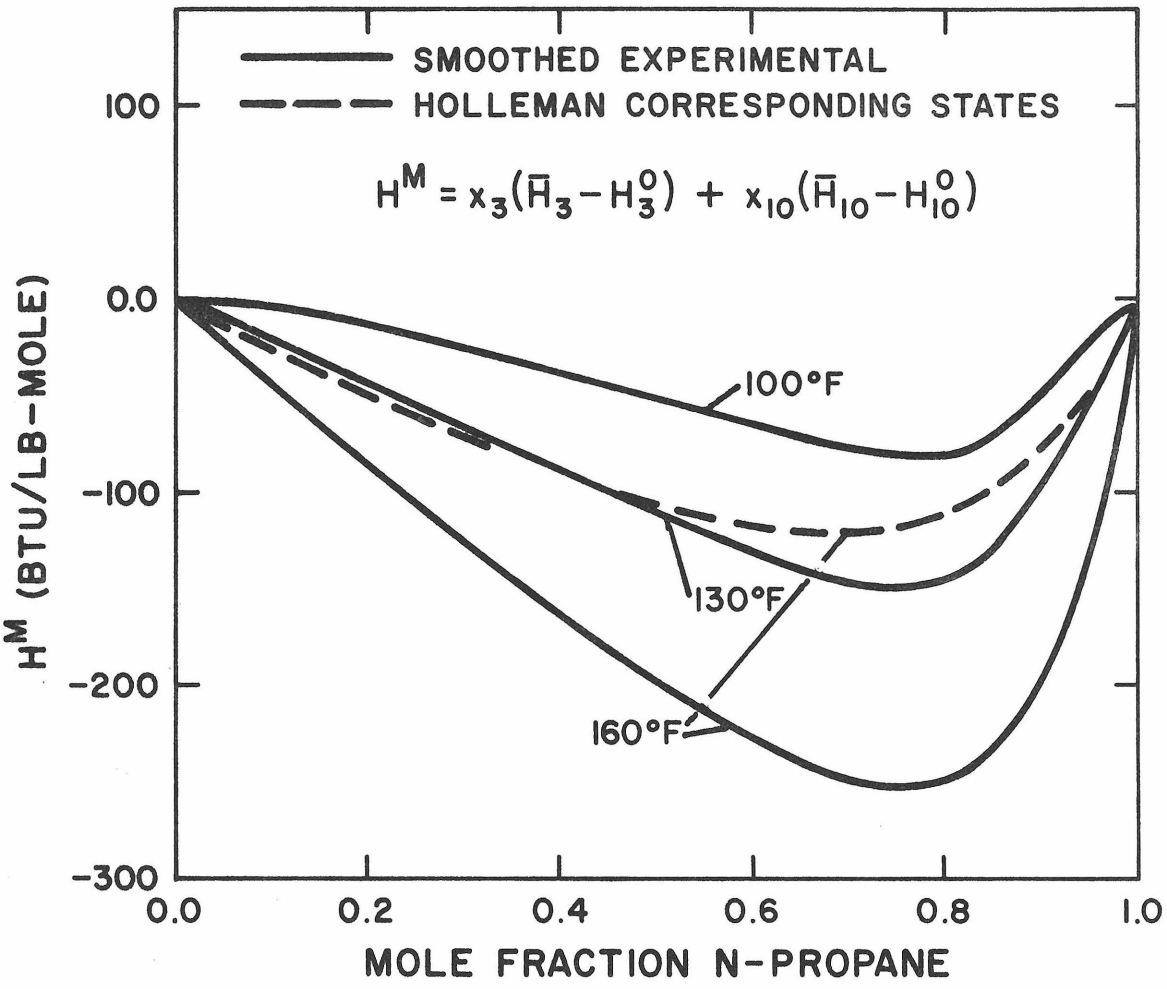

FIGURE 12. CALCULATED HEATS-OF-MIXING FOR N-PROPANE/N-DECANE LIQUID MIXTURES.

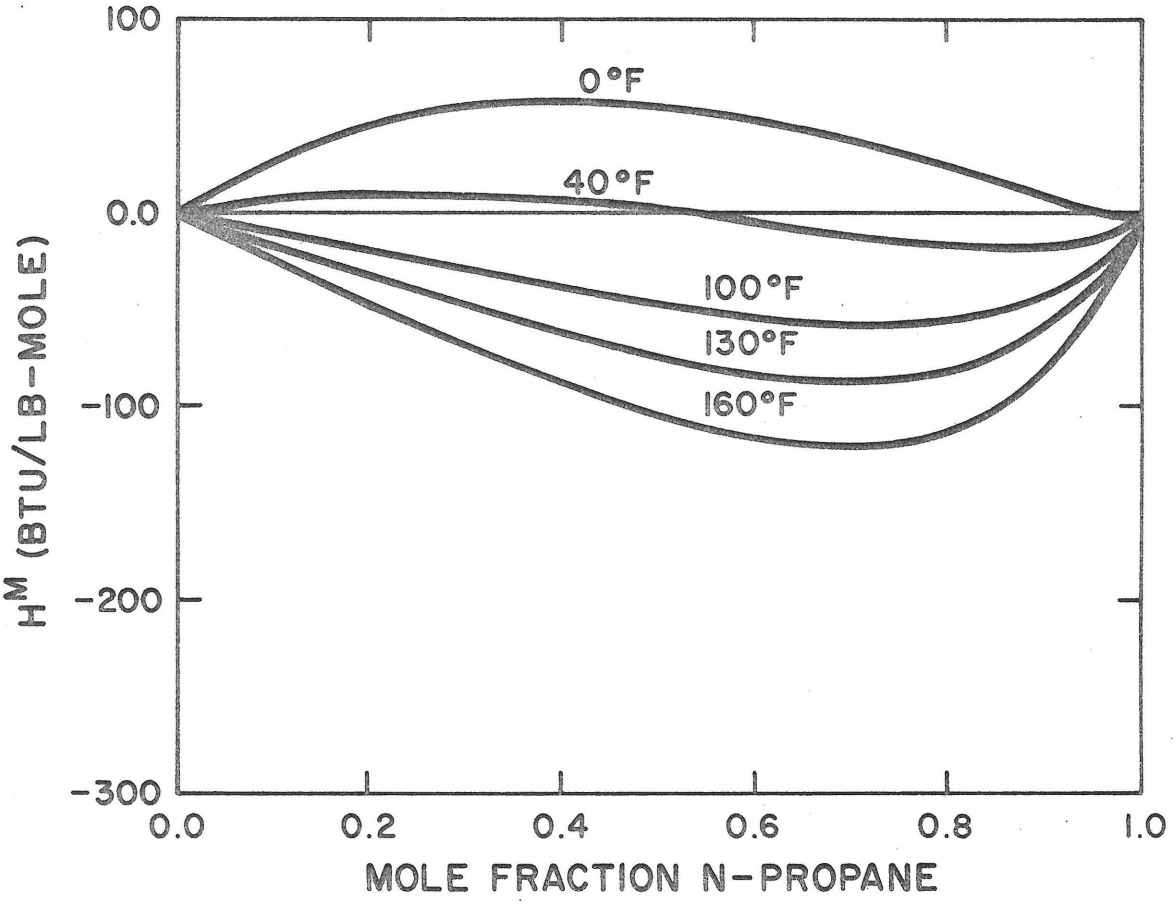

FIGURE 13. LIQUID PHASE HEATS-OF-MIXING AS PREDICTED BY CORRESPONDING STATES CORRELATION.

APPENDIX I

THERMODYNAMIC DEVELOPMENT

The enthalpy change upon vaporization for a pure, single component liquid may be defined as that energy required to transform a unit mass of liquid into a unit mass of vapor in a steady, equilibrium process. The process is isothermal, and vaporization proceeds at constant pressure, there being but one independent variable. For multicomponent systems, however, selective vaporization of the components occurs so that all but one (e.g., temperature) of the intensive variables change as a function of time.

Two types of heat-of-vaporization are often defined for the multicomponent case. The differential heat-of-vaporization refers to the energy required for a change in state resulting from the transfer of an infinitesimal amount of material from the liquid to the vapor phase under conditions of equilibrium. The properties of neither phase are affected by the transfer. Integral heats-of-vaporization refer to the energy required for the transfer of material between phases over the range of conditions resulting from vaporization of a finite amount of material (see Figure I-1). Although the former quantity, the differential heat-of-vaporization, is a thermodynamic point function, it is clear that integral values are a function of the process by which they are defined.

Any number of such processes may be considered. However, the isothermal and isobaric processes are the ones of usual interest. Of these, the heat-of-vaporization at constant pressure is often considered to be of greater practical importance as it may be applied directly

in fractionation column calculations.

Experimental measurements for the enthalpy change upon vaporization for multicomponent systems, of practical necessity, yield results of the integral type. Under certain limiting conditions, however, it is possible to deduce differential (thermodynamic point function) quantities from these experimental data. In the current investigation integral values of the heat-of-vaporization were determined for an isothermal vaporization process. A constant volume calorimeter was used. The pressure and composition of both phases changed as a function of time; however, the capacity of the calorimeter (1156 cc.) was such that the removal of a vaporization sample (~10 gms.) did not introduce large changes in the thermodynamic properties of either of the phases. Because these changes were small the thermodynamic properties of the bulk phases within the calorimeter, for calculational purposes, were assumed to be constant for the test, and were taken as the average of the thermodynamic values which described the end points of the experimental test. Thus, the partial enthalpy-of-vaporization, as calculated from the experiment (see Equation I-6 below) actually represents the mean value (indicated by *) for a sequence of states.

$$(\bar{H}_{k,g} - \bar{H}_{k,\ell})^{*} = \frac{-\int_{m_k(x_1)}^{m_k(x_2)} \left\{ \bar{H}_{k,g}\,(m_k) - \bar{H}_{k,\ell}\,(m_k) \right\} dm_k}{-\int_{m_k(x_1)}^{m_k(x_2)} dm_k}$$

$m_{k,\ell}$ represents the amount of component k present in the calorimeter and is a function of the composition of the liquid phase (x). The limits of variation are determined by the end points of the test (x_2) and (x_1).

EQUILIBRIUM CASE

McKay (15) and Huisman (8) previously presented thermodynamic analyses by which the partial enthalpy-of-vaporization of a volatile component from solution could be calculated from experimental data. The analysis shown below follows that of Huisman which was developed to describe either material addition or withdrawal processes. It was assumed that vaporization proceeded at a rate such that equilibrium was maintained throughout the calorimeter. That is, the temperature and pressure were considered uniform throughout the calorimeter and composition was considered uniform within each phase. Both of these assumptions and the limitations which are introduced by them are discussed in greater detail below.

An energy balance for a constant volume, open thermodynamic system "A" may be written (see Figure I-2) for the case of withdrawal of a differential amount of material, dm_a, at the point "a".

$$\underline{dE} = q + w + \sum_{k=1}^{n} \overline{E}_{k,a}\, dm_{k,a} \qquad (I\text{-}1)$$

Here E represents the total internal energy of the calorimetric system, and changes in it are the result of thermal energy added (q), pressure-volume work done on the system (w) and the intrinsic energy of the material added at point "a" $\sum(\overline{E}_{k,g}\, dm_{k,a})$.

The thermal transfer, q, is the sum of three terms

$$q = q_e + q_{ag} + q_{ht} \tag{I-2}$$

where q_e is the electrical energy input, q_{ag} is the energy input by the agitator and q_{ht} is the heat transferred by conduction and radiation from the surrounding vacuum jacket.

Since the vessel A is considered isochoric the work w associated with the process is limited to that concerned with the addition or withdrawal of material:

$$w = P\ dV = P \sum_{k=1}^{n} \overline{V}_{k,a}\ dm_{k,a}$$

The total change in internal energy of the system is the sum of the changes in the internal energy of each of the phases so that:

$$d\underline{E} = d\underline{E}_g + d\underline{E}_\ell + d\underline{E}_c$$

where $d\underline{E}_c$ refers to energy changes of the calorimeter.
Introducing the enthalpy, H,

$$E = H - PV$$

$$dE_g = dH_g - PdV_g - V_g\ dP$$

$$dE_{\ell} = dH_{\ell} - PdV_{\ell} - V_{\ell}dP$$

where

$$H = H\ (T,\ P,\ m_1,\ m_2,\ \ldots\ m_n)$$

The total differential of $\underline{H}_g$ is:

$$d\underline{H}_g = \left(\frac{\partial \underline{H}}{\partial T}\right)_{P,m} dT + \left(\frac{\partial \underline{H}}{\partial P}\right)_{T,m} dP + \sum_{k=1}^{n} \left(\frac{\partial \underline{H}_g}{\partial m_{k,g}}\right)_{P,T,m_{j,g}} dm_{k,\ell}$$

$$= m_g\, C_{P,g}\, dT + \left\{ \underline{V}_{\ell} - m_g T \left(\frac{\partial V_g}{\partial T}\right)_{P,g} \right\} dP + \sum_{k=1}^{n} \overline{H}_{k,g}\, dm_{k,g}$$

and similarly

$$d\underline{H}_{\ell} = m_{\ell} C_{P,\ell}\, dT + \left\{ \underline{V}_{\ell} - m_{\ell} T \left(\frac{\partial V_{\ell}}{\partial T}\right)_{P,x} \right\} dP + \sum_{k=1}^{n} \overline{H}_{k,\ell}\, dm_{k,\ell}$$

The calorimeter volume $\underline{V}$ constant

$$d\underline{V} = d\underline{V}_g + d\underline{V}_{\ell} = 0$$

and the change in internal energy of the calorimeter can be expressed

as: $$dE_c = C_c\, dt$$

where C_c is the total heat capacity of the calorimeter.

Combining the above equations and rearranging gives

$$\sum_{k=1}^{n} \bar{H}_{k,g}\, dm_{k,g} + \sum_{k=1}^{n} \bar{H}_{k,\ell}\, dm_{k,\ell}$$

$$+ \left(m_g C_{P,g} + m_\ell C_{P,\ell} + C_c\right) dT$$

$$- \left\{ m_g T \left(\frac{\partial V_g}{\partial T}\right)_{P,y} + m_\ell T \left(\frac{\partial V_\ell}{\partial T}\right)_{P,x} \right\} dP = q + \sum_{k=1}^{n} \bar{H}_{k,a}\, dm_{k,a} \qquad \text{(I-3)}$$

The left-hand side of this equation describes thermodynamic changes in state which take place within the thermodynamic system (A). The terms on the right-hand side are process variables and describe the interaction of the calorimeter thermodynamic system with its surroundings.

The terms $dm_{k,\ell}$ and $dm_{k,g}$ cannot be measured directly and must be expressed in terms of measurable quantities, and the term $dm_{k,\ell}$ will be eliminated first. A material balance for any component k can be expressed as

$$dm_{k,\ell} = (dm_{k,a} - dm_{k,g}) = d(y_{k,a} m_a) - d(y_k m_g)$$

$$= y_{k,a} dm_a - d(y_k m_g) \tag{I-4}$$

In this relation the term $m_a dy_k$ must be zero as for the case m_a = constant (zero), $dy_k = 0$. This is due to the fact that dm_a describes the process of material transfer and is not a thermodynamic variable-of-state of the system. Substituting in Equation (I-3) we obtain

$$\sum_{k=1}^{n} \{(\bar{H}_{k,g} - \bar{H}_{k,\ell}) y_{k,a}\} dm_a =$$

$$+ \sum_{k=1}^{n} (\bar{H}_{k,g} - \bar{H}_{k,\ell}) \, d(m_{k,g}) \tag{I-5}$$

$$- q + (m_g C_{P,g} + m_\ell C_{P,\ell} + C_c) \, dT$$

$$- \left\{ m_g T \left(\frac{\partial V_g}{\partial T} \right)_{P,y} + m_\ell T \left(\frac{\partial V_\ell}{\partial T} \right)_{P,x} \right\} dP$$

Up to this point no assumptions, other than that of equilibrium, have been made, and Equation (I-5) applies, rigorously, to any withdrawal or addition process which occurs in a constant volume calorimeter. Assuming an isothermal process, Equation (I-5) may be rearranged directly

to obtain an expression for evaluating the partial enthalpy-of-vaporization of the volatile component for a binary system.

$$\left\{\bar{H}_{k,g} - \bar{H}_{k,\ell}\right\}^{*} = \left[\frac{1}{y_k^{*}\Delta m_a - \Delta m_{k,g}}\right] \times$$

$$\left[-q - \left\{m_g T\left(\frac{\partial V_g}{\partial T}\right)_{P,y} + m_\ell T\left(\frac{\partial V_\ell}{\partial T}\right)_{P,x}\right\}^{*}\Delta P\right. \tag{I-6}$$

$$\left. + \left\{\bar{H}_{j,g} - \bar{H}_{j,\ell}\right\}^{*}\left\{\Delta m_{j,g} - y_j\,\Delta m_a\right\}\right]$$

The second enclosure on the right contains energy quantities. Electrical, agitation, and heat transfer energies are included in q. The second quantity is used to evaluate changes in energy of the contents of the calorimeter. It is due to the pressure changes which occur during a test. Average test values were used to evaluate the coefficient of the pressure change, ΔP. The last quantity is a correction which accounts for the amount of the heavy component vaporized.

Within the first parentheses are terms for calculating the amount of component k vaporized. Δm_a is experimentally measured from the quantity of material collected in the sample bomb. y_k^{*} is the average composition of the material collected, and $\Delta m_{k,g}$ represents the ac-

cumulation of component k within the vapor space during a test. It is evaluated from

$$\Delta m_{k,g} = \Delta \left(y_k \frac{\underline{V} - \underline{m} V_\ell}{V_g - V_\ell} \right) \qquad \text{(I-7)}$$

where $\underline{V}$ is the total volume and m the total mass of material within the calorimeter.

It should be mentioned, at this point, that Huisman included in his development the term

$$\overline{H}_{k,a} = (\overline{H}_{k,a} - \overline{H}_{k,g}) + \overline{H}_{k,g}$$

so that the quantity $\sum_k (\overline{H}_{k,a} - \overline{H}_{k,g}) y_k$ was introduced into Equation (I-5) above. The term, ostensibly, was introduced to account for variations in the thermodynamic properties of the vapor phase during sample withdrawal or for addition of material which is at a different state than that of material within the calorimeter. However, either of these conditions implies that gradients exist within the system which can then not be at equilibrium. As the entire development was based on the assumption that equilibrium existed, inclusion of the term referred to above is not appropriate. At equilibrium $\overline{H}_{k,a}$ must equal $\overline{H}_{k,g}$ for all types of processes considered. This condition is rather easily satis-

fied when a mass is being withdrawn from the calorimeter, but it is considerably more difficult to satisfy for addition processes. This is not to say that Equation (I-6) could not be used for addition processes. However, if it is, a mechanism should be included which would permit the evaluation of the irreversible mixing (both thermal and material) which must occur within the vapor phase.

IRREVERSIBLE EFFECTS AT LIQUID-VAPOR INTERFACE

It was pointed out above that for the mass withdrawal process (vaporization) gradients within the vapor phase are probably negligible. In the current experiments the liquid phase was agitated and it will be assumed that temperature and concentration gradients within the bulk liquid phase are not of any consequence. However, ample evidence (16,17) exists which shows that even at very low rates of inter-phase mass transfer small temperature differences develop at the interface between the bulk liquid and the vapor phases. In the case of a binary system concentration gradients would also be expected to develop which, along with the temperature gradients, contribute to pressure changes within the system. The purpose of this section is to provide a means for evaluating the effect which these gradients have on measurements for determining the partial enthalpy-of-vaporization.

Single Component Systems. It is not possible to maintain a bubble of a single component system in a state of equilibrium (mechanical and thermodynamic). Thermodynamic equilibrium requires that the temperatures and pressures (except for a small pressure effect due to curvature of the interface) of the contiguous phases be identical. Mechanical equilibrium requires that the sum of the forces acting on the

bubble surfaces be equal to zero. The latter consideration shows that because of the existence of an interfacial surface tension the pressure within the bubble, P_b, must be greater than the system pressure, P_s, by an amount $\Delta P = 2\sigma/r$ (σ is the surface tension of the liquid and r the radius of the bubble). Therefore, in a stable system (thermal and dynamic equilibrium)

$$P_b = P_s + \frac{2\sigma}{r} \tag{I-8}$$

For a single-component system all pressure within the bubble is derived from the vapor pressure of the surrounding liquid, $P_b = P_{vp}$. But from thermodynamic considerations $P_{vp} \leq P_s$, otherwise flashing of the liquid to vapor would occur. This leads to

$$P_b = P_{vp} \leq P_s < P_s + \frac{2\sigma}{r} \tag{I-9}$$

which shows that Equation (I-8) can never be satisfied and a stable bubble will not form. In a single component system a bubble must either be growing or collapsing, and this requires that the latent energy of phase change either be supplied to or removed from the vapor phase at the vapor-liquid interface.

The thermal gradients which exist during the growth of a bubble in a single component system are represented schematically in Figure I-3 where it is indicated that the major portion of the temperature drop between the bulk phases exists in the liquid phase. This representation may be justified by considering the thermal boundary condi-

tion at the interface

$$k_\ell \left(\frac{\partial T_\ell}{\partial z}\right)_i = m_i \, (\Delta H_v)_i + k_g \left(\frac{\partial T_g}{\partial z}\right)_i \qquad \text{(I-10)}$$

where k_ℓ and k_g are considered to be effective thermal conductivities of the liquid and vapor phases respectively and i, ℓ, and g refer to the interface and the liquid and vapor phases. (The convective term included here describes only the mean motion of the vapor phase normal to the vapor-liquid interface). The important term on the right is the convective term as the temperature gradient within the gas phase approaches zero. Therefore, energy is supplied to the interface by conduction in the liquid phase and carried away by convection in the vapor phase. Conductive resistance to heat transfer in the vapor phase is negligible. The general problem of heat and mass transfer between individual bubbles and their surrounding mediums has been analyzed in considerable detail (see e.g. 18 and 19)and the results presented here are in agreement with the applicable portion of that theory.

In processes in which evaporation occurs at the upper surface of the liquid rather than at a bubble interface,conditions similar to those described above exist. Experimental measurements of the temperature profile for this case have been reported previously by Pruger (20) (see Figure I-3). Here the large temperature gradient within the liquid phase and the small gradient in the vapor phase are evident. The discontinuity in the temperature profile at the interface is almost zero (approximately 0.002 °F). These measurements support the conclusions drawn from a consideration of the boundary conditions in the paragraph

above, and may be justified, physically, as follows. Molecules are transported to the vicinity of the interface by convection at essentially a constant temperature. To pass into the vapor phase they require an additional quantity of energy, the heat of vaporization, which is obtained by thermal conduction through the liquid layers immediately adjacent to the surface.

Binary Systems. In a system in which a second component is present and in which one component is considerably more volatile than the other it is understandable that concentration gradients in addition to temperature gradients may develop at the vapor-liquid interface. From Gibb's phase rule a two component system in which two phases exist has two independent variables. The temperature and composition of the liquid phase are set, independently, so that the system is completely specified. Therefore, as temperature and concentration changes develop between the bulk liquid phase and the interface it follows that the phase pressure also changes. When the process of vaporization starts, the measured system pressure changes from a value which corresponds to equilibrium with a bulk liquid phase to one which reflects the condition of the surface during material transfer. A small pressure change also occurs at the start of vapor flow when a single component system is being investigated. This change, however, is due only to the temperature gradient and is an order of magnitude less than those which develop in a multicomponent system.

Effect on Calculations. Pressure was described as a dependent variable in the developments above. However, the effect that pressure, temperature and concentration gradients within the calorimeter have on

calculations for the partial enthalpy change on vaporization may be treated separately. This remains to be discussed.

In Equation (I-6) pressure is used, specifically, in two places; in the pressure energy term and the relation used for determining the amount of mass evaporated. The pressure gradient occurs on the liquid side of the vapor-liquid interface, and as the thicknesses of the temperature and concentration boundary layers are small (the liquid phase is agitated), the bulk liquid remains essentially at equilibrium pressure. The interface is at a different thermodynamic state which is in equilibrium with the vapor phase. Therefore, the properties of the two bulk phases (liquid and vapor) should be evaluated for different state conditions. This procedure could have some effect on the pressure energy term ($T \frac{\partial V}{\partial T} \Delta P$) but as the entire term is relatively small only negligible improvements in evaluation of the partial heat-of-vaporization would be expected. Larger effects could result, however, from pressure changes in the vapor phase and lead to significant errors in the calculation of the mass change, $\Delta m_{k,g}$.

Based on these considerations Equation I-6 and I-7 may be rewritten to reflect the changes required for the non-equilibrium case. Those terms conceivably affected by a consideration of the irreversible effects are underlined.

$$\left\{ \underline{\underline{\bar{H}_{k,g} - \bar{H}_{k,\ell}}} \right\}^* = \left[\frac{1}{\underline{\underline{y_k}}^* \Delta m_a - \underline{\underline{\Delta m_{k,g}}}} \right]$$

$$\left[- q - \left\{ m_g T \left(\frac{\partial V_g}{\partial T} \right)_{P,y} + m_\ell T \left(\frac{\partial V_\ell}{\partial T} \right)_{P,x} \right\}^* \underline{\underline{\Delta P}} \right. \qquad \text{(I-6')}$$

$$\left. + \left\{ \bar{H}_{j,g} - \bar{H}_{j,\ell} \right\}^* \left\{ \Delta m_{j,g} - \underline{\underline{y_j}} \Delta m_a \right\} \right]$$

The process of vaporization of one component may be broken down into a series of equilibrium states through which the material to be evaporated must pass as it is transferred from the bulk liquid to the bulk vapor phase. As there are only two independent variables in the system the third, pressure, is included below only for descriptive convenience. The thermodynamic states are (see Figure I-4):

Thermodynamic State	Variables
1. Bulk condition of liquid	T_ℓ, x_ℓ, P_ℓ
2. State of liquid at surface temperature and bulk liquid concentrations	T_g, x_ℓ, P_ℓ'
3. State of liquid at surface temperature and surface concentration	T_g, x_i, P_g
4. State of vapor in equilibrium with interface of liquid	T_g, y_g, P_g

5. State of vapor at bulk vapor conditions T_g, y_g, P_g

Calorimetric measurements provide the partial enthalpy change for the overall process 1-5 which may be calculated for the overall process from Equation I-6'. Steps 1-2 and 2-3 are non-equilibrium processes. Step 3-4 is assumed to be an equilibrium process and the energy required for this change is the thermodynamica quantity, the partial heat-of-vaporization. The conditions within the vapor phase are completely uniform so that states 4 and 5 become identical. It was assummed (step 3-4) that the transfer of material from one phase to the other takes place under conditions of complete equilibrium so that any discontinuities in the temperature or concentration profiles at the vapor-liquid interface is neglected (9).

As the enthalpy change of the overall process 1-5 equals the sum of the enthalpy changes of the individual processes, the partial heat-of-vaporization may be determined by difference.

$$(\Delta\bar{H}_k)_{3-4} = (\Delta\bar{H}_k)_{1-5} - (\Delta\bar{H}_k)_{1-2} - (\Delta\bar{H}_k)_{2-3} \qquad \text{(I-11)}$$

where (see Equation I-6')

$$\Delta\bar{H}_k{}_{1-5} \equiv (\bar{H}_{k,g} - \bar{H}_{k,\ell})^*$$

Description of Correction Terms. $(\Delta\bar{H}_k)_{1-2}$ represents the cooling of the material to be evaporated, at constant composition, as it passes from the bulk liquid temperature to the interface temperature. It is normally referred to as a superheat correction and introduced in the form

$$\Delta H_{superheat} = C_{P,g}(T_{\ell} - T_g)$$

In this way the temperature of vaporization reported is the bulk liquid temperature rather than the interfacial temperature.

The evaluation of the term $(\Delta\bar{H}_k)_{3-2}$ depends upon the availability of two-phase equilibrium data from which values of y_k and x_k can be obtained, and also on the availability of heat-of-mixing data for the liquid phase. Values of the individual terms ($\bar{H}_{k,3}$ and $\bar{H}_{k,2}$) may be evaluated from heat-of-mixing curves using standard thermodynamic data handling techniques (e.g., method of intercept). Both of these terms are small and almost negligible. They are a function of the rate of vaporization, becoming smaller at low rates of vaporization. They are discussed here, mainly, because the latter quantity, $(\Delta\bar{H}_k)_{3-2}$ has not previously been considered in calculations involving binary heat-of-vaporization experiments.

THERMODYNAMIC METHOD FOR CALCULATING H^M

Heats-of-mixing are normally determined from either (21) vapor pressure measurements of a solution and of the pure components or from calorimetric measurements by mixing two liquid phases. The enthalpy per unit weight of solution is

$$H = x_1\bar{H}_1 + x_2\bar{H}_2 \qquad \text{(I-13)}$$

which for an ideal solution becomes

$$H^i = x_1 H_1^o + x_2 H_2^o \qquad \text{(I-14)}$$

Here H^o represents the enthalpy of the pure components at the same temperature and state of aggregation as the solution. The heat-of-mixing, or integral heat of solution, in which we are interested is obtained by combination of Equations (I-13) and (I-14) so that

$$H^M = x_1 (\bar{H}_1 - H_1^o) + x_2 (\bar{H}_2 - H_2^o) \qquad \text{(I-15)}$$

In this section it is shown how one of the quantities $(H_i - H_i^o)$ may be obtained from calorimetric measurements of the partial enthalpy change upon vaporization. This same quantity for the second component may then be obtained by integrating the Gibbs-Duhem equation

$$\sum_k x_k d\bar{H}_k = 0 \qquad (T,P) \qquad \text{(I-16)}$$

The two quantities may then be combined in Equation (I-15) to obtain the heat-of-mixing.

The thermodynamic analysis used for calculating the partial enthalpy of the more volatile component in a binary solution may be broken down into a series of steps as shown in Figure 10 It is assumed that the heavy component is almost completely non-volatile.

Step A Change in partial enthalpy of n-propane in liquid solution with pressure for constant temperature and composition. This

process represents an exceedingly small quantity as carried out in the present system. It may be calculated from

$$(\Delta\overline{H}_k)_A = \int \left\{ \overline{V}_k - T\left(\frac{\partial \overline{V}_k}{\partial T}\right)_{P,x} \right\} dP$$

Step B Change in partial enthalpy of n-propane upon vaporization from an n-propane/n-decane liquid solution.

$$(\Delta\overline{H}_k)_B = (\overline{H}_{k,g} - \overline{H}_{k\ell})^*$$

Step C Change in partial enthalpy of gaseous n-propane in being transferred from a mixture to a pure state at constant temperature and pressure. For the calculations presented below the change in composition of the gas phase is so small (∿0.99-1.00) that this term is assumed zero.

$$(\Delta\overline{H}_k)_C \simeq 0$$

Step D Change in enthalpy of pure n-propane in the gaseous state upon compression at constant temperature to the dew point pressure of the pure component. This may be calculated using

$$\left(\frac{\partial H}{\partial P}\right)_T = \frac{-RT^2}{P}\left(\frac{\partial Z}{\partial T}\right)_P$$

Step E Change in enthalpy upon vaporization of pure volatile component at constant temperature.

Step F Change in partial enthalpy of liquid n-propane upon mixing at constant temperature and pressure. This is the final step of the thermodynamic cycle. As the sum of the thermodynamic changes around a cycle must equal zero, the partial enthalpy upon mixing may be obtained from

$$(\Delta\bar{H}_k)_F = (\Delta\bar{H}_k)_A + (\Delta\bar{H}_k)_B + (\Delta\bar{H}_k)_C + (\Delta\bar{H}_k)_D + (\Delta\bar{H}_k)_E \qquad \text{(I-17)}$$

The calculated results depend, substantially, on the three relatively large quantities $(\Delta\bar{H}_k)_B$, $(\Delta\bar{H}_k)_D$, and $(\Delta\bar{H}_k)_E$.

For a binary system, after integration, Equation (I-16) becomes

$$\bar{H}_2 - H_2^{\circ} = -\int_{x_1=0}^{x_1} \frac{x_1}{x_2}\, d\bar{H}_1 \qquad \text{(I-18)}$$

Equations (I-17 and I-18) give results which when combined in Equation (I-15) yield the heat-of-mixing.

The features of this method for determining the heat-of-mixing for a solution may be summarized as follows

Advantages: (1) Provides method for determining H^M at high pressures. Previous experimental results have been restricted generally, to systems where both components are liquids at atmospheric pressure.

(2) Provides a method for determining H over a range of

temperatures when sufficient vaporization data are available. Heat-of-solution data in the past have normally been taken at or near room temperature.

(3) The results are obtained as a side result of experimental measurements for the partial enthalpy change upon vaporization on a binary system.

(4) Permits a comparison of experimental results for the partial enthalpy-of-vaporization to calculations for heats-of-mixing based on liquid state theories.

Disadvantages: Considering that each of the partial heat-of-vaporization measurements has an uncertainty of 0.4 Btu/#(m), this would result in an uncertainty for the H^M of about 25%. This does not compare favorably with the 2% or slightly greater error which has been estimated (21) for other experimental methods.

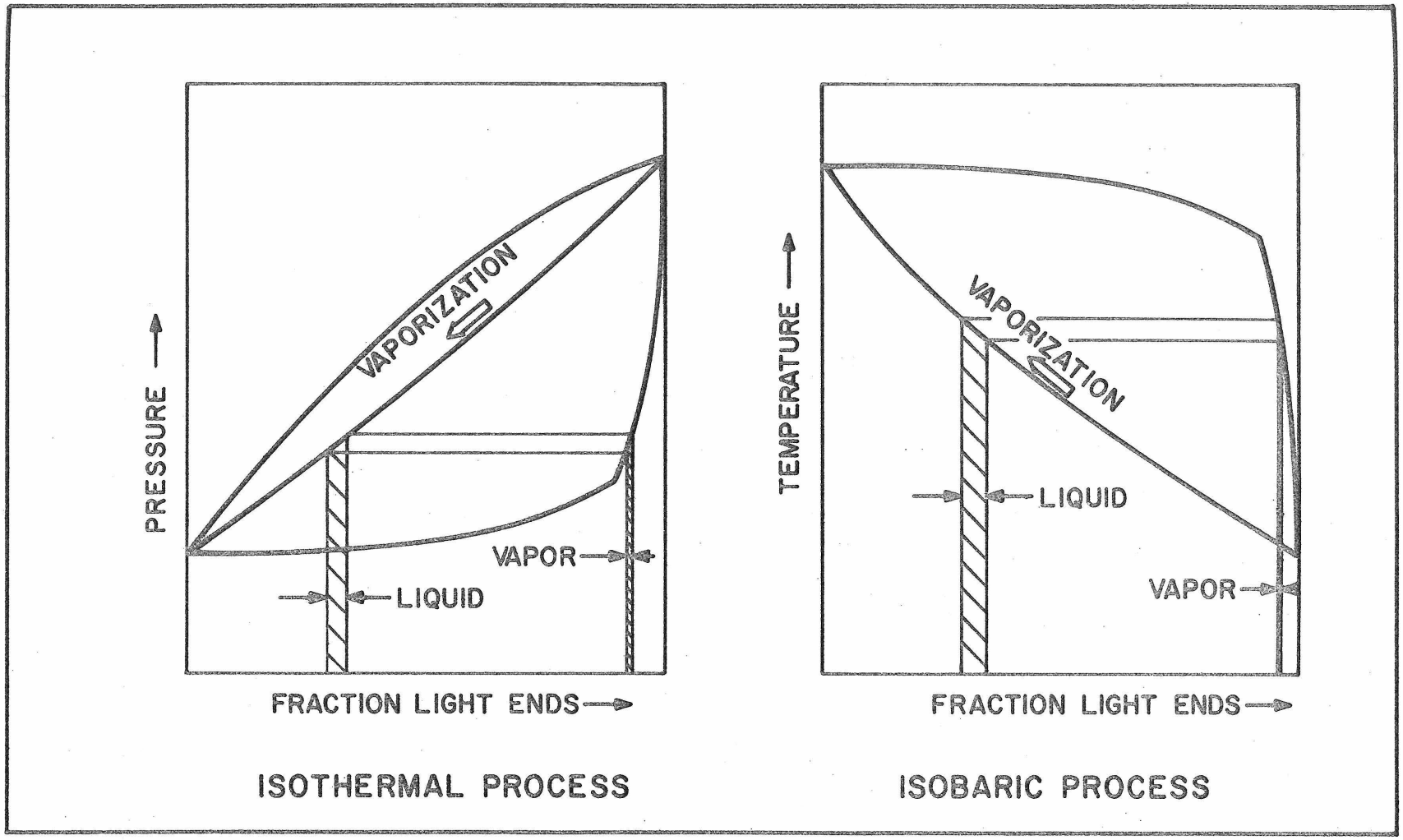

FIGURE I-1. PRESSURE, TEMPERATURE AND COMPOSITION CHANGES FOR VAPORIZATION PROCESSES IN MULTICOMPONENT SYSTEMS.

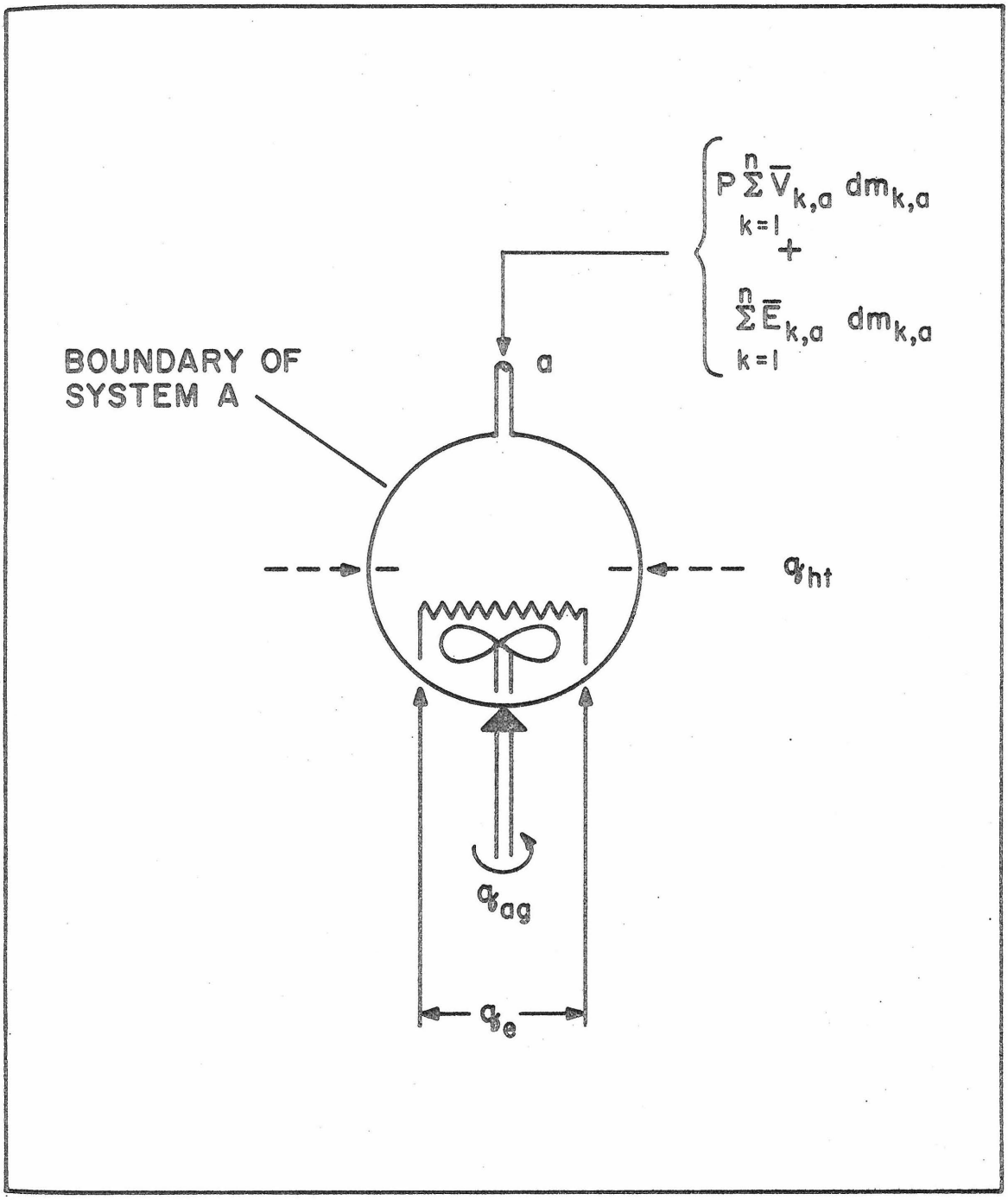

FIGURE I-2. INTERACTION OF THERMODYNAMIC SYSTEM WITH SURROUNDINGS.

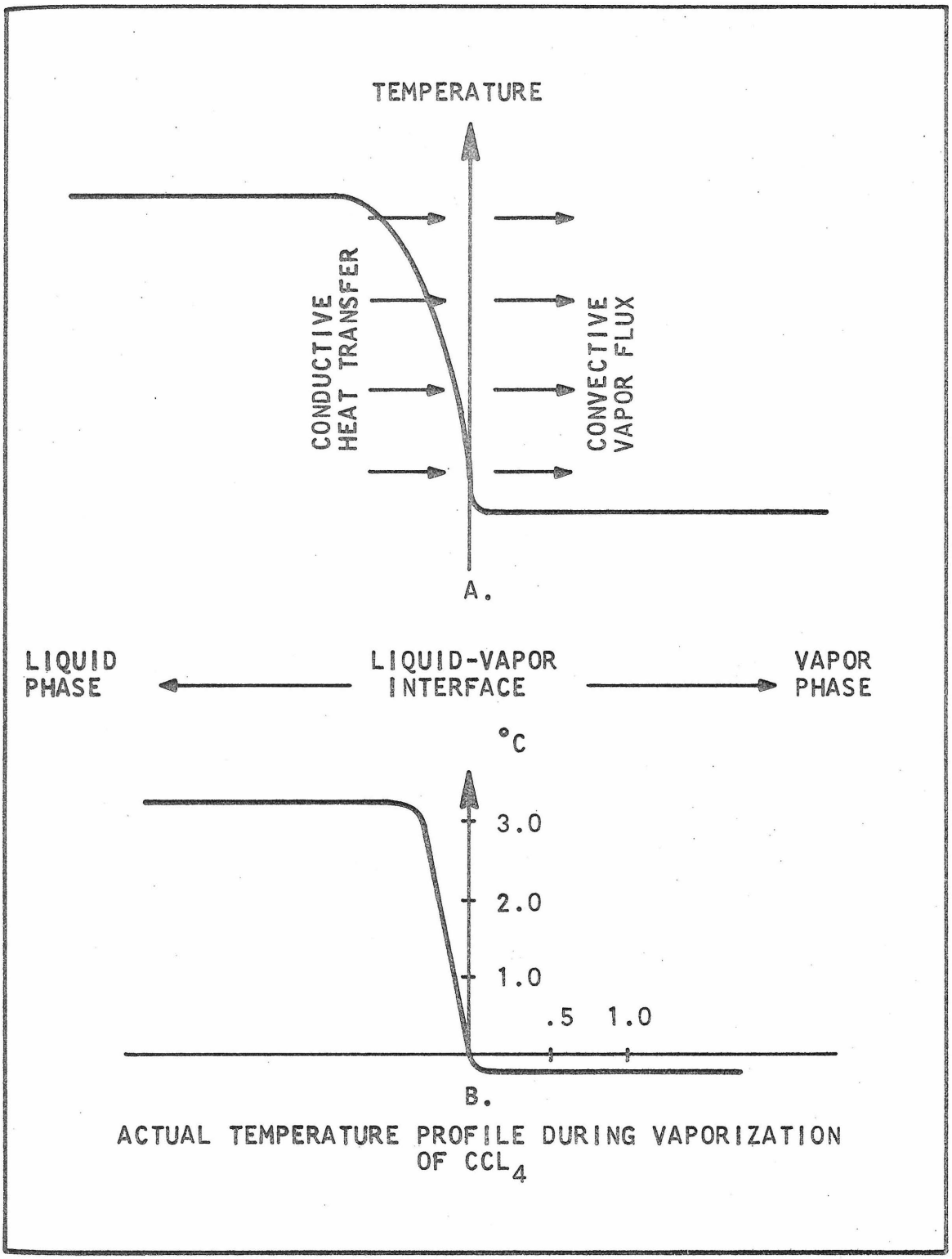

ACTUAL TEMPERATURE PROFILE DURING VAPORIZATION OF CCL_4

FIGURE I-3. SCHEMATIC REPRESENTATION (A) AND EXPERIMENTALLY MEASURED (B) TEMPERATURE PROFILE THROUGH VAPOR-LIQUID INTERFACE DURING VAPORIZATION.

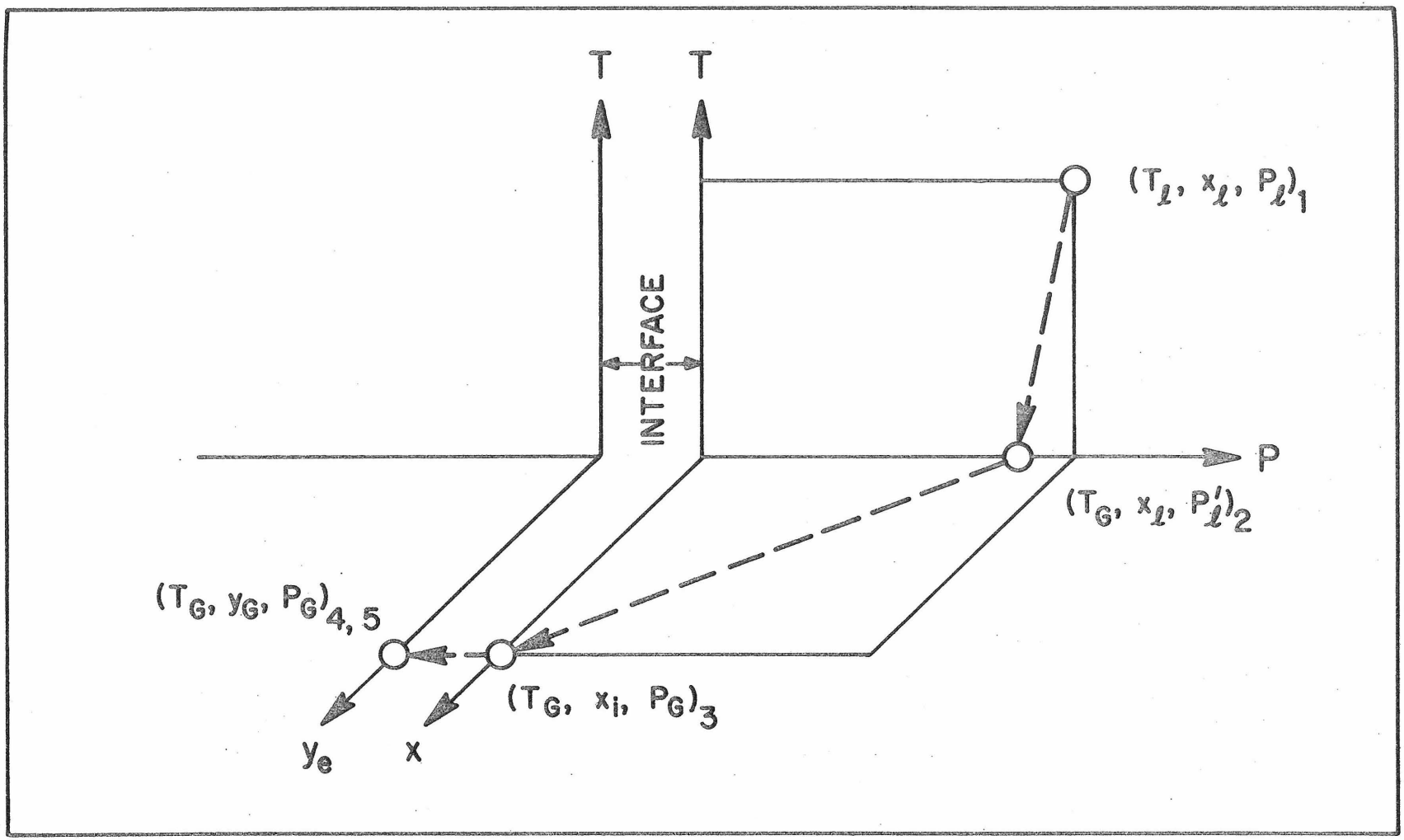

FIGURE I-4. THERMODYNAMIC STATES THROUGH WHICH MATERIAL PASSES UPON VAPORIZATION.

APPENDIX II

EXPERIMENTAL EQUIPMENT

A scale drawing of the calorimeter is presented in Figure II-1, and various other items of equipment associated with the calorimeter were shown in Figure 1. A detailed description of much of this equipment and of the instrumentation used has been presented previously (see Section II and Reference 5, 7 and 22). Therefore, only those changes which were made in conjunction with objectives of the current investigation are discussed below. These changes were motivated both by the necessity of converting the experiment from a two-man to a one-man operation and by the desirability of improving the precision and accuracy of the experimental results.

Related to the latter objective was: (1) an improved method of determining the specific volume of the vapor phase (primarily dependent upon improved pressure measurements), (2) development of a means for evaluating the effect of concentration gradients which developed within the liquid phase on the calculated results, and (3) an increased precision in calorimeter temperature measurements which would permit improvement in the accuracy of the agitator calibration.

TEMPERATURE RECORDING INSTRUMENTS

Two platinum resistance thermometers were used in the experiment. The resistance of each was determined by measurements made with a Mueller resistance bridge used in conjunction with a null detector. One thermometer was immersed in the oil bath surrounding the calorimeter and was used to determine the absolute temperature of the experiment. The null detector was a high sensitivity galvanometer. The second thermo-

meter was mounted in a helium-filled thermometer well within the calorimeter. The output of the Mueller bridge connected to this thermometer was fed through an amplifier to either a null indicating ammeter or a strip chart recorder. When the null indicating ammeter was used it was possible to obtain a precision of ± 0.0005 °F in the temperature measurement. This was two to three times better than when the galvanometer had been employed. When a reading was not being taken using the ammeter the output from the amplifier was fed to a strip chart recorder so that a continuous record of the calorimeter temperature-time history could be obtained.

The measurements recorded on the strip chart had a precision of approximately ± 0.002 °F. Much of this error was due to hysteresis in the recorder, and is approximately of the same magnitude as for measurements using the galvanometer null detector. With the recorded output, however, the temperature history and the rate-of-change of the calorimeter temperature were immediately apparent during an experimental test and corrective action for maintaining the calorimeter at a constant temperature could be taken.

PRESSURE RECORDING INSTRUMENTS

The choice of an instrument by which the calorimeter pressure could be measured was made somewhat difficult by the fact that several factors had to be considered. These difficulties were mentioned previously in Section II but are repeated here for convenience. They are:

(1) an accuracy of 0.5 psia over a pressure range of 3-300 psia,

(2) a precision of 0.05 psi over the time span of an

experimental test (∿ 45 minutes),

(3) a sufficiently rapid instrument response time so that the dynamic pressure changes in the calorimeter would not create a significant error in the reported measurements,

(4) an instrument with which individual measurements could be made in a relatively short period of time so as not to interfere with other experimental measurements which were also required.

These requirements, individually, are not all easily satisfied with standard laboratory pressure measuring instrumentation. Therefore, the chance of obtaining an instrument which would meet all of these criteria simultaneously did not appear good. Three experimental set-ups were evaluated before the final pressure measuring instrument and experimental configuration was determined. The two initial configurations employed a bench-scale, dead-weight tester as the pressure measuring instrument.

Pressure Cell. The dead-weight tester was used in conjunction with a pressure cell containing a flexible steel diaphragm (8). Fluid from the calorimeter entered the lower portion of the cell and a mercury column was supported above the horizontal diaphragm. Deflection of the diaphragm up or down caused the mercury to rise and fall in a capillary tube either closing or opening an electrical contact switch. The amount of mercury above the diaphragm was adjusted so that the on-off point of the switch was removed from the neutral position. When used previously, errors attributable to the diaphragm were reported to

to be of the order ±1.0 psi. The diaphragm cell was evaluated in connection with the present investigation, however, with the thought that a large portion of this error could be eliminated. Tests showed that the reproducibility was even worse than expected as a hysteresis of 2-3 psia was observed.

In the construction of the pressure cell provision had been made against overpressures in only one direction, and the diaphragm had apparently become strained beyond its elastic limit in the unprotected direction. When this occured a considerable amount of sensitivity was apparently lost. A physical inspection of the diaphragm revealed several small ripples which confirmed the suggestion that non-elastic deformation had taken place.

As the diaphragm, itself, was an integral part of the larger main body of the pressure cell, its replacement meant that this entire section would have to be refabricated. It was decided, instead, to attempt repairing the diaphragm and determine if it could be made functional. The surfaces were remachined and polished, but the major portion of a regular ripple remained. A retest of the pressure diaphragm showed little, if any, improvement in its operation, and it was decided that another method of measuring the calorimeter pressure would have to be used.

Mercury Trap. In spite of the hazard of possibly exposing the interior of the calorimeter (parts of which were gold plated) to mercury, the diaphragm cell was replaced with a mercury trap. In this case the balance point was again located by means of an electrical circuit which was actuated by the rise and fall of the mercury column

within the trap. The trap was also used in conjunction with the dead-weight tester.

With this configuration pressure having an accuracy of 0.2 psia and a precision of about 0.05 psi were obtainable. If the pressure was steady an individual measurement could be made in 1 to 2 minutes. However, for a dynamic pressure, that which occurs during an experimental test, accurate measurements were almost impossible to make. The test pressure changed significantly during the period of measurement so that even if the balance point was found in one direction, the system pressure changed before the necessary balance check in the opposite direction could be made. Therefore, this configuration was adequate for determining the thermodynamic conditions which existed within the calorimeter before a test began and after it ended. But it did not provide a satisfactory means of defining the transient thermodynamic states which existed during an experimental test.

Texas Instrument Gage. The third pressure measuring device evaluated was a commercially available Texas Instrument Precision Pressure Gage (TI Gage) which employed a fused quartz spiral bourdon tube as a pressure-sensitive element. This gauge satisfied all of the criteria discussed above. Absolute pressures were measurable to within $\pm$ 0.1 psi over a range of 0-500 psia with a precision better than $\pm$ 0.05 psia. The gauge had a natural frequency (50 cps) which was considerably greater than that required for the calorimeter pressure measurememements. An individual measurement could be made in 15 to 20

seconds. A more detailed description of the gauge, along with the calibration results, is given in Appendix 3.

Pressure Connections. The TI Gage was connected to the fluid pressure lines coming from the calorimeter as shown in Figure II-2. The bench-scale dead-weight tester used in conjunction with the Hg Trap was also connected to the pressure system to serve as a back-up in the event that problems should develop with the TI Gage. This contingency never developed, however, and the TI Gage was used for all experimental pressure measurements.

Almost all of the pressure lines up to valve A were 1/4 inch copper tubing. The exceptions were several short sections where it was more convenient to use steel tubing to accommodate existing fittings. All tubing on the calorimeter side of valve A was steel. The fluid on the calorimeter side of valve A was, of course, a mixture of n-decane and n-propane. Pure n-decane was used as the pressure transmitting fluid within the pressure measuring system and was interfaced with the calorimeter system through a four-inch length of small diameter (1/16"I.D.) steel tubing. It was not possible to completely eliminate the interchange of material between these two systems, however the presence of this length of small diameter tubing served to reduce mixing of the pure n-decane with the mixture by diffusion.

A great deal of care was taken in loading the pressure transmitting fluid, n-decane, into the pressure measuring system. This was to eliminate the possibility of air bubbles forming in the pressure line. If bubbles had appeared the effect of surface tension at a vapor liquid interface could not only lead to inaccurate static

pressure measurements, but could also introduce an undesirable sluggishness in the pressure measuring system. The latter would have resulted from the transient effect of a component being absorbed or desorbed from solution, and the effect would lead to a decrease in the effective time response of the pressure measuring system.

A series of valves were placed between the calorimeter and the pressure gauge. When the gauge was not being operated all of these valves were kept closed to ensure that no leaks from the calorimeter system occurred through these lines. The gauge itself was released to atmospheric pressure through a vent. The condition of the transmitting fluid was usually apparent from observations which were made at both the start and end of an experimental test. When starting a test, and the valve connecting the pressure gauge to the calorimeter was cracked, the pressure imposed on the gauge went from atmospheric to calorimeter pressure (as much as 300 psia) almost immediately. This rapid response would not have been expected if a vapor-liquid mixture had been in the pressure transmitting line rather than a pure liquid. It also made it necessary to take special care in bringing the gauge to operating pressure so as to minimize the chance of shattering the fused quartz bourdon tube with a pressure surge.

At the end of a test the gauge was released to atmospheric pressure after first isolating it from the calorimeter. Placed on the atmospheric vent was a piece of transparent tubing aligned vertically, which was partially filled with n-decane. Any bubbles which existed within the pressure line at a high pressure would have expanded when released to atmospheric pressure and caused a displacement of

liquid in the transparent tubing. If this happened (it did once) the pressure line was reloaded with a fresh quantity of n-decane.

SUMMARY OF EXPERIMENTAL MEASUREMENTS

A summary of the measurements made in conjunction with the operation of the calorimeter is shown in Figure II-3. A total of 11 differential thermocouples were monitored by measurements made with a White Potentiometer. Nine of these were to aid in determining the temperature of the vapor path between the calorimeter and the sample block and were connected to a rotary switch leading to one side of the White Potentiometer. Two more differential thermocouples (top and bottom) DTT and DTB were used to help define the temperature difference between the vacuum jacket and the oil bath and these were connected to the second side of the White Potentiometer. A third differential thermocouple (center) DTC was connected directly to a galanometer, and was used as a basis for determining the zero temperature difference between the vacuum jacket and the calorimeter (see Appendix IV). The latter measurement was, essentially, a null measurement and quantitative data were not taken. For this purpose the direct connection of the thermocouple to a galvanometer was the most sensitive means of detection available.

Measurements of the quantity of thermal energy added by the resistance heater were made with a Minneapolis-Honeywell Rubicon Potentiometer. A thyratron control unit was used to maintain the oil bath at a constant temperature ($\pm$ 0.005 ^{o}F). The calorimeter pressure and temperature measurements were discussed above.

CALORIMETER VOLUME

The volume of the calorimeter was measured and reported

previously (22). Methane was used as the calibration fluid and reported results showed the calorimeter to have a total internal volume of 1192 cc. Some changes of the internal construction of the calorimeter had been made since that original calibration, however, and it was decided to repeat it. N-propane, for which extensive compressibility values were available (10), was chosen as the calibration fluid. As n-propane condenses at a relatively low pressure at room temperature, it was easier to handle than methane and it was possible to obtain a smaller relative error in determining the sample weight than was the case for methane. The results of the calibration are shown in Table II-1.

TABLE II-1

RESULTS OF EXPERIMENTAL DETERMINATION

OF CALORIMETER VOLUME

Test	Temp. (^{o}F)	Press. (psia)	Z	Sample Wt. (gm)	V (cc)
1	99.50	47.22	0.9548	7.307	1255.32
2	101.71	54.36	0.9481	8.443	1256.05

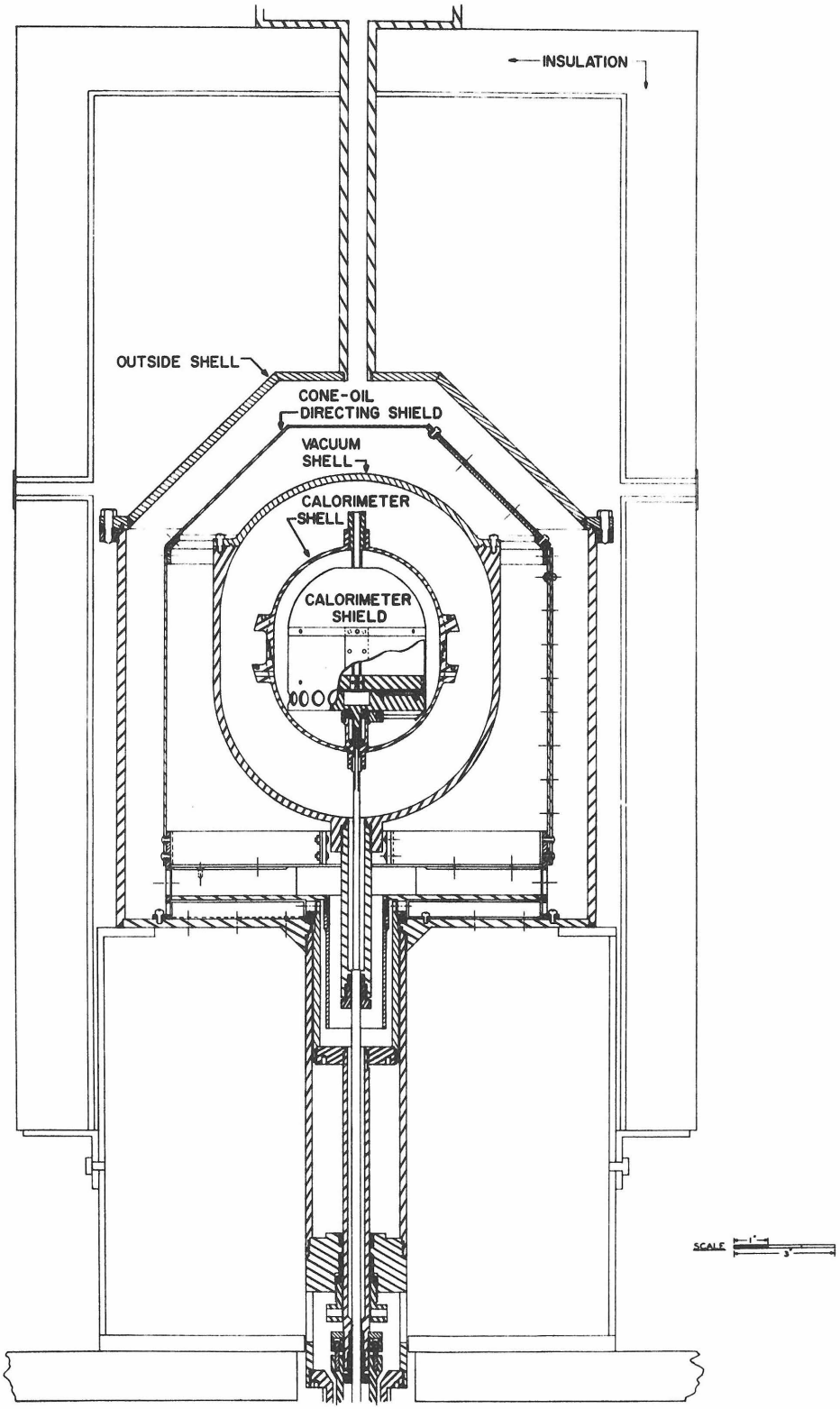

FIGURE II-1. SCALE DRAWING OF CALORIMETER.

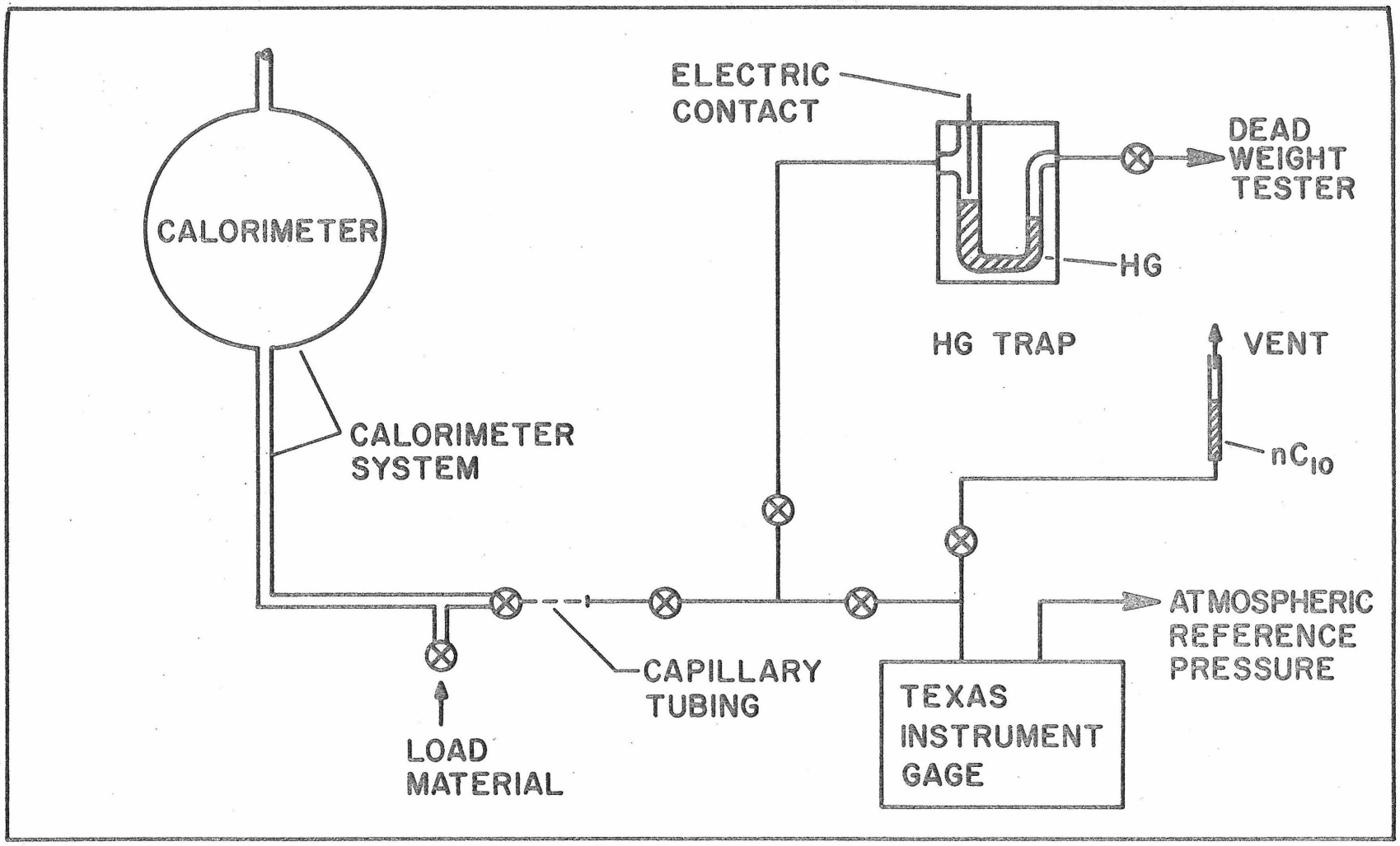

FIGURE II-2. PRESSURE MEASURING SYSTEM.

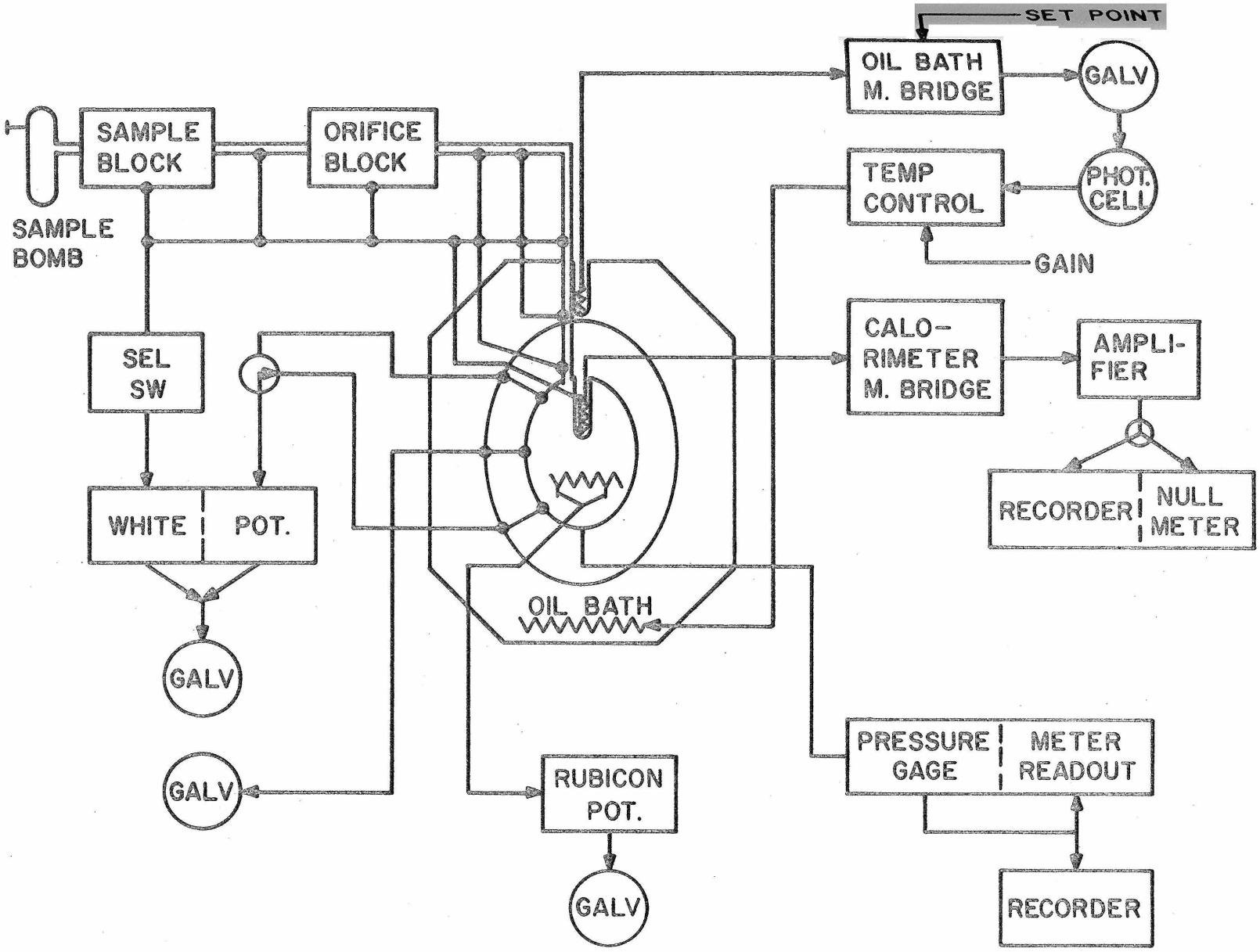

FIGURE II-3. SCHEMATIC SUMMARY OF EXPERIMENTAL MEASUREMENTS

APPENDIX III

CALIBRATION OF PRESSURE GAUGE

DESCRIPTION OF PRESSURE GAUGE

Calorimeter absolute pressures and pressure changes were determined from measurements made with a Texas Instruments Model 141 Precision Pressure Gage. The pressure sensitive element of this gauge was a fused quartz spiral tube mounted within a sealable capsule. The capsules were interchangeable, and when in use were held in a separately packaged read-out unit. Application of pressure to either of two pressure fittings on the capsule caused the bourdon tube to rotate, deflecting a light beam which was directed onto a mirror attached to the free end of the bourdon tube (see Figure III-1). The amount of deflection, measured by an optical transducer which traveled concentrically around the bourdon tube, was indicated by a set of counting wheels geared to the movement of the transducer. The magnitude of an applied pressure was found by multiplying the deflection of the bourdon tube by a scale factor determined from calibration.

The utility of the gauge depends upon two central ideas: (a) the extremely low internal viscosity of fused quartz and (b) the optical coupling between the capsule and the read-out unit. Fused quartz is an extremely elastic, although brittle material, and hysteresis effects due to material stress are reduced to a minimum. Manufacturer's literature describing the quartz elements used in the gauge states that hysteresis effects are negligible, and this statement is supported by the calibration results presented below. The optical coupling between the bourdon tube and the read-out unit made it possible to isolate the bourdon

element from any mechanical linkage and eliminated the problem of a frictional constraint.

Several other factors affect the accuracy of the gauge. The calibration curve for the gauge is highly non-linear. Therefore to obtain accuracy over an extended range in pressure a large number of calibration points must be available. When this is the case interpolation (linear or non-linear) for the intermediate pressures is possible.

Pressures can be measured as either absolute or gauge, depending upon the mechanical connections made at the capsule. Two fittings are available, one for the interior of the bourdon tube and one for the interior of the capsule which contains the bourdon tube. Either side of the bourdon tube may be used as the reference pressure, the choice being for practical considerations. If the reference pressure is chosen as atmospheric (one port open to the atmosphere) the measured output is in gauge (psi) pressure. For accurate absolute measurements, however, it is preferable to use a vacuum for reference as barometric pressure variations are then eliminated.

The resonant frequency of the bourdon tube (per manufacturer) is 50 cps. As the pressure-time profile for an experimental test was continually decreasing the time response of the pressure measuring instrument was of some concern (see Section II). However, as the maximum rate of pressure change in any test was less than 0.01 psi/sec., the time response of the Texas Instrument Pressure Gage exceeded the requirements of this experiment.

The gauge may be operated in any three modes: external, manual, or servo. In servo mode the deflection of the reflected light

beam was followed automatically. The instrument was switched to manual mode for a precision balancing of the null meter. The external mode was not used in these experiments as it proved to be inconvenient in measuring small pressure changes accurately over the relatively wide pressure range observed in individual tests.

CALIBRATION PROCEDURES AND RESULTS

The primary pressure standard for calibration of the Texas Instrument Gage was a Hart Pressure Balance which operated on the principle of a dead-weight tester. The Hart Balance has a reported accuracy of better than 1:10,000, and a reproducibility of 1:20,000 over a range of 3-3,000 atmospheres. To cover this entire range of pressures a total of eight differential pistons is available. For the range of pressures measured in this experiment, however, only two of these pistons were required; one for the range 39-290 psig, and the second for the range of pressures greater than 239 psig. The overlap in the range of these two pistons provided an opportunity to check the reproducibility of the Hart Balance against itself. For pressures lower than 39 psig a smaller (and less accurate) pressure standard was used to verify extrapolations of the calibration results from the Hart balance to zero absolute pressure. These latter results are not included in the table below.

The experimental setup for calibration is shown in Figure III-2. The output of the Hart Balance was coupled to that of the Texas Instrument Pressure Gage through an open oil/nitrogen interface which was maintained at a constant elevation throughout the calibration. For convenience, atmospheric pressure was chosen as the reference pressure. Therefore, zero pressure difference occurred when both sides of the bour-

don tube were open to the atmosphere. The scale reading for zero pressure difference was adjusted to 12.000 prior to calibration of the gauge and also prior to each subsequent use. This procedure prevented errors from any irregularity in the gear train from being injected into the pressure measurement.

Calibration points were taken for both increasing and decreasing pressure increments for the pressure range 39-417 psig. The results are presented as a tube constant $K(\Delta R) = \Delta P/\Delta R$, where ΔP is the pressure difference between the applied pressure and the reference pressure and ΔR is the change in scale reading on the pressure gauge from the initial value of 12.000. The calibration results are shown in Table III-1. Also shown are the applied pressure difference, ΔP, the change in meter reading, ΔR, an indication showing if the calibration point was taken for an increasing or decreasing pressure step and a column showing which differential piston was used.

A good indication of the precision of the calibration is obtained if experimental tests (86,90) and (104,111) are compared. Included in these four tests are data for increasing and decreasing pressure steps for both of the differential pistons that were used. The results ($K(\Delta R)$) for each individual piston are reproducible within one part in 20,000. Although the scale readings for these four calibration points are nearly identical (21.1 and 21.2) the difference is enough to cause a significant change in the calibration constant. The calibration curve changes rapidly at that point and the results for the higher deflection (21.2) should have been 0.003 higher, as determined from a fit of all the data (see below). As the difference actually was only 0.0005

the reproducibility of two different pistons becomes 1:5000, compared to the reported accuracy of the Hart Balance of 1:10,000. It should be emphasized that this comparison of the two Hart Balance pistons is based on only one data point. Although the reproducibility of the results for each piston is extremely good it is believed that several data points would be required over the pressure range of mutual applicability in order to check with any certainty the accuracy of the Hart Pressure Balance.

A comparison of other data points having equal loads shows that for all of the points taken where the applied pressure was greater than 100 psig the reproducibility was always better than 1:10,000 and usually within 1:20,000. Discrepancies of this magnitude could very well be associated with the limitations of the read-out device in the Texas Instrument Gage. Only five significant figures could be read directly (four at low pressure differentials) and the sixth could be estimated with a precision of five.

With the exception of the low pressure points the results of the calibration demonstrate the extremely high precision with which pressure changes can be measured with both the Hart Pressure Balance and the Texas Instrument Pressure Gage. The lack of agreement of the data points for the two differential pistons where the pressure ranges overlap are inconclusive.

The data presented in Table III-1 are plotted in Figure III-3. The non-linearity of the calibration constant is evident. For ease of calculation of the pressure from gauge readings the data were represented by a series of line segments; four straight lines and three quadratic

curves. The data were easily represented in this manner, and with better accuracy than could have been achieved with a polynomial fit. The line representations and the ranges for which they apply are indicated in the figure. To calculate an absolute pressure from these calibration curve segments the tube constant, $K(\Delta R)$, was determined, first, as a function of scale readings. Then

$$P_{abs} = \Delta R \times K(\Delta R) + P_{atm} + \begin{matrix}\text{head} \\ \text{correction}\end{matrix}$$

COMPARISON WITH STAINLESS STEEL BOURDON TUBE

The calibration data shown in Figure III-3 can also be plotted as a deviation (Δ) from a calculated reference pressure. If the reference pressure (ΔP_{ref}) is taken as a linear function of the scale reading

$$\Delta P = \Delta P_{ref} + \Delta = 11.522\ (\Delta R) + \Delta$$

Δ is plotted versus scale reading (ΔR) in Figure III-4.

A similar result is available from calibration data obtained when a stainless steel element was used in place of the fused quartz bourdon tube (23). Two curves result in the latter case; one for increasing pressure steps, the other for decreasing pressures. A hysteresis effect completely lacking for the fused quartz bourdon tube is evident in these measurements. However the calibration results are more nearly linear.

TABLE III-1
CALIBRATION CONSTANTS OF TEXAS INSTRUMENTS PRESSURE GAGE

TEST NO.	RANGE OF DIFFERENTIAL PISTON (psig)	DIRECTION OF PRESSURE CHANGE	ΔP (psig)	ΔR	K (ΔR)
-	-	-	0.000	0.000	-
79	39-290	Increase	39.4009	3.5005	11.2432
80	"	"	67.8798	6.0120	11.2781
81	"	"	96.3513	8.515	11.3029
82	"	"	124.8222	10.9995	11.3348
83	"	"	153.2956	13.4945	11.3472
84	"	"	181.7689	16.063	11.3034
85	"	"	210.2440	18.641	11.2660
86	"	"	238.7203	21.111	11.2452
87	"	"	267.1929	23.402	11.4048
88	"	"	289.9648	25.2175	11.4857
89	"	Decrease	267.1929	23.404	11.4038
90	"	"	238.7203	21.112	11.2947
91	"	"	233.0163	20.659	11.2666
92	"	"	221.6330	19.655	11.2636
93	"	"	210.2444	18.6405	11.2663
94	"	"	181.7689	16.062	11.3041
95	"	"	153.2956	13.4955	11.3464
96	"	Increase	158.9881	14.016	11.3307
97	"	Decrease	147.5941	12.9935	11.3464
98	"	"	124.8222	11.0005	11.3343
99	"	"	96.3513	8.516	11.3015
100	"	"	67.8798	6.015	11.2725
101	"	"	62.1728	5.513	11.2649
102	"	"	50.7895	4.513	11.2415
103	"	"	39.4009	3.502	11.2384
104	> 239	Increase	239.8379	21.209	11.2957
105	"	"	275.2859	24.061	11.4248

TABLE III-1 (Continued)
CALIBRATION CONSTANTS OF TEXAS INSTRUMENTS PRESSURE GAGE

TEST NO.	RANGE OF DIFFERENTIAL PISTON (psig)	DIRECTION OF PRESSURE CHANGE	ΔP (psig)	ΔR	K (ΔR)
106	> 239	Increase	310.7504	26.878	11.5486
107	"	"	346.2044	29.906	11.5635
108	"	"	417.1811	36.256	11.4937
109	"	Decrease	346.2044	29.9065	11.5633
110	"	"	310.7504	26.879	11.5482
111	"	"	239.8379	21.210	11.2952

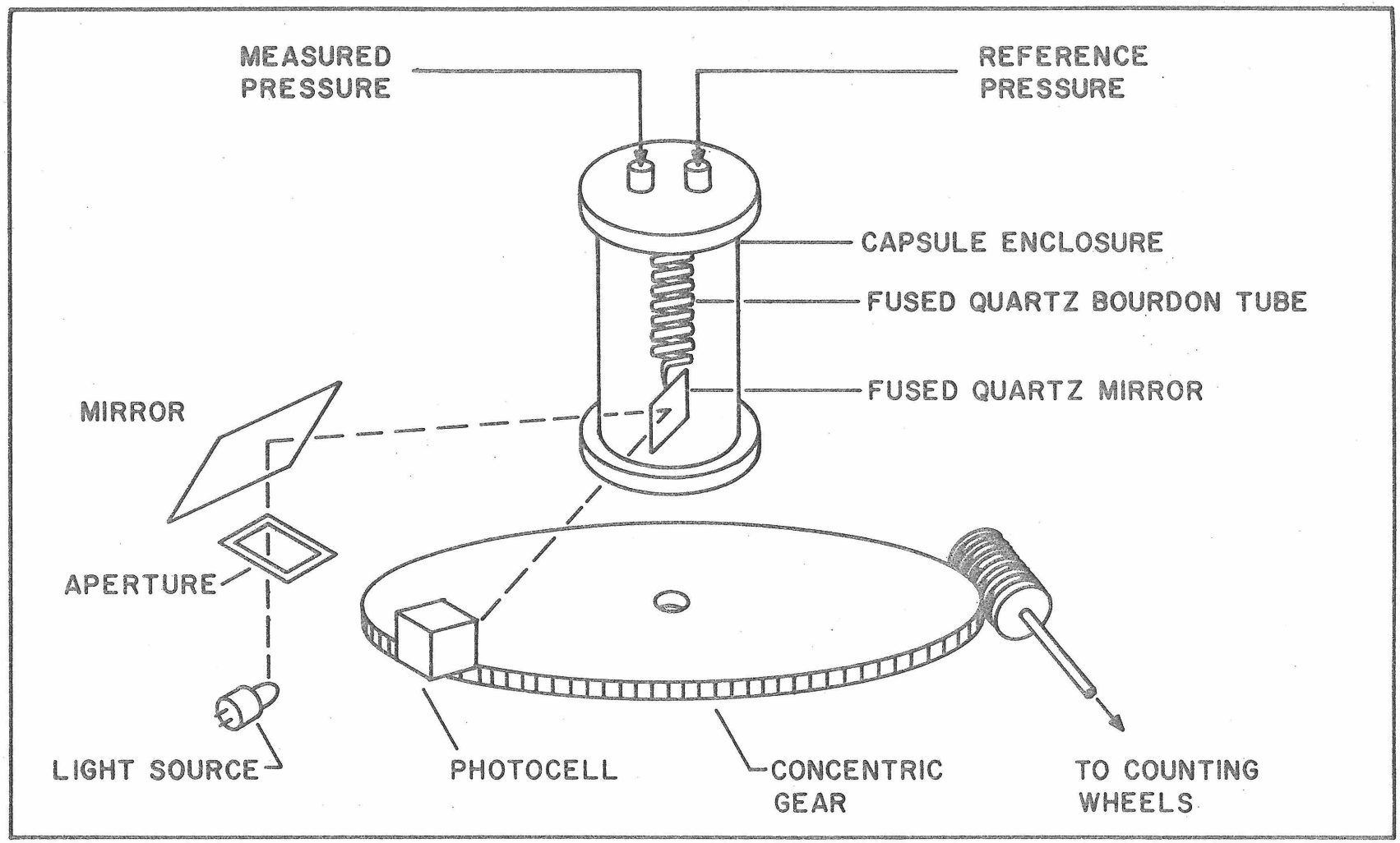

FIGURE III-1. SCHEMATIC DIAGRAM OF TEXAS INSTRUMENT PRESSURE GAGE, MODEL 141

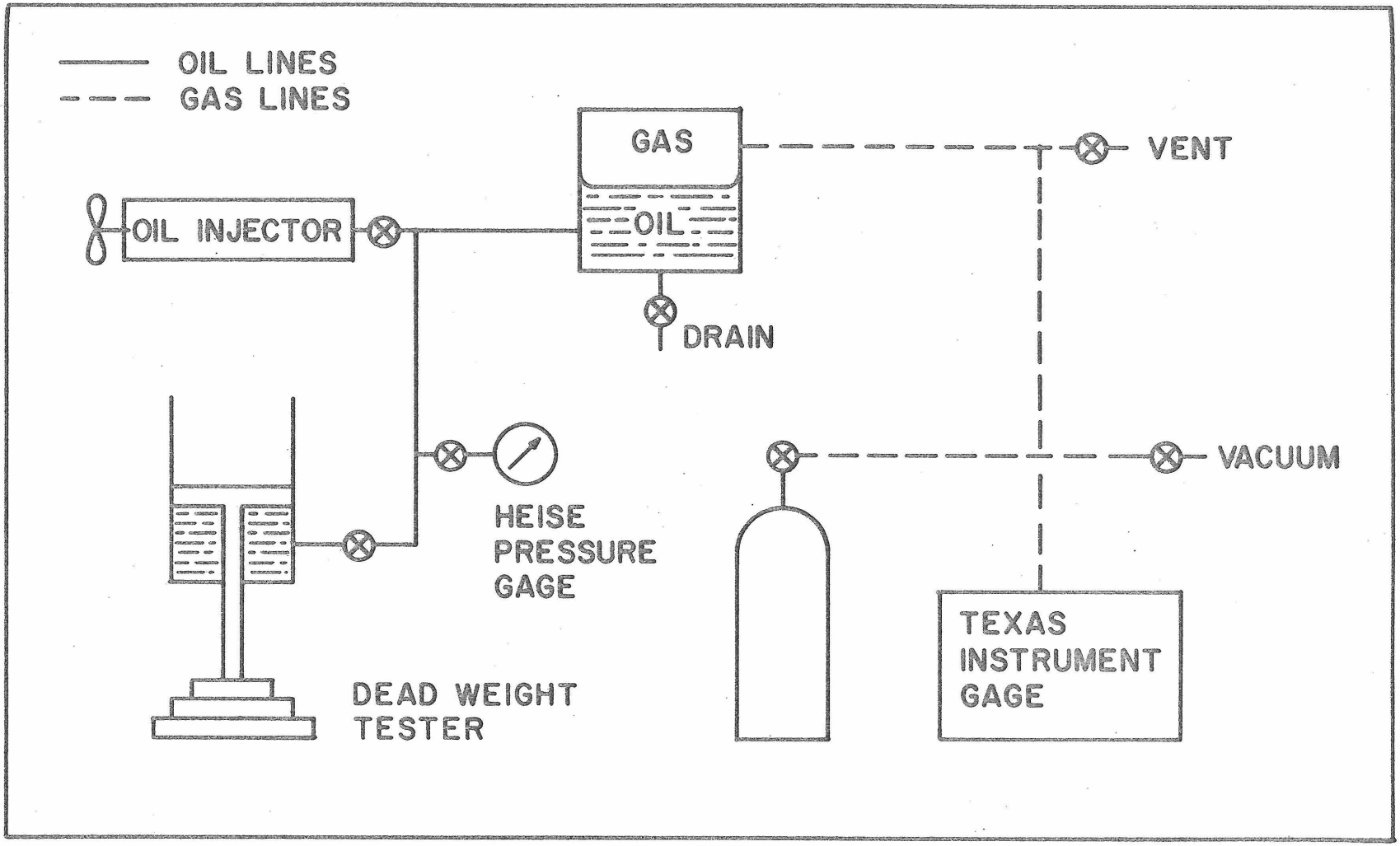

FIGURE III-2. APPARATUS FOR CALIBRATION OF PRESSURE GAGE.

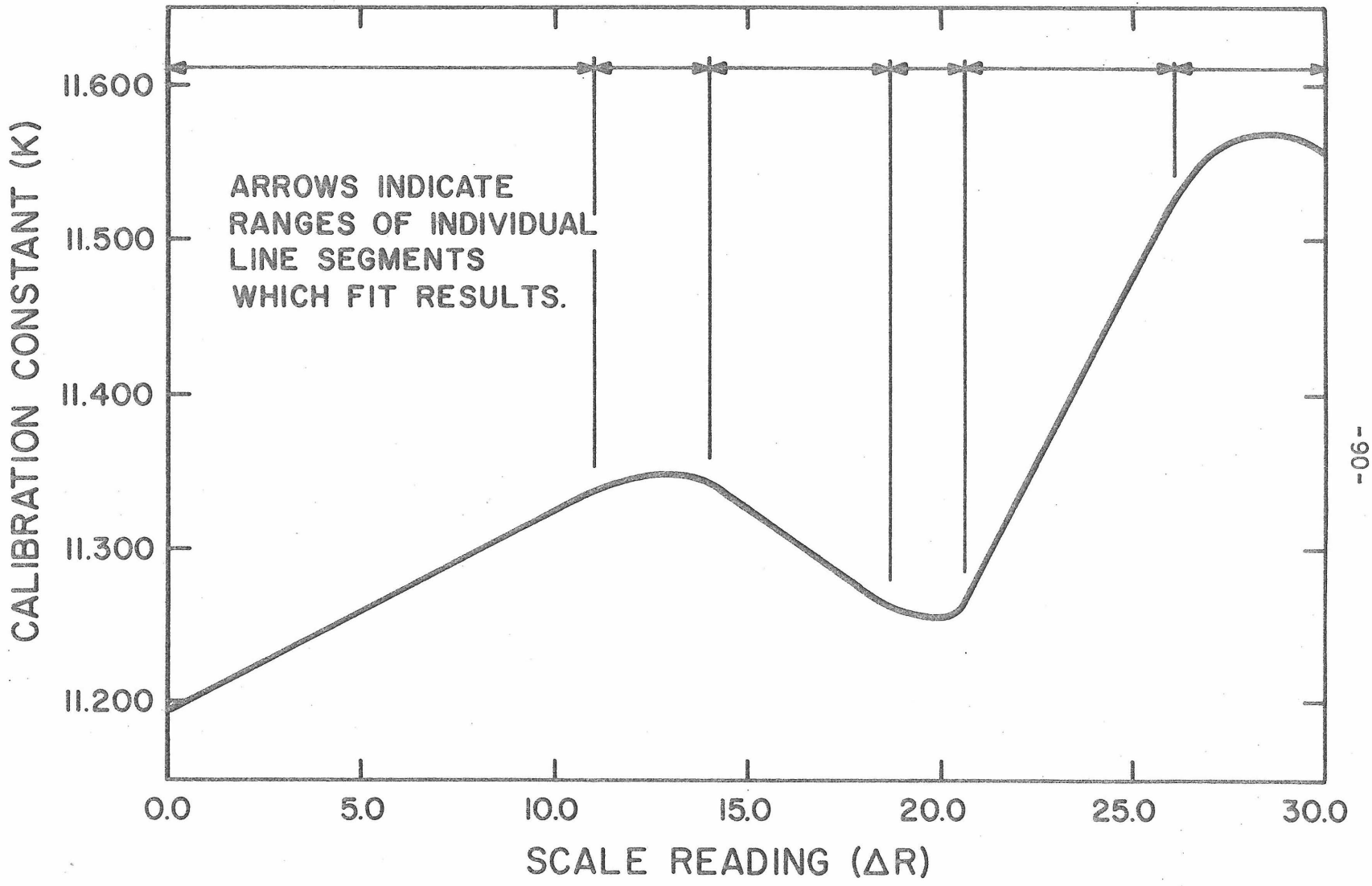

FIGURE III-3. RESULTS OF CALIBRATION FOR TEXAS INSTRUMENT GAGE.

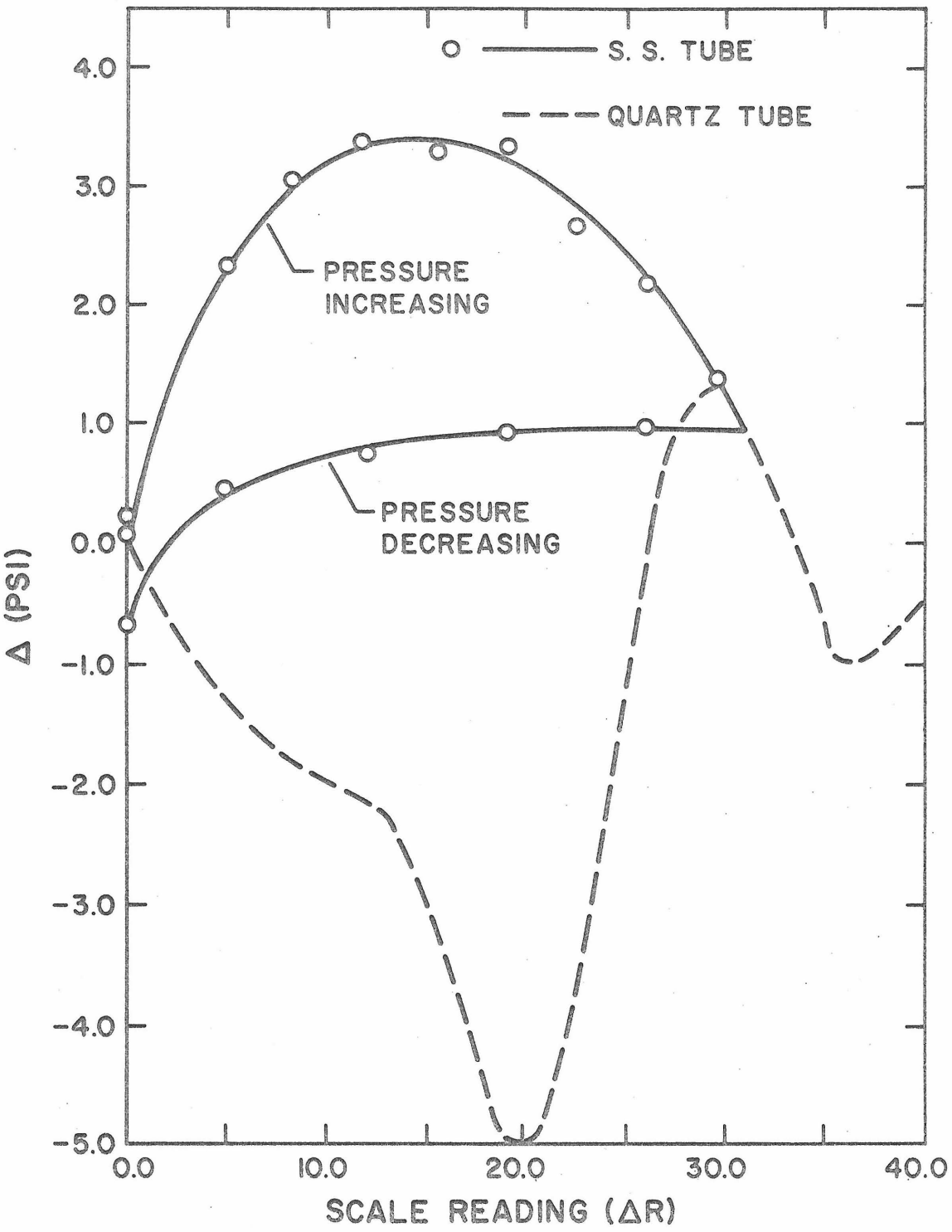

FIGURE III-4. COMPARISON OF CALIBRATION RESULTS FOR QUARTZ AND STAINLESS STEEL HELICAL COILS.

APPENDIX IV

CALORIMETER TEMPERATURE MEASUREMENTS

This appendix is included for several reasons. They are:

(1) To evaluate the uncertainty of the reported absolute temperature at which vaporization takes place.

(2) To establish a base for making heat transfer and agitator energy calibrations.

(3) To evaluate the method used for estimating the subcooling of the vapor phase during vaporization.

(4) To investigate the temperature dynamics of the calorimeter.

Concern for the first three of these goals is understandable. The importance of the latter objective may not be evident and is discussed in the paragraph below.

In the calculations to obtain the latent heat of vaporization from experimental data it was assumed that the temperature of the calorimeter was maintained constant throughout a test. In addition to the desirability of satisfying the process specification of an isothermal test this assumption also permitted neglecting the temperature change term of Equation (I-5). Actually, the temperature did not remain precisely constant during a test, but small variations occurred. However, if the response of the temperature sensing device to calorimeter temperature changes were sufficiently fast, and if temperature gradients existing within the calorimeter remained stationary during a test, it would have been possible to start and stop a test within the precision of the temperature measuring instrument being used.

In this case temperature changes of less than 0.001 ^{o}F were monitored with the platinum resistance thermometer mounted within the calorimeter thermometer well. Temperature measurements of this precision would have been sufficient to reduce the start-stop temperature error to a negligible amount. However, there was a finite delay time involved with the temperature sensing device, and the temperature gradients which developed within the calorimeter were subject to variations with respect to time. Therefore, a discussion is included to provide an estimate of the time response of the platinum resistance thermometer and also to point out the conditions under which temperature transients within the calorimeter may become the source of significant experimental error.

REPORTABLE TEMPERATURE OF VAPORIZATION

The absolute temperature at which each experimental test was conducted was determined from the resistance measurements of a platinum resistance thermometer immersed in the oil bath surrounding the vacuum jacket. Differential thermocouples were used to determine the temperature difference between the oil bath and the calorimeter itself. The reported temperature of vaporization, therefore, includes the inaccuracies associated with both the resistance thermometer and the differential thermocouple measurements. (The platinum resistance thermometer mounted within the thermometer well of the calorimeter was used only for determining temperature changes of the calorimeter once an experiment was underway). A scale drawing showing the location of the resistance thermometers and four differential thermocouples located within the calorimeter is shown in Figure IV-1.

From measurements of the platinum resistance thermometer, the absolute temperature of the oil bath was determined to within 0.01 ^{o}F. The uncertainty associated with the differential thermocouple temperature measurements was greater. With the calorimeter and oil bath in apparent thermal equilibrium a consistent discrepancy in the measurements of three of the differential thermocouples was observed. The apparent temperature profile of the calorimeter relative to the oil bath, as determined from thermocouple measurements, is shown in Figure IV-2. The center thermocouple (DTC) always indicated that the calorimeter was at a slightly higher temperature than did the top (DTT) and bottom (DTB) differential thermocouples. This uneven temperature profile of the calorimeter could have been attributed to several factors: (1) temperature gradients within the calorimeter wall, (2) temperature gradients within the vacuum jacket wall, (3) residual voltages in the thermocouple circuits which indicated temperature inequalities when in fact there were none.

The possibility that a temperature gradient existed within the wall of the calorimeter adjacent to the liquid phase may be eliminated almost immediately. There was no source of thermal energy within the calorimeter wall, and the presence of the circulating liquid phase, with its large thermal capacity, would make it highly improbable that a measurable temperature gradient could have been sustained. In the upper part of the calorimeter there was no similar effect as the vapor phase was relatively stagnant and had a small thermal capacity. Therefore, it was possible that temperature gradients existed within the upper part of the calorimeter adjacent to the vapor phase, and this could account for

the differences observed for readings from the upper and center differential thermocouples (this point is discussed further below under Static Conditions). It cannot, however, explain the differences between the lower two differential thermocouples as these were both attached to that portion of the calorimeter wall which was in contact with the liquid phase.

The possibility that unevenness in temperature distribution existed within the wall of the vacuum jacket is related to the fact that this surface was closer to the temperature variations of the environment. The circulating oil bath and an adiabatic jacket served to isolate the vacuum jacket from the surroundings. Although it does not seem likely that temperature gradients of the size reported could have existed in the wall of the vacuum jacket, there is no way of knowing this.

The remaining alternative is that the discrepancies in the reported readings were due to residual voltages either in the thermocouples themselves or in the thermocouple lead junctions. Some checks were made of the thermocouple lead junctions and small ($\sim$0.5 microvolts) residual voltages were observed. But even finding these did not remove the possibility that similar residual voltages may be present at inassessable thermocouple junctions on the walls of the calorimeter and vacuum jacket. An uncertainty in the temperature of the amount described here,however, did not seem to justify what would have been a major effort in disassembly and reassembly of equipment in attempting to locate and correct such errors; especially since the equipment was working satisfactorily otherwise. Therefore, it was decided to make an operational check of the equipment and approach the problem from a different

point of view. If the point of zero heat transfer between the calorimeter and the vacuum jacket could be determined, that point could also be used as a definition of zero temperature difference between the oil bath and the calorimeter.

ZERO HEAT TRANSFER

To make this check the oil bath was set on control at a convenient temperature. The calorimeter was then brought to a temperature which was ∿1.0 °F warmer than the oil bath and the agitator was turned off. (At small temperature differences the agitator represented the major source of thermal energy for the calorimeter, and if left running, the agitator, rather than heat transfer, would have controlled the rate-of-change of the calorimeter temperature). The temperature of the calorimeter was then monitored as a function of time with the calorimeter platinum resistance thermometer to determine the rate of temperature drift. If the point of zero drift could be determined this, ostensibly, would be the point of zero heat transfer and could also be used to define the point of zero temperature difference between the calorimeter and the oil bath.

At small temperature differences between the calorimeter and the vacuum jacket other factors became important, however. As noted above, the agitator could not be run during these tests because of the thermal energy that would have been generated. But it also became increasingly important to maintain the calorimeter at a uniform (well-mixed) temperature when temperature differences between the calorimeter and the vacuum jacket were small so that small average temperature changes of the calorimeter (0.001 °F) could be measured. These two require-

ments were in conflict. In order to maintain a well-mixed liquid phase within the calorimeter frequent activation of the agitator was required. But, initiating the agitator action resulted in an energy addition for which corrections could not be introduced.

As the temperature differences between the oil bath and the calorimeter became small the thermal capacity of the calorimeter and its contents became large relative to the rate of heat transfer between the vacuum jacket and the calorimeter, and relatively long periods of time were required before a measurable temperature drift could be detected. For this condition the stability of temperature control for the oil bath also became a factor.

These effects combined to make it impractical to determine the point of zero heat transfer to a precision of better than $\sim$0.05 ^{o}F. As the error involved in this measurement is of the same magnitude as the discrepancies indicated by the three differential thermocouples discussed above, determination of the zero point heat transfer, by this method, did not provide any measurable improvement in the determination of the absolute temperature of the calorimeter. It did help, however, to confirm the limits of accuracy which were attributed to the differential thermocouples.

A second approach for determining the point of zero heat transfer was tried also, but without success. This method involved comparing the drift-rate of the calorimeter temperature for the cases where (a) the calorimeter was warmer than the oil bath and (b) the calorimeter was colder than the oil bath. The temperature of the oil bath was maintained constant over the period of both tests which were conducted con-

secutively. If the experimental conditions could be determined such that the rate of decreasing temperature for case (a) was equal to the rate of increasing temperature for case (b), the midpoint between these two conditions could be taken as the point of zero heat transfer. For case (b), however, the temperature of the sample injection line leading from the base of the calorimeter became greater than that of the calorimeter (it passed through the warm oil bath surrounding the calorimeter), and apparently caused vapor bubbles to form in the sample loading tube which ascended into the calorimeter bomb. This action amounted to, essentially, the addition of a large pulse of thermal energy to the calorimeter which became evident as large unstable variations, of both the calorimeter temperature and pressure. Thus a thermodynamic system which had been assummed to be closed became open and the character of the test was violated.

In view of the lack of definitive information from either of the above tests it was decided to use the null point of the center differential thermocouple (DTC) to define a point of zero heat transfer.

CALORIMETER TEMPERATURE GRADIENTS

Static Conditions. The fact that temperature gradients, or apparent temperature gradients, developed within the calorimeter when the agitator was off was easily observed when, after a period of being off, the agitator was reactivated. Measurements from the calorimeter resistance thermometer showed that the temperature of the calorimeter fluctuated for a period of several seconds after which it again became stable.

The expression "apparent temperature gradient" was used above

to describe a further effect of agitation. By merely flicking the agitator on and off after the calorimeter and oil bath had been brought to a stable pseudo-equilibrium, the calorimeter resistance thermometer indicated temperature changes of 0.002-0.003 ^{o}F. (The time required for the calorimeter resistance thermometer to respond to these operational changes was $\sim$ 5 seconds, and this fact will be used below in discussin the dynamic temperature changes of the calorimeter). The fact that a small change in temperature did occur is indicative that there was a measurable temperature gradient within the calorimeter even under these ideal circumstances. If a small gradient existed in the thermometer well it would be understandable as the well extends from the vapor phase down into the liquid phase. (The possibility of thermal gradients in the calorimeter wall adjacent to the vapor phase was discussed above).

This apparent gradient could lead to a temperature differential between the liquid phase and the sensing element of the calorimeter resistance thermometer in the lower part of the thermometer well. In this case, heat would continually be flowing between the liquid phase and the thermometer. By turning the agitator on and off the flow field around the thermometer well and the liquid phase heat transfer coefficient would be changed. The rate of heat transfer between the liquid phase and the resistance thermometer would be changed and this affected the temperature of the platinum sensing element.

The results seem to indicate that a measurable temperature gradient probably did exist in the walls of the calorimeter adjacent to the vapor space, but they do not provide a means of calculating its magnitude. It must be concluded, then, that the variation in the calori-

meter temperature profile shown in Figure IV-2 is probably not all due to residual voltages present in the measuring circuits, but that these measurements may actually reflect a degree of thermal nonequilibrium which exists within the calorimeter even under the most ideal circumstances.

Dynamic Conditions. In addition to knowledge of the temperature gradients which exist within the calorimeter under static conditions it may be helpful to gain some understanding of how these values change when the calorimeter is operated normally (changing thermodynamic conditions). The temperature-time history of the output of several of these devices for a contrived test is shown in Figure IV-3. To obtain these measurements the oil bath and the calorimeter were brought to a pseudo-equilibrium condition (no vapor was flowing). That is, the oil bath and the calorimeter were maintained at a steady, controlled temperature and were in thermal equilibrium with each other, as determined by the center differential thermocouple. The agitator was operating. At time zero the circuit providing electrical energy to the calorimeter heater was activated for 30 seconds. The temperature response of the calorimeter, as indicated by the several different thermocouples, is shown by the curves. The oil bath was maintained at a constant temperature throughout the test.

There was a wide range of response times in the measurements recorded. The measurement with the fastest response was the bottom differential thermocouple (DTB), although even with this measurement there was approximately a 30 second delay between the start of the energy addition process and the initial response of the thermocouple. The re-

sponse of the center thermocouple was only slightly slower than the lower thermocouple (see Figure IV-3a). This could be due to the fact that the center portion of the calorimeter was influenced to some extent by the lagging vapor phase temperature. The liquid flow patterns within the calorimeter (see Figure VI-3) were also such that the lower part of the calorimeter wall may have been affected by temperature changes before other areas. The platinum resistance thermometer (not shown) had a response time comparable to that of the center thermocouple.

The measurements having the slowest response were the top differential thermocouple and the differential thermocouple located within the thermometer well (see Figure IV-3b). Of course, both of these measurements reflect temperatures of the calorimeter wall adjacent to the vapor phase. The initial change of DTW is rapid, reflecting a change in the temperature of the liquid phase. The output then slowly decreases to zero as the vapor and liquid phases equilibrate. DTU shows the change of the calorimeter wall temperature with respect to time. Its response appears to be somewhat faster than DTW.

The total response of the center (DTC) and bottom (DTB) differential thermocouples can be broken down into several components only one of which, at this point, can be evaluated with any confidence. Such a breakdown might consist of:

(1) The time required to bring the resistance heater to a steady state temperature once the electrical circuit is energized.

(2) The time required for the liquid to transport thermal energy from the heater to the calorimeter wall.

(3) The time required for thermal energy to diffuse through the calorimeter wall to the thermocouple mounted on the exterior surface.

An estimate of the latter response time can be made using the one-dimensional transient heat conduction equation and calculating the time required for a step change to penetrate from the inner surface to the outer surface of the calorimeter wall. As the actual liquid temperature change would be approximated more by a ramp than a step input, it will be assumed, for purposes of calculation, that 50 percent of a step change must penetrate the thickness of the wall in order for it to be sensed by the thermocouple. Solutions for this problem are available (24). For a 50 percent response to a step input $\alpha t/b^2 = 0.4$ (α is the thermal diffusivity of stainless steel, b the wall thickness, and t is the time) the diffusion time, t, becomes 1.5 seconds. This result indicates that there is probably a negligible temperature gradient through the wall of the calorimeter and that of the three time delays described only the first two are significant.

The response times of the top (DTU) and of the thermometer well (DTW) differential thermocouples were also investigated by a second test. Starting with the calorimeter and the oil bath in thermal equilibrium the liquid phase immersion heater was turned on and vapor flow was started in such a way as to minimize liquid phase temperature transients in coming to a pseudo-steady-state condition. Upon initiation of the vaporization process the temperature of the liquid-vapor interface rapidly approached a temperature 0.2-0.3 ^{o}F less than that of the bulk liquid-phase. (The magnitude of this temperature change was a function of

the rate of vaporization and was discussed more fully in Appendix I). The measured output of the two thermocouples for this test is shown in Figure IV-4a as a function of time. The response of the upper differential theremocouple was, again, considerably faster of the two.

It is not possible to determine the cause of the time lag in these measurements, but there are certain factors which may be considered. The driving force for any change to occur is the change in the temperature of the vapor adjacent to the liquid vapor interface. Thus, it is apparent that the upper wall and the upper portion of the thermometer well are cooled by virtue of their contact with a cooler vapor. But even though the temperature of the liquid vapor interface approximates a step change, the vapor temperature does not. Mixing and diffusion along with conduction between the upper calorimeter walls and the liquid vapor interface and convection of evaporated material all contribute to the thermal condition of the vapor phase. The flush-out time of material in the vapor space is about five minutes; therefore, it may be anticipated that part of the time lag is due to the time required to cool the vapor phase. The fact that the calorimeter wall responds much more rapidly than the thermometer well indicates that a resistance other than the vapor-solid heat transfer coefficient is probably operative. The higher thermal capacity/per unit area of exposed surface of the thermometer well may be a factor or there may be a significant amount of heat transport by the helium gas from the bottom to the top of the thermometer well (high thermal diffusivity) by conduction.

In spite of the uncertainty concerning the nature of the overall process it is helpful to compare the measurements to the time-depen-

dent solution for a step temperature change applied to a one-dimensional slab of finite thickness (25). The physical and analytical models for this calculation and a discussion of them is presented in Appendix VI (see Figure VI-1) For the time-dependent solution conduction along the calorimeter wall is neglected.

The heat transfer coefficient, H is anticipated to be in the range 1-50 (Btu/Hr-Ft^2 ^oF) and calculated results are shown for several values in Figure IV-4b. Considering the nature of the assumptions involved in the model, the calculated and experimental results are in reasonable agreement and seem to indicate that the top differential thermocouple (DTT) probably serves as a good indication of the temperature of the upper calorimeter wall and of the condition of the vapor phase.

The output of the thermocouple within the thermometer well appears to characterize only itself and to some extent possibly the thermometer well which encloses it. This distinction is important not only as an improvement in the method of determining the amount of vapor phase subcooling, but more importantly as an aid in determining the thermodynamic condition of the calorimeter at starting and stopping times for experimental tests.

SUMMARY

The uncertainty of the reported absolute temperature of vaporization ($\sim$0.1 ^oF) was not improved, however, the sources of error were defined. Several attempts at refining this measurement were unsuccessful. It was found that some of the uncertainty may be due to the measureable temperature gradients which existed within the calorimeter even under the most ideal circumstances. Because of the uncertainty

involved in determining the temperature difference between the calorimeter and the vacuum jacket and also because of the difficulty of experimentally establishing a point of zero heat transfer the latter condition was defined as the null point of the center differential thermocouple (DTC) as the basis.

Measurements reported showed that significant time delays existed between the application of electrical energy to the calorimeter and the accompanying response of the calorimeter resistance thermometer. It could not be determined whether this time delay was characteristic primarily of the heater or of the temperature measuring device. The measurement also showed that the upper portions of the calorimeter responded much more slowly to changing conditions than did that part in contact with the liquid phase. The output of the top differential thermocouple (DTT) provided a better means of characterizing the vapor space and the calorimeter wall than did the thermocouple within the thermometer well (DTW). These results show that in making the assumption of identical temperatures for the starting and stopping points of a test the temperature history of the calorimeter must be considered. A period of approximately 10 minutes (DTT) should be allowed in order to permit the dissipation of transient temperature gradients which may have developed during operational changes.

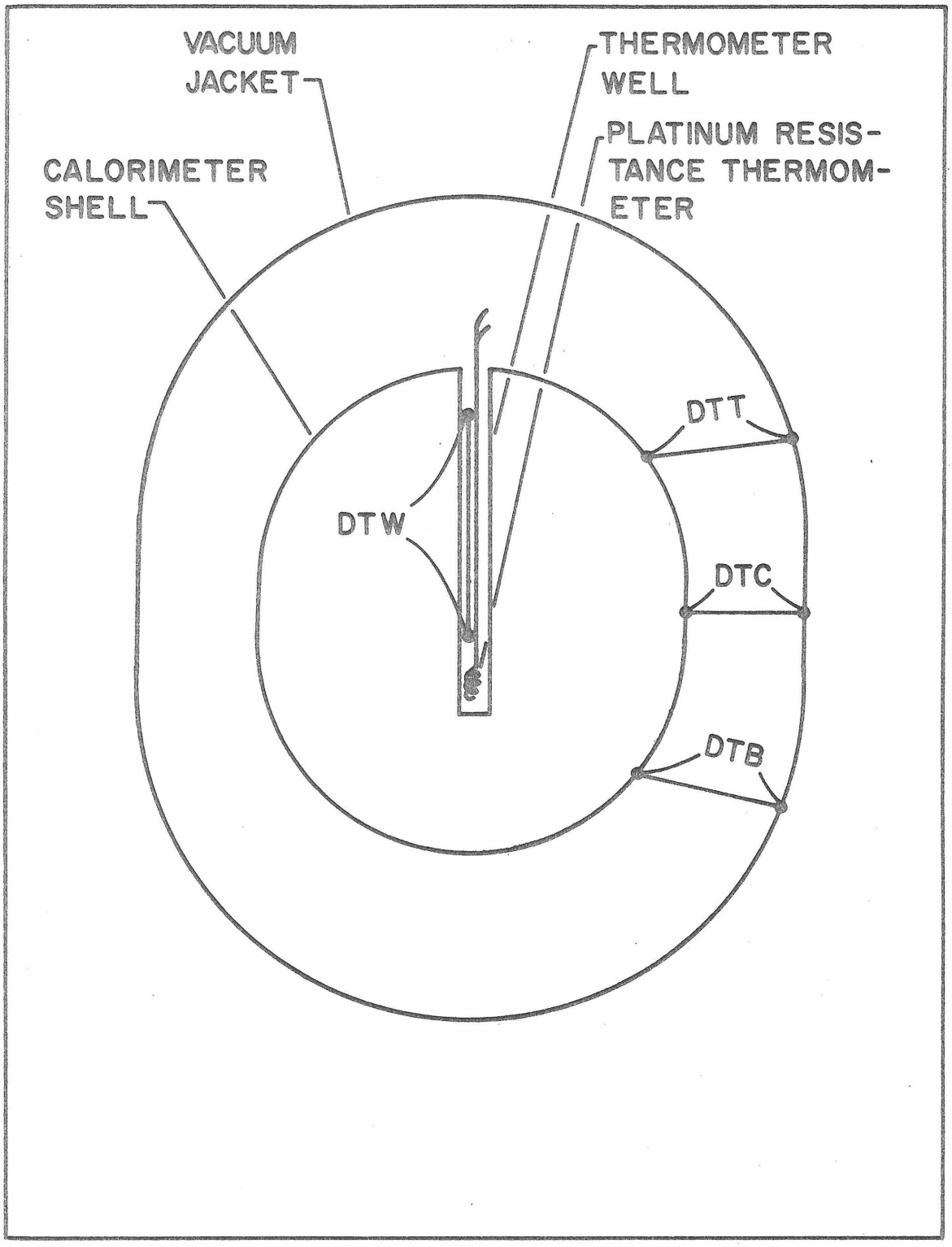

FIGURE IV-1. SCALE DRAWING SHOWING LOCATION OF TEMPERATURE SENSING DEVICES USED IN CONJUNCTION WITH CALORIMETER.

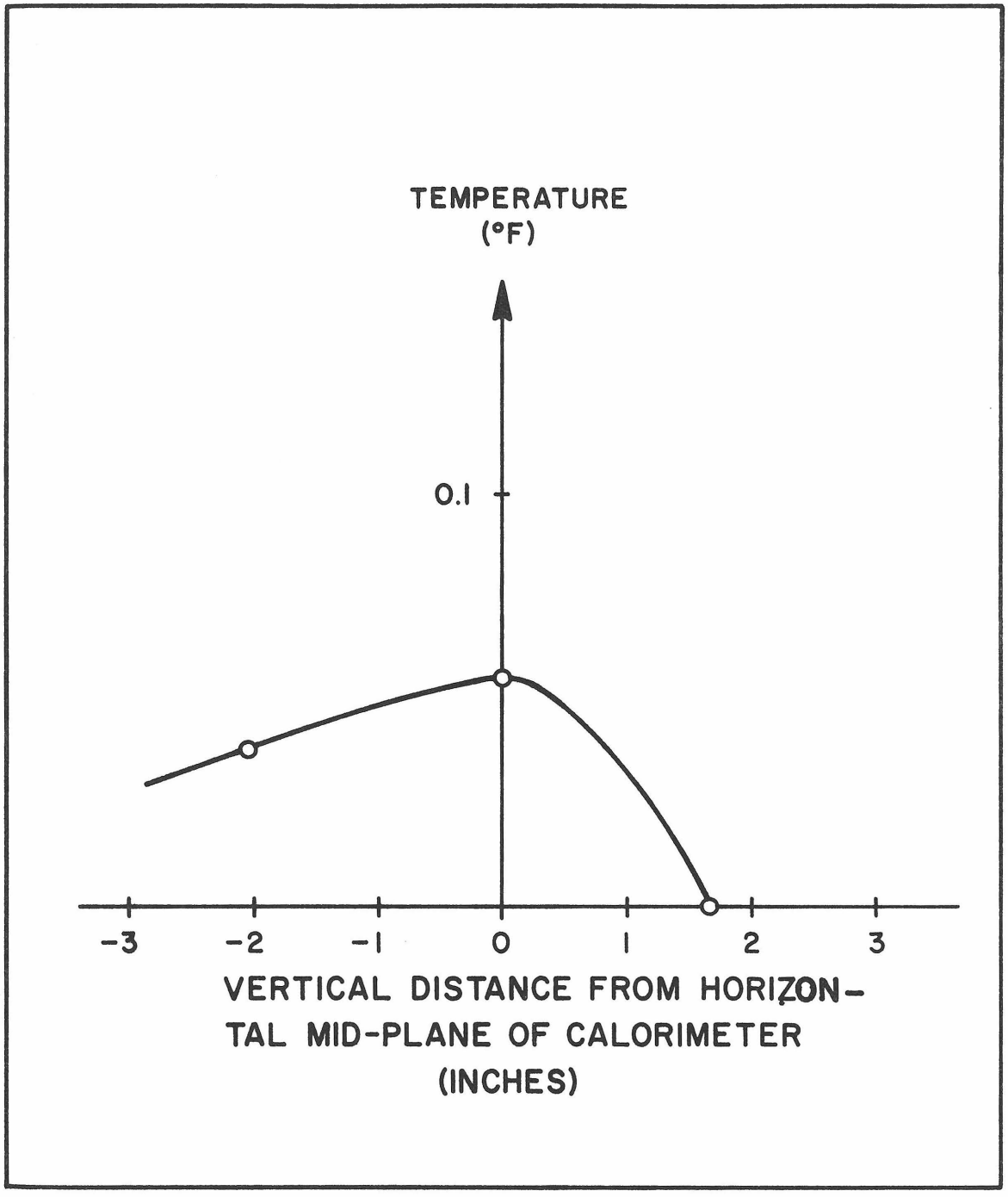

FIGURE IV-2. APPARENT TEMPERATURE PROFILE OF CALORIMETER FOR EQUILIBRIUM CONDITIONS.

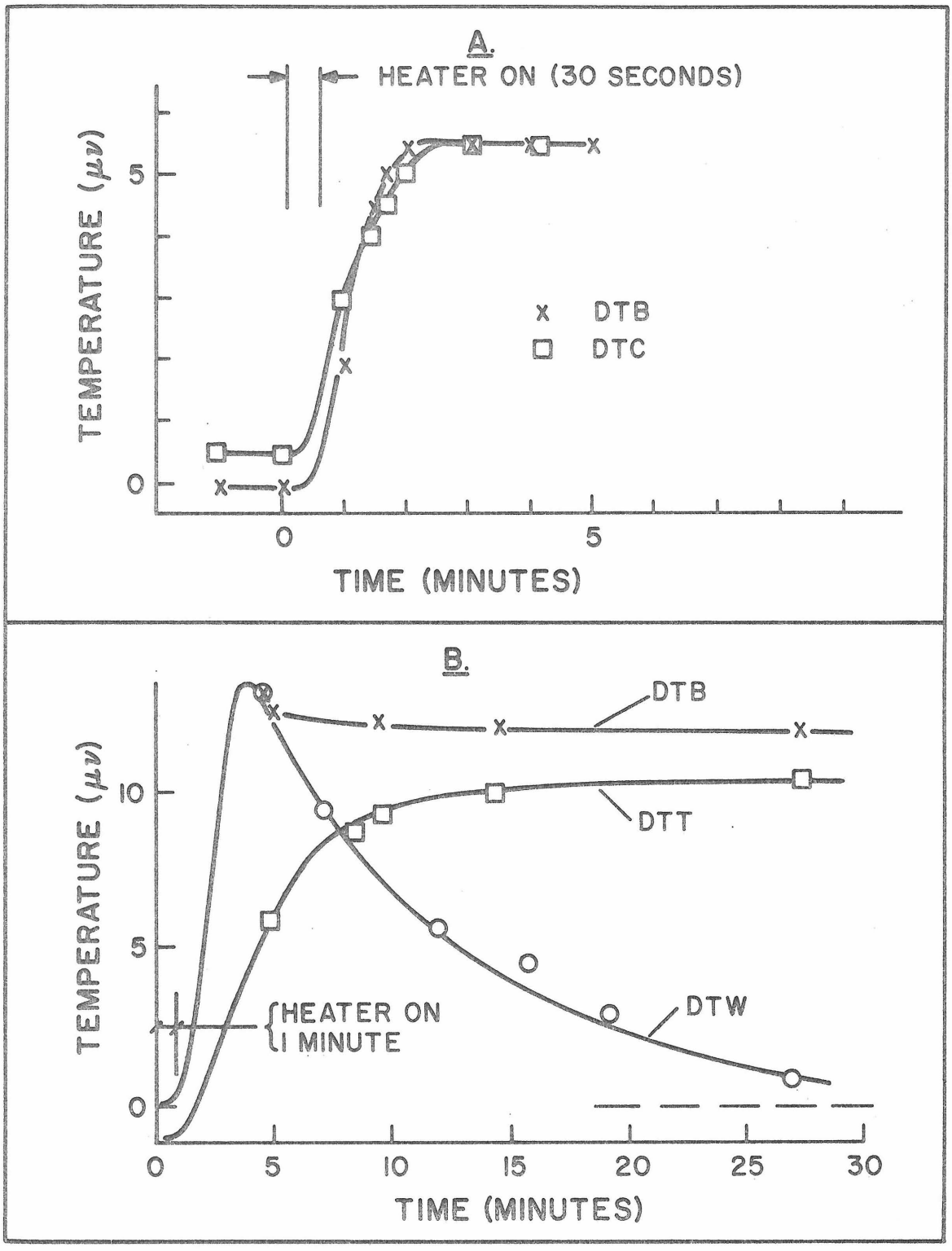

FIGURE IV-3. TIME RESPONSE OF THERMOCOUPLES TO ENERGY PULSE FROM ELECTRICAL HEATER.

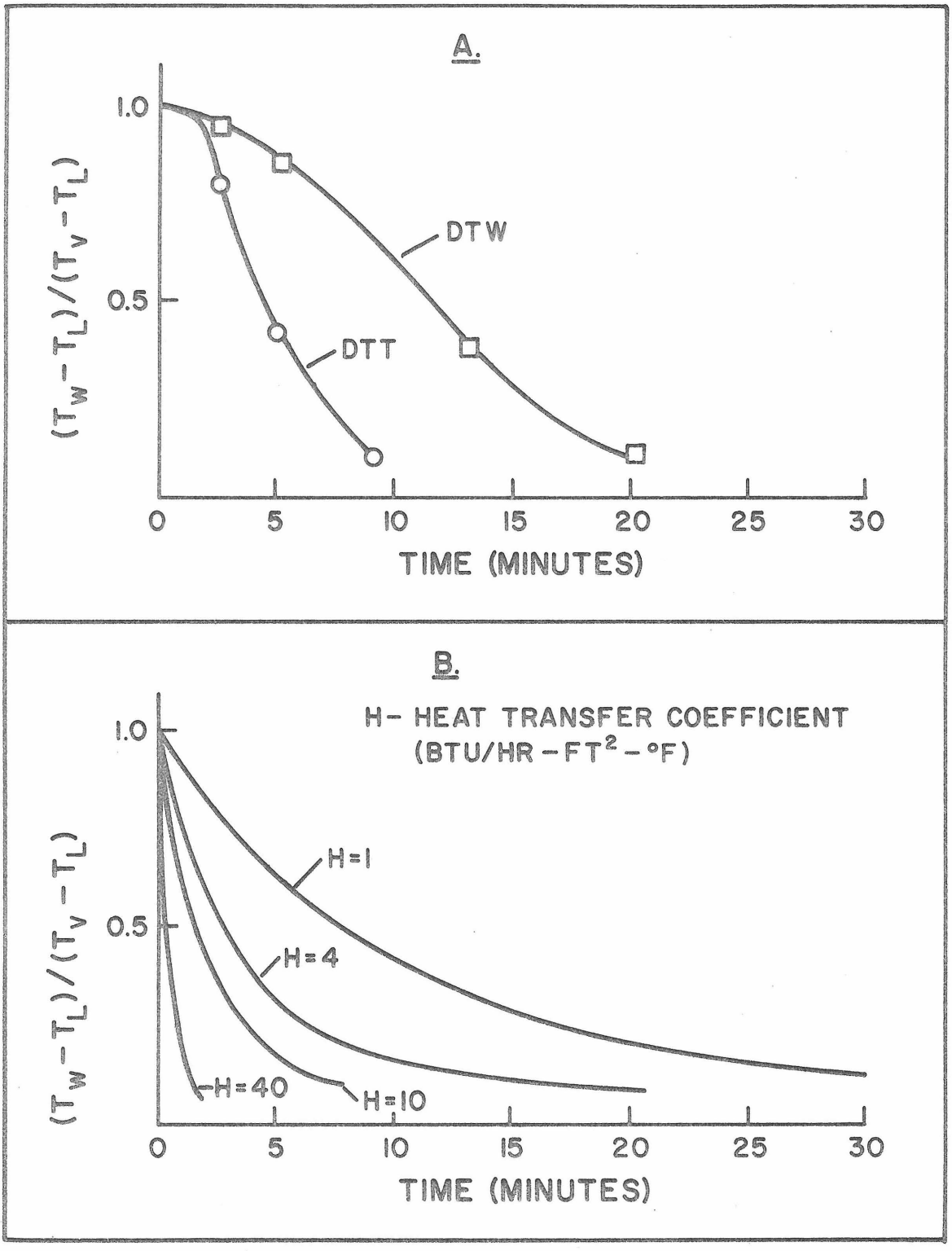

FIGURE IV-4. TIME RESPONSE OF DIFFERENTIAL THERMOCOUPLES (DTT, DTW) TO INITIATION OF VAPOR FLOW. EXPERIMENTAL (A) AND ANALYTICAL (B).

APPENDIX V

ANALYTICAL REPRESENTATION OF HEATS-OF-MIXING

The procedure for calculating heats-of-mixing from experimental data for the partial enthalpy of vaporization was described in Appendix I. A review of several of the methods which have been used to correlate heats-of-mixing for solutions of n-alkanes is given below.

Traditionally, heats-of-mixing measurements have been limited to chemical systems in which both components are relatively non-volatile and in the liquid state at normal temperature and pressure. The non-volatile nature of the components of these liquid systems, however, may make the experimental determination of the latent heat-of-vaporization extremely difficult because of the low vapor pressures involved. In the present system (n-propane/n-decane) vapor pressures of up to 300 psia are encountered for the isotherms investigated so that heats-of-mixing cannot be determined by conventional methods. However, heats-of-vaporization can be measured. In this particular case the availability of a thorough study of the volumetric and phase behavior of the binaary system made possible the calculation of heats-of-mixing from latent heat measurements. The results must be considered semi-quantative, but they do represent heats-of-mixing information which is not otherwise available from standard experimental techniques.

The heats-of-mixing of n-alkane systems have been studied widely both from an experimental and from a theoretical point of view. The first analytical representation was an empirical rule proposed by Bronstad and Kofoed (26), called the "Principle of Congruence". The

essence of this rule is that the thermodynamic properties of a liquid mixture (two or more n-alkane components) can be described in terms of the mean molecular chain length. When applied to heats-of-mixing for a binary system the rule takes the form

$$H^M = A\ (n_2-n_1)^2(x)(1-x) \qquad (V-1)$$

where A is constant along an isotherm, (n_2-n_1) is the difference in the number of carbon atoms of the two components, and x and (1-x) are mole fractions. The resultant heats-of-mixing curves are symmetrical with respect to composition for each mixture and decrease in magnitude with increasing temperature. At sufficiently high temperatures the curve crosses the horizontal axis and becomes negative.

In the early 1960's the results of several new theoretical and experimental investigations for n-alkane mixtures were presented. It was shown that excess properties for n-alkane mixtures were not always symmetric with respect to composition, and that this asymmetry could be explained in terms of an u extended principle of congruence (27, 28, 29). As temperature increased not only did the heat-of-mixing curve pass downward, but it took on a sigmoid shape as it passed through the horizontal axis. As temperature was further increased the curve again became quadratic with respect to composition. These features were accurately recorded experimentally (30, 31, 32) and also explained theoretically.

Hijman's pursued these developments further than most, and eventually presented a corresponding states theory to describe the

excess volume and the excess enthalpy of liquid n-alkane mixtures has the function of a reduced mean hydrocarbon chain length and a reduced temperature (6, 33). Although the fit of the measured experimental data to the general correlation is not as good as the precision of the data itself, the results represent the most comprehensive attempt, yet available, at correlating the excess thermodynamic properties of diverse n-alkane systems. As such these results were chosen as the standard of comparison for the heats-of-mixing calculations for the n-propane/n-decane system.

In Figure V-1 is shown a heat-of-mixing curve which Hijman derived from data for n-alkane systems for a range of temperatures. This curve may be represented by an equation of the form

$$H^M (n_1,n_2,n,T_{20}) = (n_2 - n)(n - n_1) \qquad (V\text{-}2)$$

$$X(A_1 + \frac{A_2}{n} + \frac{A_3}{n^2} + \ldots)$$

where n_1 and n_2 are the chain lengths of the components of the mixture, n is the mean chain length and T the temperature. In order to apply this result to mixtures at other temperatures, Hijman showed that the following relations may be used.

$$H^M (n_1',n_2',n',T') = \frac{\alpha(n')}{\alpha(n)} H^M (n_1,n_2,n,T) \qquad (V\text{-}3)$$

where

$$\frac{\alpha(n')}{\alpha(n)} = \frac{(1 + \lambda n')}{(1 + \lambda n)} \qquad \text{(V-4)}$$

$$n' = f(n,y) = \frac{(y^{1/u} - 1)(\lambda y^{1/u} - \mu)n}{(\lambda - \mu y^{1/u}) - \lambda\mu\,(y^{1/u} - 1)n} \qquad \text{(V-5)}$$

and

$$y = T'/T$$

Here, if T represents the base temperature for a mixture composed of molecules of chain length n_1 and n_2 and a mean chain length of n, the above values translate to n_1', n_2' and n' for T' according to Equation (V-5). H^M for that mixture is calculated from Equations (V-3, V-4).

The parameters $\lambda = 0.564$, $\mu = 0.254$ and $u = 2.245$ were evaluated from thermodynamic data describing pure n-alkanes and are independent of the thermodynamic state. Thus, the necessary information is available by which heats-of-mixing for non-standard thermodynamic states can be calculated.

(1.) $NC_6 - NC_{16}$ 40°C

(2.) $NC_{13} - NC_{62}$ 135°C

(3.) $NC_8 - NC_{62}$ 106°C

(4.) $NC_8 - NC_{24}$ 96°C

(5.) $NC_6 - NC_{36}$ 76°C

(6.) $NC_6 - NC_{24}$ 60°C

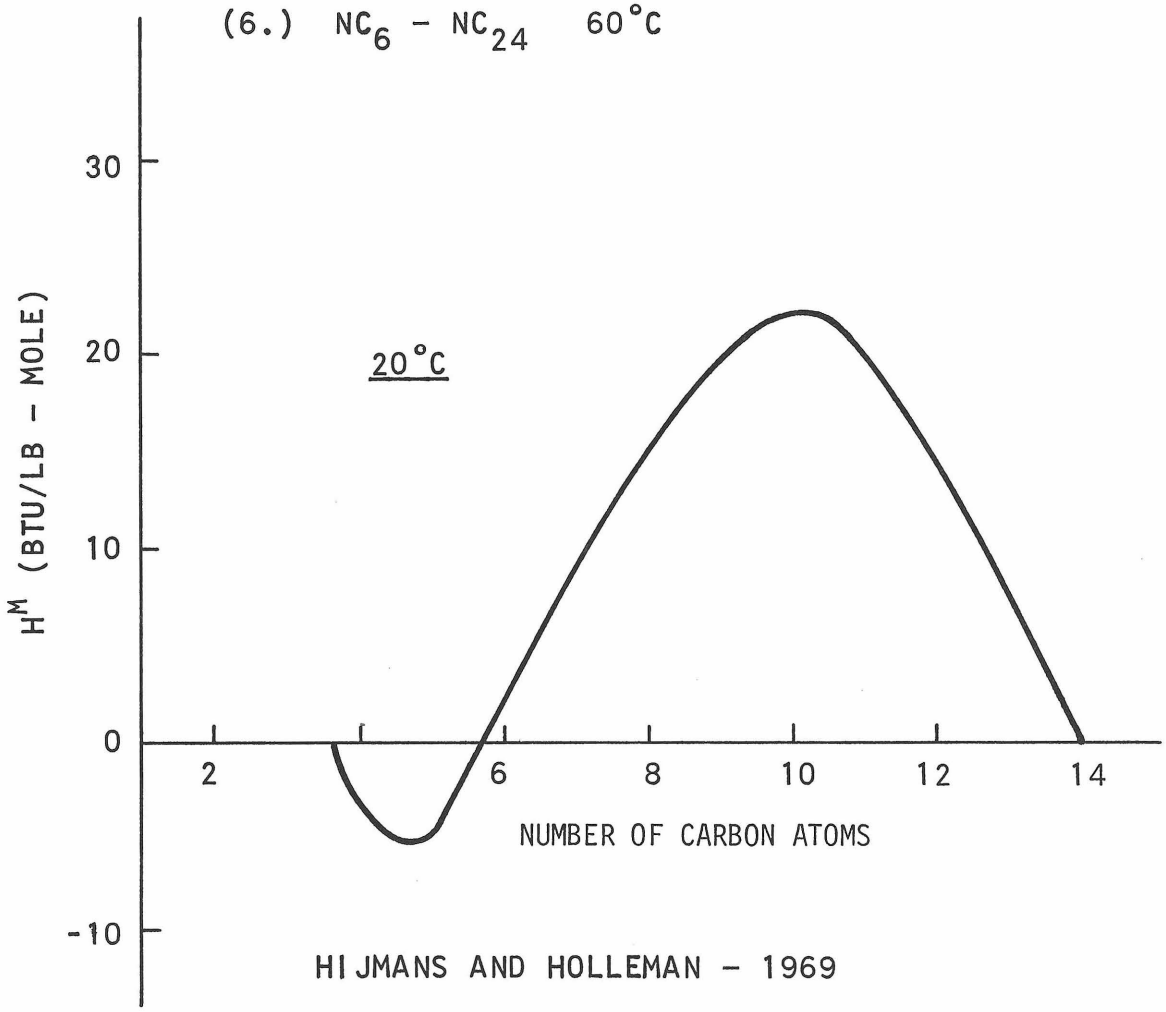

FIGURE V-1. HEATS-OF-MIXING AT 20°C FOR N-ALKANE LIQUID MIXTURES.

APPENDIX VI

HEAT TRANSFER AND AGITATOR CALIBRATION

In addition to the electrical energy provided to the calorimeter by the electrical resistance heater, corrections for agitator energy addition and energy transmitted by radiation and conduction between the calorimeter and the vacuum jacket must also be considered. The agitator energy comprised between 0.5 and 1.5 percent of the total energy added during an experimental test, but the heat transfer accounted for less than 0.01 percent. Because of its small contribution to the final results it is difficult to justify attempts at improving the heat transfer correction. However, the agitator correction is of sufficient magnitude to merit attention.

The uncertainty of the agitator energy addition process has previously been evaluated as about 20 percent (7,8) which may be interpreted as a 0.2-0.3 percent contribution to the total uncertainty of the experimental results. Therefore improvement in the method of determining an agitator calibration would seem to be a worthwhile objective. The results of such an investigation are given below. Also presented is a new procedure for calculating the heat transfer correction term. The latter is presented not so much because of the need for a new procedure, but because it provides a truer account of the transport processes as they actually occur in the calorimeter.

In Appendix IV it was pointed out that the uncertainty in the measurements made to determine the temperature difference between the calorimeter and the vacuum jacket was of the order of 0.1 ^{o}F. Information was also presented to show that this same uncertainty applied to

the determination of the point of zero heat transfer between the calorimeter and the vacuum jacket. Because of this it became necessary to assume a point of zero heat transfer and this was defined as that condition when the output of the center differential thermocouple (see Figure IV-1) was zero. The calorimeter, as far as could be determined, was in a condition of thermal equilibrium. The agitator was calibrated under these conditions and any error of energy exchange due to the assumption of a zero temperature difference between the calorimeter and the vacuum jacket was then absorbed in the results of the agitator calibration.

HEAT TRANSFER CALIBRATION

McKay (7) describes three methods by which the rate of heat transfer between the calorimeter and the vacuum jacket may be determined. The calibration provided a coefficient, k (T), which could be used in the relation

$$q_{ht} = k(T) \int_{t_o}^{t_f} (T_j - T_c) \, .dt \qquad \text{(VI-1)}$$

where q_{ht} is the amount of heat transferred to the calorimeter per unit time and T_j and T_c are temperatures of the vacuum jacket and calorimeter respectively. Heat transfer due to radiation is proportional to the fourth power of the absolute temperature, however at small temperature differences terms of higher order than the first power may be neglected. Heat transfer due to conduction in the various leads and connecting tubes, of course, is linear with the temperature difference.

Values of k(T) were experimentally determined for two temperatures and the results are shown in Table VI-1 along with a comparison

of results obtained by McKay for similar conditions. McKay also obtained calibration points at several additional temperatures which showed that a linear relationship existed between k and the absolute temperature for the temperature range of interest (560-660 ^{o}R). Because of the good agreement between the two series of tests, the results of McKay, being more extensive, were used for the evaluation of the heat transfer correction term.

The procedure for evaluating the temperature difference $(T_j - T_c)$ was changed from that used previously, however. In determining the difference in temperature the average of the center and lower differential thermocouples (see Figure IV-1) had been used. The oil bath was maintained at a constant temperature and variations of the calorimeter temperature alternately placed the calorimeter above and below that of the oil bath. The integral average of $(T_j - T_c)\ \Delta t$ was then used to calculate the heat transfer correction. No account was taken of the fact that as the vaporization process proceeded the temperatures of the calorimeter wall adjacent to the vapor phase decreased by as much as 0.3 ^{o}F. This is a considerable change when compared to the fact that temperature excursions of the calorimeter from a mean nominal temperature were of the order of only .01 ^{o}F.

The procedure described here attempts to account for this change in wall temperature. Rather than maintaining the oil bath at a constant temperature it was maintained at a temperature identical to that of the calorimeter wall adjacent to the liquid phase. This required that small adjustments in the oil bath temperature be made during the experimental tests. As described above, the zero temperature dif-

ference was defined by the null point of the center differential thermocouple (DTC), and the changing calorimeter wall temperature was treated as a deviation from the zero-point temperature difference. The temperature profile of the upper part of the calorimeter was a function of time; however, once a test was underway and at a pseudo-steady-state, the profile for purposes of heat transfer calculations was considered to be independent of time.

In Figure VI-1 are shown the physical and analytical models which were used for estimating the steady-state calorimeter wall temperature profile for different values of the vapor phase heat transfer coefficient, H. The physical model for the calculation is shown in Figure VI-1 (A). The temperature of the liquid phase changes abruptly from that of a temperature in equilibrium with the vapor temperature at its surface to that of the bulk liquid (see Figure I-3). The calorimeter wall temperature adjacent to the liquid can be assumed equal to that of the liquid. The calorimeter wall adjacent to the vapor phase will, at steady-state and at a distance from the vapor-liquid interface, assume the temperature of the vapor phase. Heat transfer due to radiation and conduction from the vacuum jacket may be neglected in this calculation and the boundary condition for the external surface of the calorimeter wall becomes $(\partial T/\partial y)_{y=0}=0$. At the top of the calorimeter is a plane of symmetry so that $(\partial T/\partial x)_{L}=0$.

This physical model may be represented with sufficient accuracy using a well-known, one-dimensional steady-state heat conduction solution for a rectangular cooling fin. (See Figure VI-1 (B)). A plane of symmetry along the center of the fin gives the boundary condi-

tion $(\partial T/\partial y)_{y=0}=0$ and the end of the fin is assumed adiabatic so that $(\partial T/\partial x)_{x=L}=0$. The solution (34) is

$$\frac{T - T_v}{T_L - T_v} = \frac{\cosh \frac{HL^2}{kB} (1 - X/L)}{\cosh \frac{HL^2}{kB}}$$

Here, the heat transfer coefficient, H, for which the vapor phase is essentially saturated n-propane vapor in the pressure range of 3-300 psia, is estimated to be of the order 1.0 - 100 BTU/HR - FT^2 - ^oF.

Calculated results for three values of the heat transfer coefficient (H) are shown in Figure VI-2. For reasonably high coefficients (> 10 BTU/HR - FT^2 - ^oF) the wall adjacent to the vapor phase approaches the vapor phase temperature within a short (< 1.0 inch) distance of the liquid surface. For smaller coefficients a more gradual gradient develops.

Experimental measurements provide an indication of the calorimeter wall temperature at one location on the surface of the calorimeter (upper differential thermocouple) which may be compared to the calculated results. See Figure VI-2). Because of the fact that H varied considerably for the different tests and can only be estimated, and also because spherical curvature is neglected, the results of the calculations are only approximate. The important consideration, however, is that reasonable agreement between the calculated and experimental results was obtained.

It is also of interest to consider the dynamic response of

the upper calorimeter wall to a change in vapor temperature. In Appendix IV it was shown that the time required for the calorimeter wall to respond to a change in vapor temperature ranges from 5 to 10 minutes. Assuming a steady-state condition for the calorimeter the heat transfer correction was broken into two terms so that

$$q_{ht} = k(T)\left[A_L \int_{t_o}^{t_f} (T_j - T_c)dt + A_V \int_{t_o}^{t_f} (T_j - T_c)dt\right] \qquad \text{(VI-2)}$$

where the subscripts L,V refer to the portions of the calorimeter wall in contact with the liquid and vapor phases respectively. By the manner in which the experiment was conducted, however, $(T_j - T_c)_L$ equals zero and $(T_j - T_c)_V$ was determined by measurements of the DTT. A_V was the fraction of the calorimeter wall adjacent to the vapor phase.

AGITATOR CALIBRATION

It was pointed out above that the largest single source of uncertainty in the experimental determination of the partial heat-of-vaporization is the correction term for energy addition due to agitation of the liquid phase. The experimental methods for determining this calibration constant have been described previously (7) and consist of a comparison of the measured rate-of-rise of the calorimeter temperature both with and without a measured rate of electrical energy addition. The agitator remained operative during both portions of this test and the vapor flow and the temperature difference $(T_j - T_c)_L$ were both maintained at zero. The rate of energy addition due to agitation then becomes

$$P_{ag} = \frac{s_2}{s_2 - s_1} \quad e$$

where e is the rate of electrical energy addition and s_2 and s_1 are the slopes of the calorimeter temperature-time profiles with and without electrical energy addition respectively. The agitator energy corrections for experimental tests can then be determined from the relationship

$$q_{ag} = \int_{t_o}^{t_f} P_{ag}(t)dt \qquad \text{(VI-3)}$$

For an individual test P_{ag} may be taken as an average of the values determined from the initial and final conditions of the experimental test.

No discussion has been previously presented which has attempted to explain, in detail, the cause of the uncertainty of the agitator calibration. The calibration involves the measurement of small temperature changes and this, certainly, contributes to the difficulty of improving the accuracy of the calibration. However, it is now believed that something more fundamental may have been the major obstacle to improving the accuracy.

Several variables influence the rate of agitator energy addition. Fundamentally, the rate of degradation of mechanical energy to thermal energy may be described by (35)

$$P_{ag} = \int_{V_L} \mu \, \Phi \, dV_L \qquad \text{(VI-4)}$$

where μ is the normal viscosity of the liquid phase, Φ is the dissipation function, and dV_L a liquid volume element. Of course μ is a function of temperature and composition, and the dissipation function depends upon several variables so that for a constant geometry

$$\Phi = \Phi\ (\mu,\ \rho,\ V_L,\ \text{RPM}) \qquad \text{(VI-5)}$$

RPM refers to angular velocity of the agitator and V_L to the total volume of the liquid phase. μ and ρ are necessary to determine the velocity flow field which is set up within the liquid phase. The agitator was driven by a constant-speed electric motor so that RPM was assumed constant.

The internal configuration of the calorimeter shown in Figure VI-3 illustrates how the volume occupied by the liquid phase may become a significant variable. Depending upon the liquid level different flow patterns may be taken by the circulating liquid. If it is accepted that velocity gradients set up in the calorimeter away from the agitator may make significant contributions to the total energy of dissipation, changing flow paths could be important. Recognizing that the viscosity and density are both functions of the independent variables T and x we may write Equation (VI-4) as

$$P_{ag} = \int_{V_L} \mu\ (T,x) \quad \Phi\ (T,x,V_L)\ dV_L$$

so that

$$P_{ag} = P_{ag}\,(T,x,V_L) = P_{ag}'\,(\mu,\rho,V_L)$$

Of the three experimental values s_1, s_2, and e used to determine P_{ag}, e was measured to four significant figures so that errors in this measurement made a negligible contribution to the total uncertainty. Values of s_2 were such that errors in temperature measurement for that portion of the test where electrical energy was being added were small. The largest uncertainty was associated with measurement of the slope s_1, which was determined from a calorimeter temperature measurement made over a period of 2-3 hours. In this period a total calorimeter temperature change of 0.060 ^{o}F occurred. New instrumentation made it possible to determine temperature changes of $\pm$ 0.0005 ^{o}F so that the uncertainty of the measured temperature changes became only 2-3 percent. With this improvement in precision of temperature measurement it should have been possible to improve on the 20 percent uncertainty of the agitator calibration quoted previously.

It was decided to, first, check the reproducibility of the agitator calibration. Measurements were repeated on the same day and also on the following day for identical experimental conditions. Electrical energy was not added. The temperature-time profiles for these tests are shown on Figure VI-4. It is not believed that the irreproducibility of these results can reasonably be attributed to any of the three measurements described, (s_1,s_2,e). Rather, it seems that a more fundamental problem may be involved.

The agitator is driven by a shaft enclosed by the material loading tube as it passes through the oil bath and the vacuum jacket to the calorimeter (see Figure II-1). The shaft is magnetically coupled to the output of an electrical drive motor. It would not seem unreasonable to think that, at certain locations along this drive path, there may exist a frictional resistance which in some cases may be steady but in others may be periodic over portions of the angular revolution. It would seem that the temperature and the temperature history of both the calorimeter and the surroundings may be important variables in this event so that the intensity of a periodic frictional resistance may depend on the thermal expansion of the materials involved. As the drive shaft is only loosely coupled to the drive motor a periodic resistance could result in an uneven motion of the agitator to the liquid phase. A change in the temperature of the surroundings - even for constant calorimeter conditions - could result in a new pattern of agitator motion and a resulting change in P_{ag}.

TABLE VI-1

RESULTS OF MEASUREMENTS FOR DETERMINING
CALORIMETER HEAT TRANSFER CORRECTION

Temperature (°F)	k(Exp.) (WATT-SEC/OHM-SEC)	k(McKay(7)) (WATT-SEC/OHM-SEC)
100	1.25	1.229
130		1.369
160		1.505
190	1.58	1.642
220		1.781
250		1.918
280		2.057

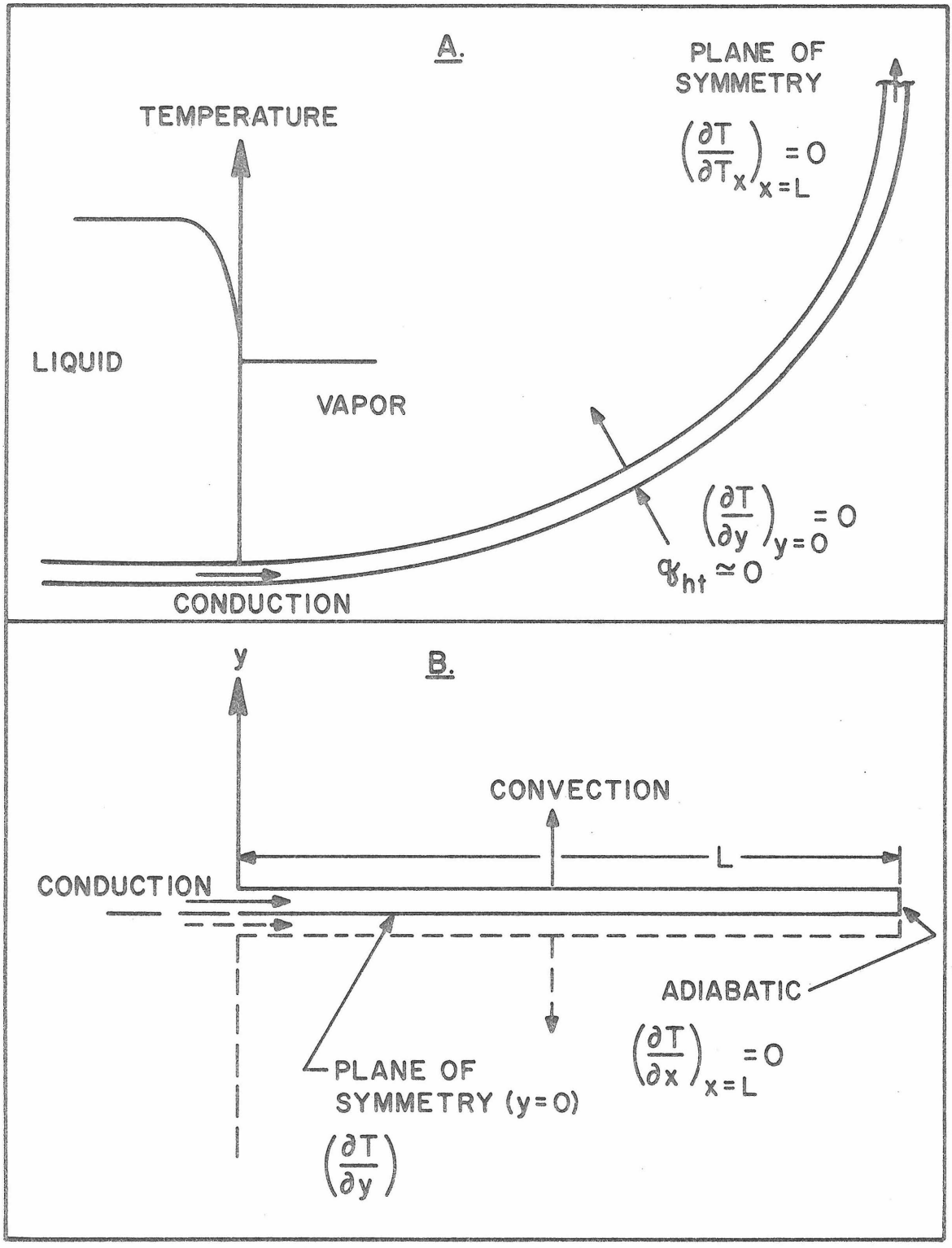

FIGURE VI-1. PHYSICAL (A) AND ANALYTICAL (B) MODELS FOR HEAT TRANSFER TO THE CALORIMETER WALL.

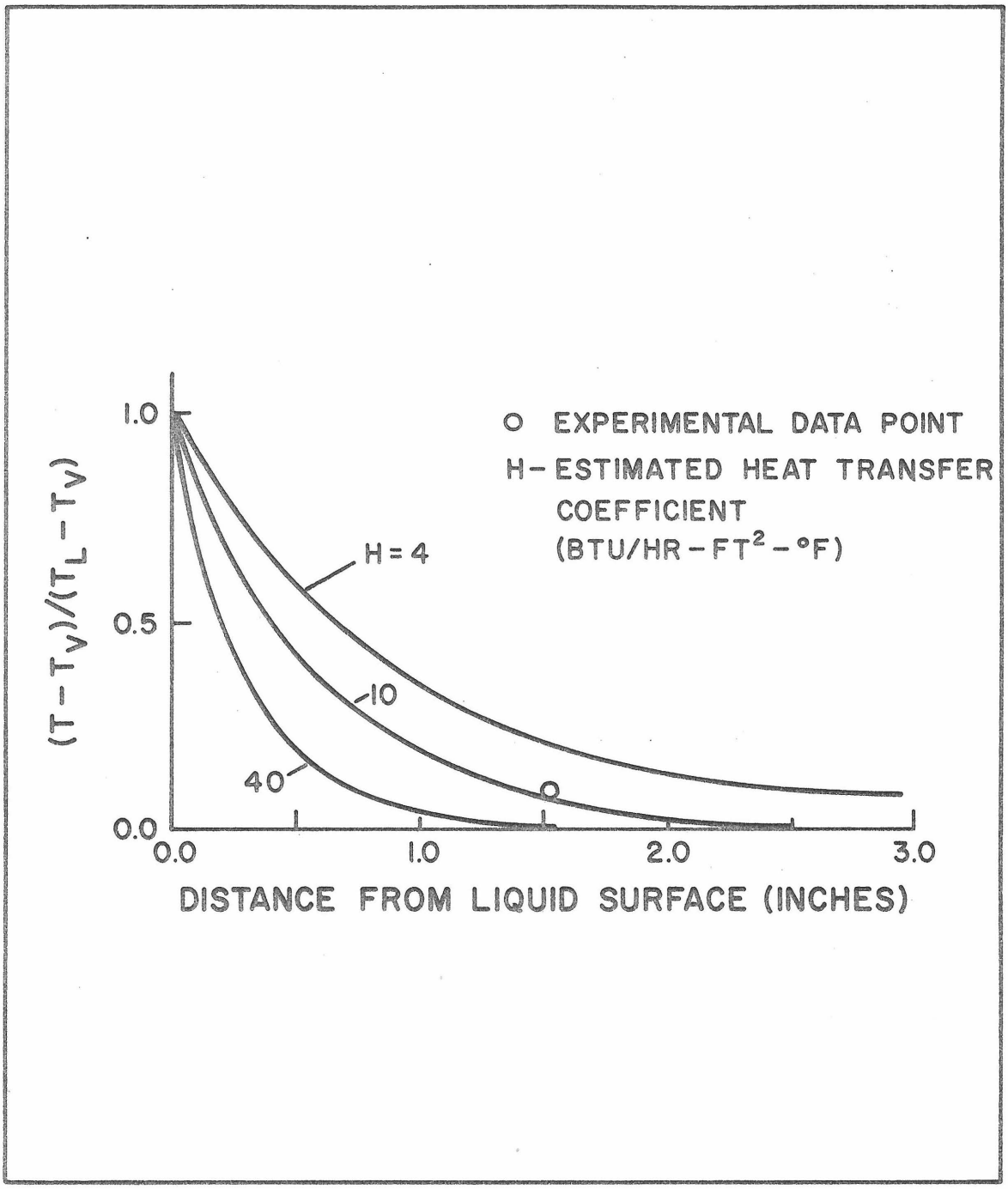

FIGURE XI-2. CALCULATED TEMPERATURE PROFILE OF CALORIMETER WALL.

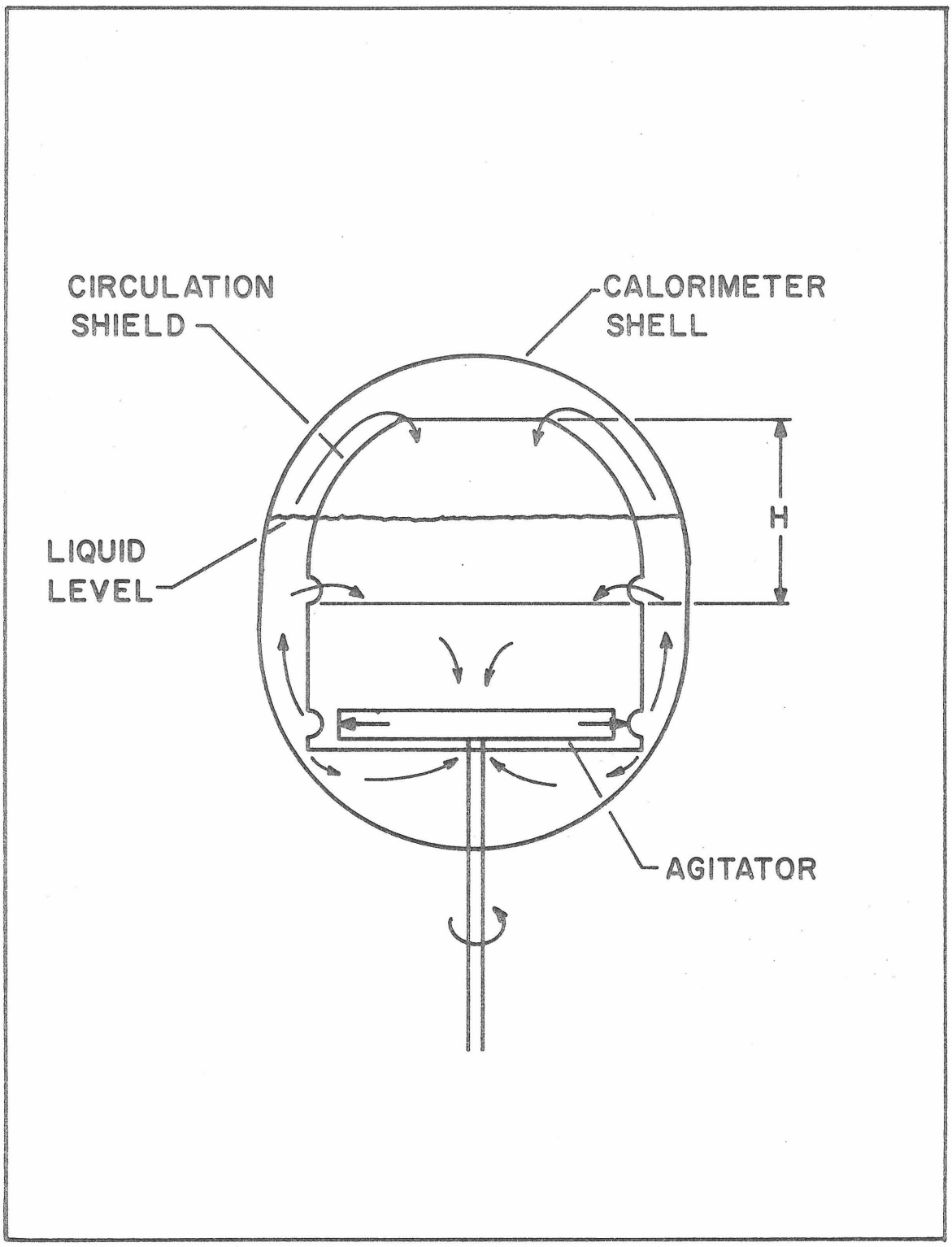

FIGURE VI-3. LIQUID FLOW FIELD WITHIN CALORIMETER.

APPENDIX VII

TABULAR SUMMARY OF EXPERIMENTAL RESULTS

A breakdown of the estimated uncertainty of the experimental measurements is given in Table VII-1. It is greater than the root-mean-square deviation of the data reported in the CALCULATIONS AND RESULTS section above, which was obtained from a best-fit curve. The r-m-s deviation is a measure of only the random errors associated with the experimental measurements (37). An estimate of the accuracy of the results, which includes the additional effect of constant errors that may appear in all of the experimental data, is not given here. However, a comparison of previously reported measurements (13) to other data available in the literature (1) indicates an accuracy of the order of one percent.

A summary of the test data is given in Table VII-1. Weights of test sample are given in grams, but the energy quantities are shown as BTU. This is to provide an easy grasp of the quantities involved. The final result is shown in BTU/LB.

Table VII-3 is a summary of the quantities involved in calculating heats-of-mixing from experimental data. CALRES is the residual partial enthalpy as shown by the solid curve in Figure 9. Based on this residual curve, calculations were made for the composition indicated in the first column. The energy quantities shown are BTU/LB except for the last three columns which are in BTU/LB-MOLE. The column headings for the enthalpy changes are as defined in Appendix 1.

TABLE VII-1

ESTIMATED UNCERTAINTY OF EXPERIMENTAL MEASUREMENTS

Source of Uncertainty	Percentage Uncertainty
Electrical energy	0.05
Agitator energy	0.10
Pressure energy	0.05
Weight of material withdrawn	0.02
Subcooling of vapor	0.03
Volumetric correction factor	0.10
Precision of temp. measurement	0.05
Accuracy of temp. measurement	0.02
Total	0.42

TABLE VII-2

SUMMARY OF TEST RESULTS

TEST	TEMPERATURE (°F)	X3 (WT.FR.)	Y3 (WT.FR.)	m (gm)	Δm_a (gm)	$\Delta m_{k,g}$ (gm)
60300	160.0	0.1366	0.9840	579.338	16.377	-0.252
60400	160.0	0.2507	0.9888	667.424	14.888	0.495
60500	160.0	0.2128	0.9876	630.386	24.869	0.443
60800	160.0	0.1416	0.9843	577.979	13.805	-0.196
60900	160.0	0.1186	0.9826	563.827	9.813	-0.238
61000	160.0	0.0953	0.9798	546.162	14.035	-0.516
61400	160.0	0.2536	0.9888	663.879	20.399	0.689
61600	160.0	0.1816	0.9864	598.885	29.446	0.080
61700	160.0	0.1344	0.9838	569.128	21.219	-0.366
61800	160.0	0.0756	0.9761	533.513	14.818	-0.619
62000	100.0	0.2968	0.9966	699.639	8.957	0.193
62100	100.0	0.2733	0.9963	679.268	11.362	0.206
62200	100.0	0.2496	0.9961	656.600	13.490	0.183
62400	100.0	0.2287	0.9958	639.879	8.961	0.079
62500	100.0	0.2057	0.9954	619.729	11.961	0.036
62600	100.0	0.1712	0.9948	592.985	11.306	-0.025
62700	100.0	0.1415	0.9940	572.896	11.480	-0.138
62900	100.0	0.1114	0.9929	553.792	10.035	-0.178
63000	100.0	0.0851	0.9912	535.158	12.324	-0.346
63100	100.0	0.0488	0.9863	513.284	9.270	-0.382
63400	130.0	0.2687	0.9841	667.210	21.160	0.469
63500	130.0	0.2375	0.9828	644.209	12.642	0.159
63600	130.0	0.2091	0.9814	618.323	18.767	0.236
63800	130.0	0.1303	0.9768	563.797	12.945	-0.238
64200	130.0	0.2680	0.9841	666.026	14.121	0.304
64300	130.0	0.2473	0.9832	648.570	9.866	0.145
64400	130.0	0.2209	0.9820	627.769	10.943	0.160

TABLE VII-2, Continued

TEST	ΔP (PSI)	FINAL PRESSURE (PSIA)	RUN TIME (SECONDS)	ELECTRICAL ENERGY (BTU)	AGITATOR ENERGY (BTU)	PRESSURE ENERGY (BTU)	DECANE ENERGY (BTU)	$\Sigma(\bar{H}_{k,g}-\bar{H}_{k,\ell})$ (BTU/LB)
60300	-14.79	99.52	3984.74	4.8726	0.0718	-0.0872	0.0021	136.
60400	- 8.49	168.40	1823.90	4.4504	0.0346	-0.0463	0.0005	130.82
60500	-16.56	144.34	3461.18	7.4327	0.0623	-0.0942	0.0014	132.57
60800	-12.13	104.16	2696.32	4.1243	0.0486	-0.0708	0.0017	136.70
60900	- 9.27	90.20	2204.32	2.9236	0.0397	-0.0542	0.0019	137.75
61000	-14.88	70.95	3854.60	4.1505	0.0694	-0.0861	0.0036	138.69
61400	-11.65	168.27	2468.13	6.0914	0.0444	-0.0624	0.0007	130.58
61600	-22.83	123.37	2893.28	8.8282	0.0521	-0.1300	0.0027	134.38
61700	-19.14	95.83	2564.19	6.3591	0.0462	-0.1112	0.0030	136.88
61800	-15.71	55.93	1816.15	4.4529	0.0327	-0.0892	0.0050	140.43
62000	- 2.14	99.30	2380.97	2.9323	0.0451	-0.0107	0.0001	147.05
62100	- 2.90	93.59	2013.69	3.7428	0.0382	-0.0150	0.0001	147.65
62200	- 3.91	87.37	2541.92	4.4394	0.0482	-0.0210	0.0002	148.16
62400	- 2.94	82.58	1804.68	2.9402	0.0342	-0.0163	0.0002	148.40
62500	- 4.55	75.59	2707.90	3.9196	0.0513	-0.0254	0.0003	149.16
62600	- 4.28	65.81	2818.10	3.6143	0.0534	-0.0240	0.0003	146.50
62700	- 5.53	55.86	1830.30	3.7379	0.0347	-0.0318	0.0005	149.59
62900	- 5.04	45.85	1936.25	3.2716	0.0367	-0.0292	0.0007	150.87
63000	- 7.48	34.81	3060.08	4.0084	0.0580	-0.0435	0.0012	152.33
63100	- 6.67	20.22	2681.84	2.9768	0.0508	-0.0388	0.0022	152.52
63400	- 8.02	130.21	3338.72	6.6142	0.0633	-0.0418	0.0009	139.09
63500	- 5.60	120.23	2040.20	3.9716	0.0377	-0.0303	0.0008	140.94
63600	- 9.52	107.35	3390.11	5.8829	0.0627	-0.0524	0.0016	140.60
63800	- 8.99	72.74	2239.12	4.0529	0.0414	-0.0528	0.0015	144.27
64200	- 5.44	131.27	2628.21	4.4074	0.0498	-0.0330	0.0006	139.05
64300	- 4.26	124.52	1915.68	3.0880	0.0363	-0.0231	0.0006	140.45
64400	- 5.23	114.14	1933.95	3.4355	0.0367	-0.0289	0.0008	140.60

TABLE VII-2

SUMMARY OF TEST RESULTS

TEST	TEMPERATURE (°F)	X3 (WT.FR.)	Y3 (WT.FR.)	m (gm)	Δm_a (gm)	$\Delta m_{k,g}$ (gm)
65600	130.0	0.5096	0.9919	564.450	11.381	0.626
65700	130.0	0.4844	0.9912	541.060	10.481	0.501
65900	130.0	0.4401	0.9900	495.738	13.590	0.488
66000	100.0	0.4215	0.9976	464.579	18.831	0.344
66300	160.0	0.4975	0.9937	536.495	19.974	1.547
66400	160.0	0.4583	0.9930	497.283	18.065	1.048
66500	160.0	0.4144	0.9922	461.863	19.802	0.776
66600	160.0	0.3744	0.9915	429.146	20.479	0.419
66700	160.0	0.3355	0.9907	403.261	17.215	-0.038
66900	100.0	0.5579	0.9984	619.457	11.300	0.459
67000	100.0	0.5377	0.9983	595.685	13.093	0.502
67100	100.0	0.5124	0.9982	571.402	14.873	0.523
67300	100.0	0.3624	0.9972	419.287	14.726	0.054
67400	100.0	0.3317	0.9969	402.768	10.669	-0.050
67500	100.0	0.4848	0.9980	518.740	12.238	0.354
67600	100.0	0.4622	0.9979	497.906	13.805	0.347
67700	100.0	0.4384	0.9977	477.792	13.055	0.277
67800	100.0	0.4087	0.9975	453.919	15.144	0.230
68000	100.0	0.3788	0.9973	433.781	13.808	0.119
68100	130.0	0.4170	0.9893	464.894	14.130	0.372
68200	130.0	0.3831	0.9883	437.737	13.099	0.192
68300	130.0	0.3392	0.9868	412.937	14.121	-0.004
68400	100.0	0.5698	0.9985	623.363	13.360	0.559

TABLE VII-2, Continued

TEST	ΔP (PSI)	FINAL PRESSURE (PSIA)	RUN TIME (SECONDS)	ELECTRICAL ENERGY (BTU)	AGITATOR ENERGY (BTU)	PRESSURE ENERGY (BTU)	DECANE ENERGY (BTU)	$\Sigma(\bar{H}_{k,g}-\bar{H}_{k,\ell}$ (BTU/LB)
65600	-1.97	198.80	1636.48	3.4281	0.0326	-0.0126	0.0005	130.18
65700	-2.32	193.05	1828.75	3.1548	0.0364	-0.0173	0.0007	131.00
65900	-3.64	181.90	2135.00	4.1152	0.0425	-0.0291	0.0014	132.94
66000	-3.99	122.57	3073.18	6.0224	0.0641	-0.0309	0.0004	143.23
66300	-5.35	268.38	1706.44	5.6207	0.0307	-0.0467	0.0009	118.06
66400	-6.36	255.11	1759.95	5.0895	0.0317	-0.0588	0.0014	120.01
66500	-8.50	238.63	1650.61	5.6079	0.0297	-0.0820	0.0020	122.38
66600	-10.71	222.36	1816.82	5.8079	0.0327	-0.1029	0.0026	124.46
66700	-11.14	206.22	1654.81	4.8708	0.0298	-0.1063	0.0027	126.54
66900	-1.19	144.70	1624.48	3.6447	0.0323	-0.0070	0.0000	141.56
67000	-1.45	141.81	1806.11	4.2042	0.0359	-0.0090	0.0001	141.16
67100	-2.00	137.95	2187.84	4.7866	0.0435	-0.0130	0.0001	141.91
67300	-4.43	111.64	2356.13	4.7420	0.0469	-0.0354	0.0006	145.87
67400	-3.76	105.89	1824.33	3.4198	0.0363	-0.0309	0.0005	146.29
67500	-1.98	133.84	1620.56	3.9372	0.0323	-0.0144	0.0002	142.45
67600	-2.49	130.07	1785.08	4.4403	0.0355	-0.0186	0.0002	142.84
67700	-2.58	126.15	1695.46	4.2039	0.0337	-0.0196	0.0003	143.49
67800	-3.51	120.59	1953.70	4.8572	0.0389	-0.0273	0.0004	143.64
68000	-3.72	115.09	1801.04	4.4495	0.0358	-0.0297	0.0004	145.10
68100	-4.46	175.65	1870.54	4.2864	0.0355	-0.0375	0.0019	133.94
68200	-5.03	166.42	1767.06	3.9629	0.0335	-0.0434	0.0024	134.80
68300	-6.66	153.30	1943.00	4.2734	0.0368	-0.0573	0.0033	136.55
68400	-1.23	146.25	1957.75	4.2913	0.0390	-0.0073	0.0000	140.86

TABLE VII-3

CALULATIONS OF HEAT-OF-MIXING FROM HEAT-OF-VAPORIZATION DATA (160° F)
(See Appendix I for definition of $\Delta\bar{H}$ terms.)

WEIGHT FRACTION	MOLE FRACTION	RESIDUAL $(\bar{H}_{k,g}-\bar{H}_{k,\ell})$ (BTU/LB)	PRESSURE (PSIA)	$(\Delta H_k)_A$ (BTU/LB)	$(\Delta\bar{H}_k)_B$ (BTU/LB)	$(\Delta\bar{H}_k)_D$ (BTU/LB)	$(\Delta\bar{H}_k)_E$ (BTU/LB)	$\bar{H}_3-\bar{H}_3^\circ$ (BTU/LB-MOLE)	$\bar{H}_{10}-H_{10}^\circ$ (BTU/LB-MOLE)	ΔH^M (BTU/LB-MOLE)
0.0	0.0	-0.009	0.40	-0.48	144.19	-35.08	-97.40	-494.88	0.0	0.0
0.005	0.016	-0.047	5.01	-0.48	143.92	-34.80	-97.40	-495.95	0.01	-7.91
0.010	0.032	-0.084	9.55	-0.47	143.65	-34.55	-97.40	-495.18	0.01	-15.62
0.015	0.047	-0.121	14.02	-0.47	143.38	-34.30	-97.40	-494.15	0.01	-23.14
0.020	0.062	-0.158	18.43	-0.46	143.11	-34.07	-97.40	-493.00	-0.02	-30.48
0.025	0.076	-0.195	22.77	-0.45	142.83	-33.83	-97.40	-491.77	-0.08	-37.65
0.030	0.091	-0.232	27.06	-0.45	142.56	-33.59	-97.40	-490.50	-0.18	-44.67
0.035	0.105	-0.269	31.30	-0.44	142.29	-33.35	-97.40	-489.23	-0.32	-51.54
0.040	0.119	-0.306	35.49	-0.44	142.02	-33.12	-97.40	-487.94	-0.50	-58.26
0.045	0.132	-0.343	39.64	-0.43	141.75	-32.88	-97.40	-486.62	-0.72	-64.84
0.050	0.145	-0.380	43.73	-0.43	141.48	-32.65	-97.40	-485.28	-0.98	-71.29
0.060	0.171	-0.453	51.76	-0.42	140.94	-32.18	-97.40	-482.51	-1.63	-83.76
0.070	0.195	-0.526	59.57	-0.41	140.40	-31.71	-97.40	-479.58	-2.44	-95.68
0.080	0.219	-0.598	67.19	-0.40	139.86	-31.25	-97.40	-476.52	-3.40	-107.06
0.090	0.242	-0.670	74.61	-0.39	139.32	-30.79	-97.40	-473.31	-4.51	-117.92
0.100	0.264	-0.742	81.86	-0.38	138.78	-30.34	-97.40	-470.00	-5.76	-128.27
0.120	0.306	-0.883	95.83	-0.36	137.70	-29.44	-97.40	-462.98	-8.68	-147.49
0.140	0.344	-1.022	109.16	-0.35	136.63	-28.55	-97.40	-455.50	-12.21	-164.87
0.160	0.381	-1.158	121.88	-0.33	135.55	-27.67	-97.40	-447.61	-16.44	-180.56
0.180	0.415	-1.291	134.02	-0.31	134.49	-26.81	-97.40	-439.30	-21.50	-194.73
0.200	0.446	-1.420	145.62	-0.30	133.42	-25.96	-97.40	-430.59	-27.55	-207.50
0.220	0.476	-1.546	156.68	-0.29	132.36	-25.11	-97.40	-421.44	-34.76	-219.00
0.240	0.505	-1.667	167.24	-0.27	131.30	-24.29	-97.40	-411.87	-43.31	-229.32
0.260	0.531	-1.784	177.34	-0.26	130.25	-23.47	-97.40	-401.94	-53.46	-238.57
0.280	0.557	-1.896	187.00	-0.25	129.20	-22.67	-97.40	-391.66	-65.38	-246.83
0.300	0.580	-2.004	196.26	-0.24	128.16	-21.88	-97.40	-381.07	-79.24	-254.15
0.320	0.603	-2.105	205.16	-0.22	127.12	-21.10	-97.40	-370.32	-94.17	-260.67
0.340	0.624	-2.201	213.74	-0.21	126.09	-20.32	-97.40	-359.46	-111.82	-266.44
0.360	0.645	-2.291	221.98	-0.20	125.06	-19.56	-97.40	-348.40	-131.72	-271.43
0.380	0.664	-2.375	229.92	-0.19	124.04	-18.80	-97.40	-337.16	-154.00	-275.65
0.400	0.683	-2.451	237.55	-0.18	123.03	-18.06	-97.40	-325.75	-178.77	-279.10
0.420	0.700	-2.521	244.91	-0.17	122.02	-17.32	-97.40	-314.18	-206.16	-281.80
0.440	0.717	-2.583	252.00	-0.17	121.02	-16.60	-97.40	-302.46	-236.28	-283.74
0.460	0.733	-2.638	258.83	-0.16	120.03	-15.89	-97.40	-290.60	-269.26	-284.91
0.480	0.749	-2.684	265.43	-0.15	119.05	-15.18	-97.40	-278.63	-305.23	-285.31
0.500	0.763	-2.723	271.80	-0.14	118.08	-14.49	-97.40	-266.54	-344.32	-284.94
0.520	0.778	-2.752	277.94	-0.13	117.11	-13.81	-97.40	-254.36	-386.69	-283.80
0.540	0.791	-2.773	283.89	-0.13	116.16	-13.14	-97.40	-242.10	-432.50	-281.86
0.560	0.804	-2.784	289.63	-0.12	115.21	-12.48	-97.40	-229.76	-481.94	-279.15
0.580	0.817	-2.785	295.19	-0.11	114.27	-11.83	-97.40	-217.38	-535.24	-275.64
0.600	0.829	-2.776	300.57	-0.10	113.34	-11.19	-97.40	-204.96	-592.62	-271.34
0.620	0.840	-2.758	305.77	-0.10	112.43	-10.56	-97.40	-192.50	-654.39	-266.23
0.640	0.852	-2.728	310.81	-0.09	111.52	-9.95	-97.40	-180.04	-720.88	-260.33
0.660	0.862	-2.688	315.69	-0.09	110.62	-9.34	-97.40	-167.59	-792.50	-253.62
0.680	0.873	-2.636	320.43	-0.08	109.74	-8.74	-97.40	-155.17	-869.71	-246.12
0.700	0.883	-2.572	325.02	-0.07	108.87	-8.16	-97.40	-142.80	-953.11	-237.81
0.720	0.892	-2.497	329.48	-0.07	108.01	-7.58	-97.40	-130.50	-1043.39	-228.69
0.740	0.902	-2.409	333.80	-0.06	107.16	-7.01	-97.40	-118.29	-1141.42	-218.76
0.760	0.911	-2.309	338.00	-0.06	106.32	-6.46	-97.40	-106.19	-1248.29	-208.00
0.780	0.920	-2.195	342.08	-0.05	105.50	-5.91	-97.40	-94.22	-1365.38	-196.40
0.800	0.928	-2.069	346.05	-0.05	104.69	-5.38	-97.40	-82.39	-1494.46	-183.93
0.820	0.936	-1.929	349.91	-0.04	103.90	-4.85	-97.40	-70.74	-1637.89	-170.56
0.840	0.944	-1.775	353.94	-0.04	103.11	-4.29	-97.40	-61.05	-1798.87	-157.92
0.860	0.952	-1.606	357.92	-0.03	102.35	-3.74	-97.40	-51.84	-1981.90	-144.54
0.880	0.959	-1.423	361.82	-0.03	101.59	-3.19	-97.40	-43.06	-2193.59	-130.26
0.900	0.967	-1.226	365.65	-0.02	100.85	-2.64	-97.40	-34.72	-2444.19	-114.93
0.920	0.974	-1.013	369.41	-0.02	100.13	-2.10	-97.40	-26.83	-2750.90	-98.32
0.940	0.981	-0.784	373.11	-0.01	99.42	-1.57	-97.40	-19.40	-3146.01	-80.05
0.960	0.987	-0.540	376.74	-0.01	98.73	-1.04	-97.40	-12.43	-3701.96	-59.47
0.980	0.994	-0.279	380.30	-0.00	98.06	-0.52	-97.40	-5.94	-4650.11	-35.13
1.000	1.000	-0.002	383.80	0.0	97.40	0.0	-97.40	0.07	0.0	0.0

PROPOSITION I*

A physical model is developed which describes the various processes involved in the ignition of aircraft fuel-tank vapors by lightning discharges. A solution which includes all of the effects important in the problem is not included, however the results of several special cases of the heat conduction problem are presented and the method of application of the model to the evaluation of the ignition hazard is indicated.

---

* Major portions of this proposition have been extracted from a previously published report, "Ignition Beneath Titanium Aircraft Skins Exposed to Lightning", T.C. Kosvic, N.L. Helgeson and M. Gerstein, NASA CR-120827, September, 1971.

INTRODUCTION

It is not uncommon for aircraft to be struck by lightning discharges and appropriate safety measures are often observed in both the structural design and the operational characteristics of aircraft to counteract this potential hazard. The ways in which a lightning discharge may damage an unprotected aircraft are many, but it is only that hazard associated with the attachment of a lightning discharge to the skin enclosing the fuel tank that is of interest here. A previous investigation (1) has shown that if the skin is aluminum a thickness of 0.080" is sufficient to protect the aircraft from possible ignition of fuel tank vapors by even the stronger lightning discharges. Recent interest in titanium as a possible aircraft skin material, however, has revived interest in this possible problem area. This proposition is concerned with the development of a physical model which characterizes the ignition of fuel tank vapors which may result from lightning discharges.

Ignition of the fuel tank vapors by simulated lightning discharges has been observed to occur by either of two mechanisims (1,2): (a) thermal ignition due to the formation of a hot-spot on the interior of the aircraft skin, or (b) direct exposure of combustible vapors to the plasma of the lightning discharge following "burn-through" of the skin material. (This excludes the case of internal arcing which is not considered here). Ignition by the second process may be thought of as arc-initiated and ignition is almost instantaneous. Thermal ignition of a combustible mixture, however, requres that the mixture be exposed to the source of ignition for a finite period of time called the ignition

delay. The ignition delay is dependent primarily on the temperature of the ignition source and below a particular temperature, the thermal explosion limit, ignition may never occur regardless of the length of exposure time. That is, for case (a), ignition is dependent upon the intensity and duration of the arc "attachment" and also upon the thermal properties of the protective skin material.

A lightning discharge attaches itself to the skin of a moving aircraft at discrete locations. It becomes "attached" at one location and remains there until the electric field, the movement of the aircraft, and various other factors (3) cause it to shift to a new location. Thus, the stroke may become attached at several different places on a wing surface as the aircraft moves through the path of the discharge. Determination of this "dwell-time" of the stroke at each point of attachment and of the parameters which control it are not the subject of this discussion. However, it is evident that the length of this dwell-time would be an important factor in determining the hazard associated with a lightning strike.

The second part of the problem, the thermal response of the wing materials to lightning discharges has been described previously (1,2,3) but the models used have been oversimplified. The purpose of this discussion is to construct a physical model from which it may be possible to predict those experimental conditions which may lead to an ignition of fuel tank vapors. It is believed that the model developed incorporates all of the essential parameters of the problem and also corrects some previous misconceptions.

ANALYSIS

The exterior of the fuel tank is exposed to the arc heating of the lightning discharge. The combustible gas mixture within the fuel tank is exposed only to the underside of the fuel tank wall. Therefore, prediction of an ignition rests on (1) the determination of the thermal response of the wall material to the arc discharge and (2) the ignition processes of the combustible gas adjacent to the underside of the fuel tank wall. As the transfer of energy from the wall to the gas is a relatively slow (almost adiabatic) process, the two problems may be considered independently of one another. The thermal response of the skin is determined from solution of the diffusion equation with appropriate boundary conditions. An empirical correlation available in the literature serves to describe the ignition phenomea.

Sources of Thermal Energy. An analysis of the thermal energy effects that accompany arc discharges is presented by Cobine (4). He reports that the arc power density, q, for hi-level arc discharges may be expected to fall within the range of $5 \times 10^4 - 1 \times 10^6$ watts/cm^2. From this it may easily be shown that when arc discharges of this power range are brought to bear on a solid body the surface temperature rises to the melting point almost instantaneously ($\sim$0.1 msec). The temperature of the surface does not continue to rise indefinitely, however, as at some point the losses of thermal energy become important and a steady-state develops. As the surface temperature reaches the melting point, a pool of molten metal forms which begins to boil (see Figure 1), and the energy absorbed by the evaporating electrode material becomes a dominant factor in balancing the energy input from the arc. The anode spot (area

directly under the arc) temperature then stabilizes at a value that may be several hundred degrees higher than the boiling point of the electrode material. The experimental measurements of the temperature of the anode spot which exist in the literature refer to this molten phase (4).

In the heat transfer problem with which we are concerned, however, it is required that we know the temperature of the surface of the "solid" electrode material as that is what forms the boundary condition for the solution of the heat conduction equation of the solid phase. In one portion of his paper Cobine identified the surface temperature of the solid electrode as the same as that of the anode spot. This may not be justified, however, as if this were the case an enormous amount of superheating of the solid phase would have to occur. As an example, for titanium, the temperature of the anode spot is reported to be of the order of 7000-8000 ^{o}F whereas the melting temperature is 3200 ^{o}F. Ubbelohde (5) reports that although liquid melts may be super-cooled tens or even hundreds of degrees it has frequently been verified that solids cannot be heated appreciably above the melting point. For example, a maximum of 0.54 ^{o}F has been observed for ice and this value is larger than for most other materials. In the present case it is not possible to predict the degree of superheating that may occur at the solid phase boundary. However, the above information does suggest that superheating of the solid phase should not be significant.

In addition to the intense heat provided by formation of the anode spot, electrical resistance heating also represents a possible source of thermal energy. The energy generated from this is proportional to the square of the current density and to the resistivity of the

electrode material. Although resistance heating can be shown to be of secondary importance it may be accounted for if necessary. The electrical discharge is a direct current and therefore the current distribution from the anode spot may be determined using Laplace's equation for the electric field and the boundary conditions of the homogeneous skin material. Knowing this the rate of energy generation/unit volume can be determined.

The Diffusion Equation. Once the sources of heat that result from a lightning stroke have been determined, the thermal diffusion equation can be used to calculate the temperature-time history of the surface of the skin opposite to the lightning strike. The problem may be formulated in terms of cylindrical coordinates (see Figure 2a). Thermal properties are assumed to be constant.

$$\frac{1}{\alpha}\frac{\partial v}{\partial t} = \frac{1}{r}\frac{\partial}{\partial r}\left(r\frac{\partial v}{\partial r}\right) + \frac{\partial^2 v}{\partial z^2} + f'(r,z) + \frac{U_s}{\alpha}\frac{\partial v}{\partial z} \qquad (1.)$$

where $v = T-T_o/T_s - T_o$

T = temperature (^oF)

T_o = initial temperature (^oF)

T_s = surface temperature (^oF)

α = thermal diffusivity, $k/\rho c$

r = radial distance

z = longitudinal distance

f' = strength of thermal energy source (energy/volume-time)

U_s = velocity of moving boundary

It is assumed that heat conduction is symmetrical in the radial direction (no angular dependence) and that the thermal properties of the skin material are independent of temperature. The formation of the anode hot spot enters the solution of this equation as a boundary condition and resistance heating is accounted for by the source term $f'(r,z)$. The erosion of the anode spot may be taken into account as a moving boundary and the term including the velocity, U_s, is included to facilitate this.

The initial and boundary conditions to be solved for are:

$$\text{I.C.} \quad v(r,z,o) = 0$$

$$\text{B.C.} \quad v(\infty,z,t) = 0$$

$$\frac{\partial v}{\partial z}(r,L,t) = 0 \tag{2.}$$

$$\frac{\partial v}{\partial z}(r,o,t) = 0 \quad (r>R)$$

$$-k \frac{\partial v(r,s,t)}{\partial z} = \dot{q} - U_s \rho \Delta H_v \quad (r<R)$$

Special Cases. Several approximate solutions to the above general set of comditions are discussed in order to illustrate several important features of the problem. The most important effect which has not been previously accounted for is the moving boundary. The electrode surface is eroded by the arc discharge at a rate which changes as a function of time. Therefore, we seek a solution for a finite plate

where one boundary is allowed to move at a finite velocity toward the other. An analytical method for solving the one-dimensional problem without sources was developed by Landau (6). He used the transformation of variables

$$\xi = \frac{L - z}{L - s(t)} \tag{3.}$$

to fix the boundary conditions at $\xi = 0.0$ and $\xi = 1.0$. This transformation was used in a numerical computation procedure to calculate temperature profiles through a simulated skin material. The number of nodes in the calculation remained constant and the transformation served to change the position of the nodes, relative to the boundaries, as a function of time. The results of a calculation for a power density, $\dot{q}$, which is anticipated for a 100 ampere discharge is shown in Figure 3. The temperature of the exposed surface is constant at the melting point of titanium (3200 ^{o}F), and the rate of regression increases as a function of time.

In Figure 4 are shown calculated temperature profiles for the case where the power input is interrupted at 25 and 50 msec. In these one-dimensional calculations the temperature of the undersurface rises substantially after current interruption, and even though only a small part of the skin was eroded thermal ignition is a possible result.

In the above calculations neither radial dissipation nor resistance heating was taken into account. However, the effect of radial dissipation can be estimated from analytical solution available in Carslaw and Jaeger(7). Thus from a given assumed temperature profile through the skin, at time zero, Figure 5 compares calculated temperature

of the underside of the skin for the cases both with and without radial dissipation. The effect is considerable, however resistance heating, also not accounted for, would tend to counteract the radial dissipation.

The results of one additional calculation will be presented in order to show the effect of an increased power input ($\dot{q}$). In this case a high erosion rate is obtained and the temperature profile through the skin becomes very steep (Figure 6). That is, the effect of the thermal wave reaches the lower surface almost simultaneously with the eroding surface. The results of Figures 3 and 6, are compared in Figure 7 where the physical interpretation of a hot-spot or burn-through ignition becomes apparent.

Chemical Ignition Delay. For the purposes of showing a complete ignition model it is necessary to provide a description of the ignition process. It will be assumed that if the lower surface stays at T longer than τ_I (T), ignition occurs. Here T is defined as the minimum spontaneous ignition temperature, which has been determined for many hydrocarbons as summarized by Gerstein (8). Studies have shown that the least wall temperature that will ignite an adjacent hydrocarbon/air mixture is around 900-1100 ^{o}F . Therefore, it would be desirable to have ignition data starting at approximately 900 ^{o}F and extending to the higher temperatures.

The results of several investigations on the ignition delay (τ_I for hydrocarbon/air mixtures are available in the literature. But often they are not directly comparable to each other, nor to the conditions of the current program. Adomeit (9) reported experimental measurements from which chemical ignition delay times are available and the data

appear to be applicable, with some adjustment, to the present problem. Among the data reported are results for ignition of a homogeneous gas-phase mixture of pentane and air. The source of ignition was cylindrically-shaped chromium-nickel rod .35 cm (.14 in.) in diameter. The rod was heated to a prescribed temperature by an electrical discharge in a time period that was small compared to the ignition delay. The growth of the thermal boundary layer, by conduction, about the hot wire, and the time of the thermal ignition were observed and recorded on interferrograms. Ignition occurred within a time interval such that free convection had not yet set in.

To permit the use of this data in the present case it must be re-evaluated in terms of the planar geometry of the fuel tank wall. The effect of geometry is, basically, a difference in heat flux ($\dot{q}_I$). In cylindrical coordinates ($\dot{q}_I$) may be evaluated for large times graphically (10) and for small times either graphically or from the following:

$$\dot{q}_I = \frac{k\Delta T}{a} \left\{ \left(\frac{a^2}{\pi\alpha t}\right)^{1/2} + \frac{1}{2} - \frac{1}{4}\left(\frac{\alpha t}{a^2\pi}\right) + \frac{\alpha t}{8^2\pi} \cdots \right\} \qquad (4.)$$

where a is the radius of the hot body. For planar geometry

$$\dot{q}_I = \frac{k\Delta T}{\sqrt{\pi\alpha t}}$$

which is the first term of the expansion in Equation (4). If $\dot{q}_I$(planar) is specified, the equivalent $\dot{q}_I$(cylindrical) may be calculated and τ_I may then be obtained from the ($\dot{q}$,τ_I) correlation (9). Results for planar

and cylindrical geometries are shown in Figure 8.

Other ignition delay data for propane/air mixtures have also been reported in the literature. Brokaw and Jackson (11) preheated the fuel and air streams separately and, after rapidly mixing the reactants, measured the ignition delay as the time to ignition following the mixing operation. A typical result indicated that the ignition delay at a temperature of 1000 ^{o}K (1340 ^{o}F) was about 1 second. Chang (12) preheated the air stream and fed a cold stream of fuel into it. A typical result from his measurements showed the ignition delay to be about 0.1 second at 1000 ^{o}K (1340 ^{o}F). The correlation given above, if extrapolated to 100 ^{o}K (1340 ^{o}F), would indicate an ignition delay time of about 0.1 second. This agreement is satisfactory.

Ignition Threshold. The ignition criterion is arbitrarily stated as follows: If the lower surface remains above a temperature T* for a period exceeding the chemical delay τ_I corresponding to T*, then ignition occurs. In symbols,

$$\text{If} \quad T(L,t) \geq T^* \qquad \text{for } \Delta t \geq \tau_I(T^*) \longrightarrow \text{Ignition}$$

where τ_I (T*) is defined in Figure 8. It is apparent that the existance of a finite chemical response time (τ) can prevent ignition for intermediate temperatures in the range 1300-2000 ^{o}F. However, if the underside of the skin reaches a temperature of 2240 ^{o}F even momentarily, ignition is essentially unavoidable. At lower temperatures (say 1600 ^{o}F), the chemical ignition delay is of the order of 100 msec and whether ignition occurs clearly could depend upon the length of time which a hot spot

persists. We have seen in a previous section that the peak temperature of the underside of the skin may not occur until after the lightning stroke has ceased to flow and that the temperature of the skin may persist at relatively high temperatures. This becomes important, then in determining the minimum dwell time of a lightning strike that could initiate a thermal ignition. For although an arc may be attached at a particular spot for only several milliseconds, a significant amount of thermal energy may have accumulated in the skin material to cause a delayed ignition

In order to illustrate the use of this ignition criterion, estimated temperature histories of the inner surface of the fuel tank are presented in Figure 9. Curves of T* are derived from Figure 9 and replotted in Figure 10. On this same plot is superimposed a chemical ignition delay curve taken from Figure 8, but with the zero taken as the time at which the underside reaches peak temperature. Any temperature history breaking above the no-ignition envelope will cause ignition, according to the model. Particular cases are:

Curve A (Low current, short duration)

The ignition delay is essentially infinite at 550 ^{o}F, the maximum temperature reached by the inner surface. No ignition.

Curve B (Low current, moderate duration)

The underside spends 100 msec above 982 ^{o}F, but this is not sufficient for ignition.

Curve C (Moderate current, moderate duration)

The underside remains above 1520 ^{o}F for over 2000 msec. Ignition in this case is guaranteed.

Curve D (High current)

Ignition and puncture occur in quick succession around 75 msec.

Summary. This discussion has outlined how the calculated results can be used to evaluate the hazard associated with lightning strikes to fuel tank skin materials. The model for predicting undersurface temperatures appears to be essentially developed, but to achieve realistic results a more complete numerical analysis of the diffusion equation is required. This would not be difficult, in principle, however, considerable computation time and cost is involved.

REFERENCES

1. Robb, J. D., E. L. Hill, M. M. Newman, and J. R. Stahmann, "Lightning Hazards to Aircraft Fuel Tanks", NACA TN 4326, September, 1968.

2. Kester, F. L., M. Gerstein, and J. A. Plumer, "A Study of Aircraft Hazards Related to Natural Electrical Phenomena", NASA CR-1076, June, 1968.

3. Kofoid, M. J., "Lightning Discharge Heating of Titanium Aircraft Skins", Boeing Scientific Research Laboratories Document 01-82-0752, September, 1968.

4. Cobine, J. D., and E. E. Burger, "Analysis of Electrode Phenomena in the High-Current Arc", J. of Applied Physics, 26, 1955, p. 895.

5. Ubbelohde, A. R., Melting and Crystal Structure, Oxford University Press, 1965, London.

6. Bankoff, S. G., "Heat Conduction or Diffusion With Change of Phase", Advances in Chemical Engineering, Vol. 5, 1964, Academic Press, p. 94.

7. Carslaw, H. S., and J. C. Jaeger, Conduction of Heat in Solids, 2nd Edition, Oxford University Press, 1959, p. 101, London.

8. Gerstein, M., and R. D. Allen, "Fire Protection Research Program for Supersonic Transport", APL-TDE-64-105, October, 1964, p. 87.

9. Adomeit, G., "Proceedings of the 1963 Heat Transfer and Fluid Mechanics Institute", Stanford University Press, 1963, p. 160.

10. Carslaw, H. S., and J. C. Jaeger, op. it., p. 334.

11. Brokaw, R. S., and J. L. Jackson, "Effect of Temperature, Pressure, and Composition on Ignition Delays for Propane Flames", Fifth Symposium (Intl) on Combustion, Rhienhold, 1955, p. 563.

12. Chang, C. J., "Ignition Delay of Propane in Air Between 725-880°C Under Isothermal Conditions", Seventh Symposium (Intl) on Combustion, Buttersworth, 1959, p. 431.

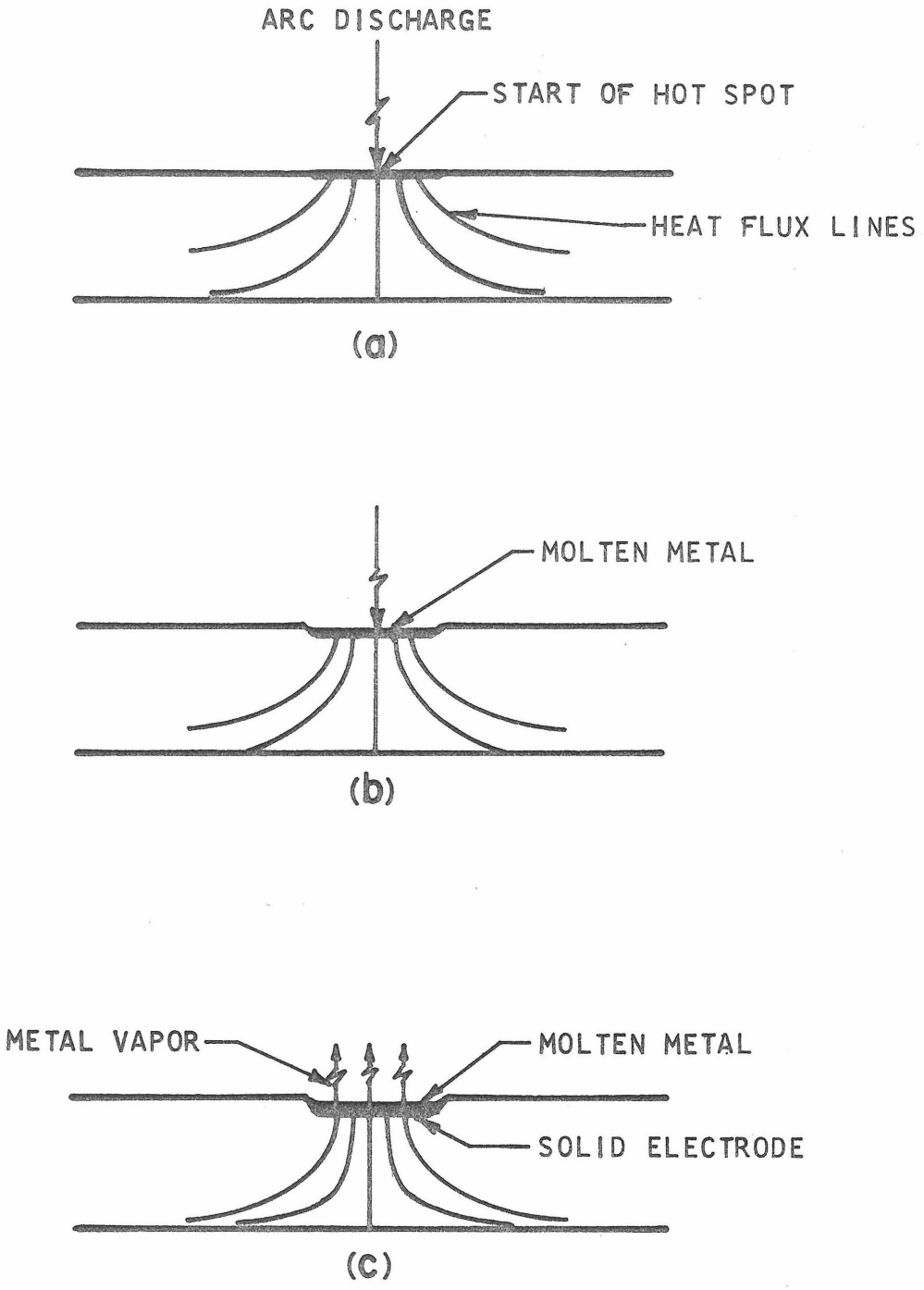

FIGURE 1. HISTORY OF HOT SPOT DEVELOPMENT

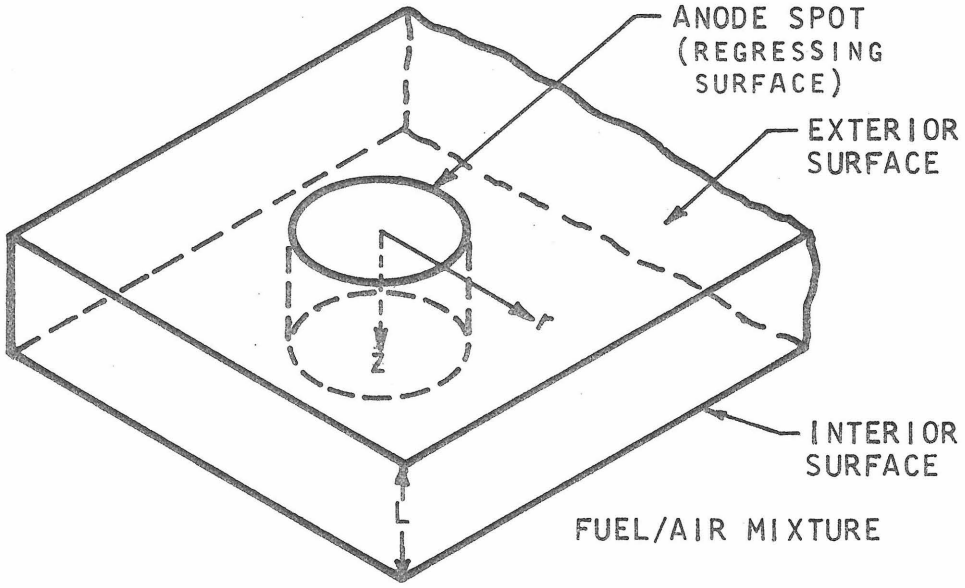

(a) CYLINDRICAL COORDINATE SYSTEM

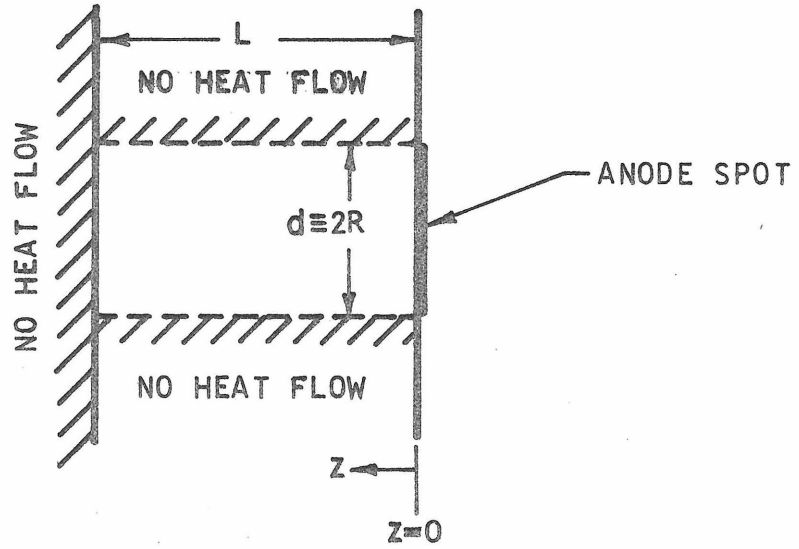

(b) MODEL FOR ONE-DIMENSIONAL FINITE BODY

FIGURE 2. COORDINATE SYSTEM FOR HEAT CONDUCTION ANALYSIS

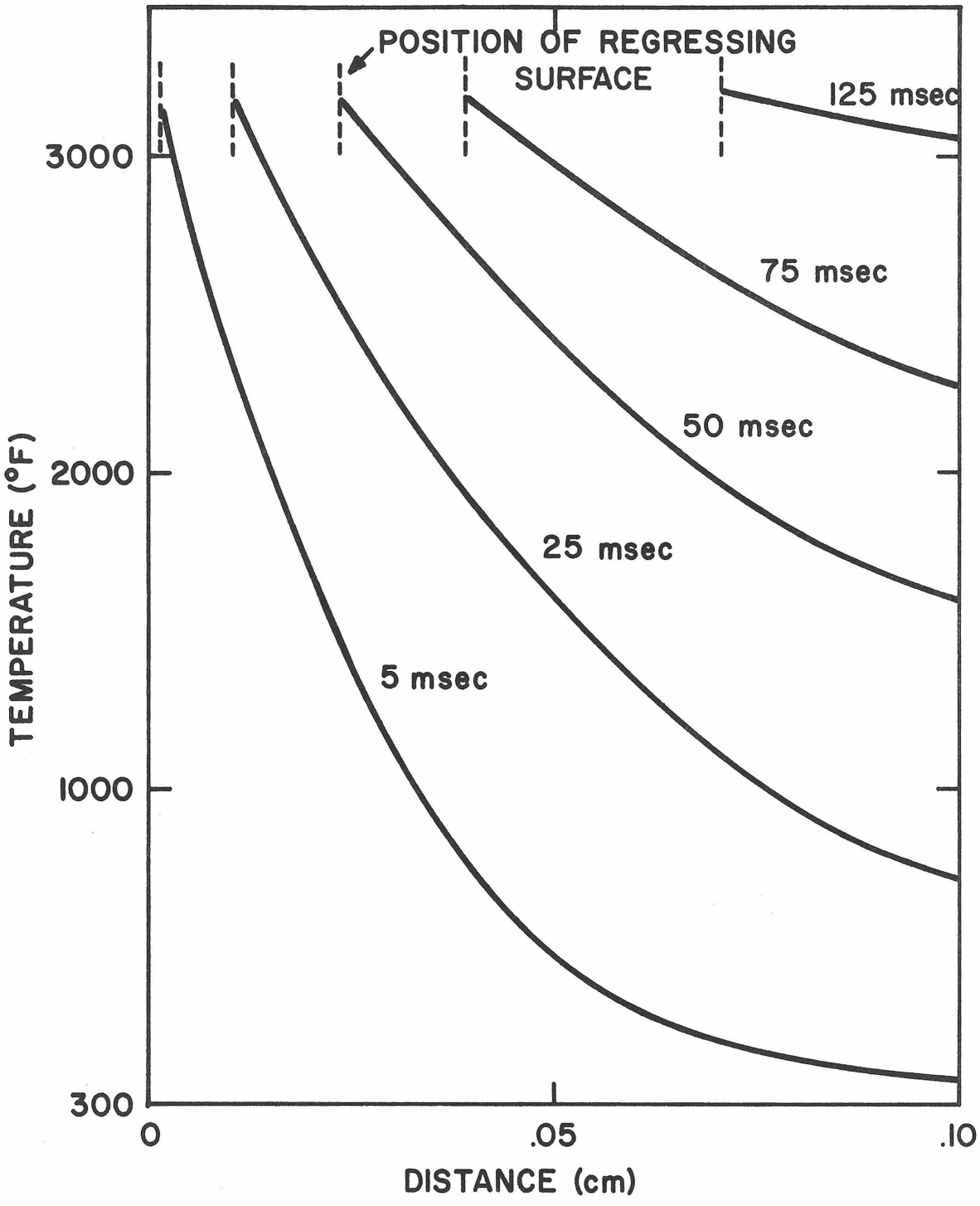

FIGURE 3. CALCULATED TEMPERATURE PROFILE AND REGRESSION RATE FOR 100 AMPERE CURRENT.

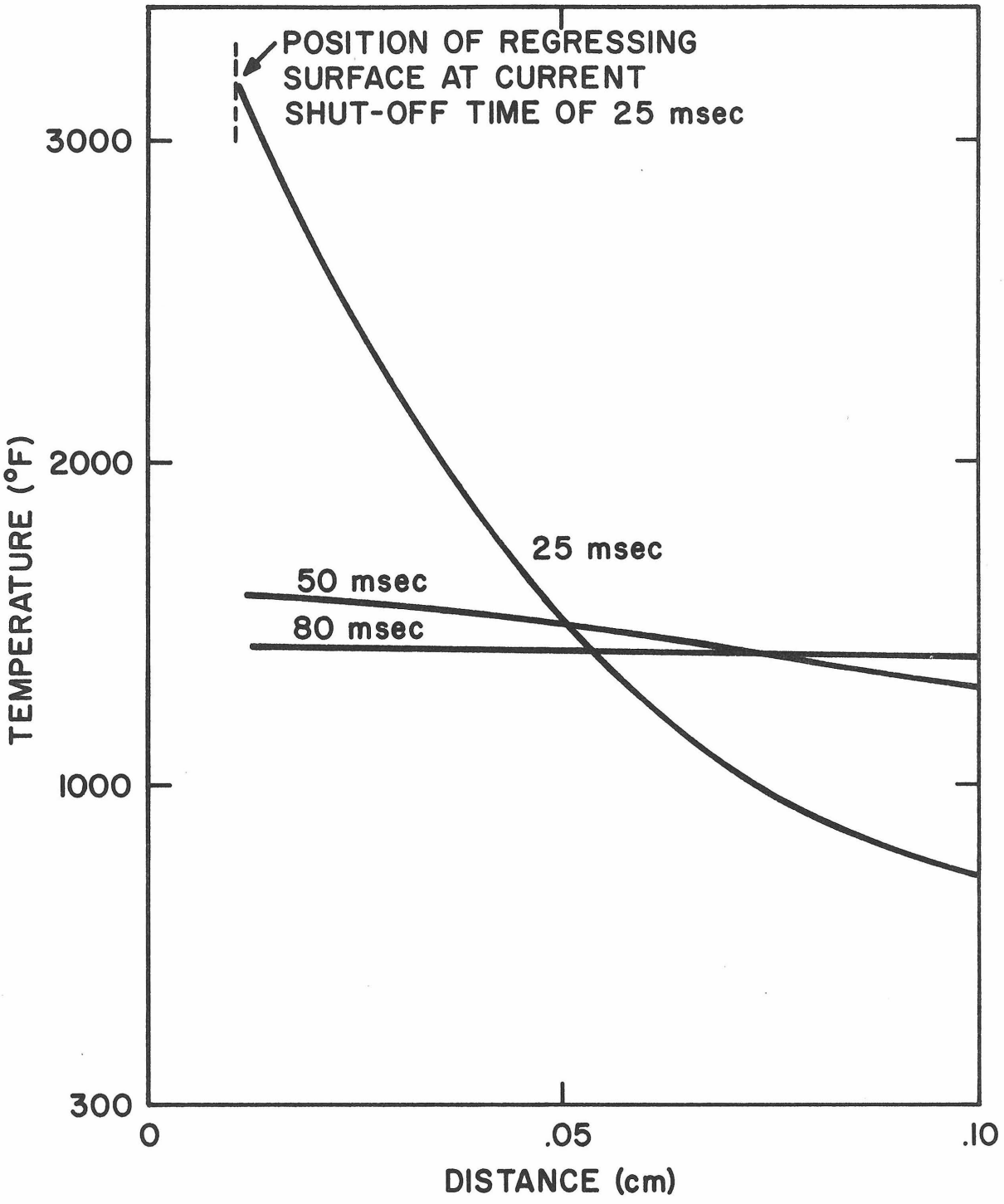

FIGURE 4. LONGITUDINAL TEMPERATURE EQUILIBRATION FOLLOWING CURRENT INTERRUPTION.

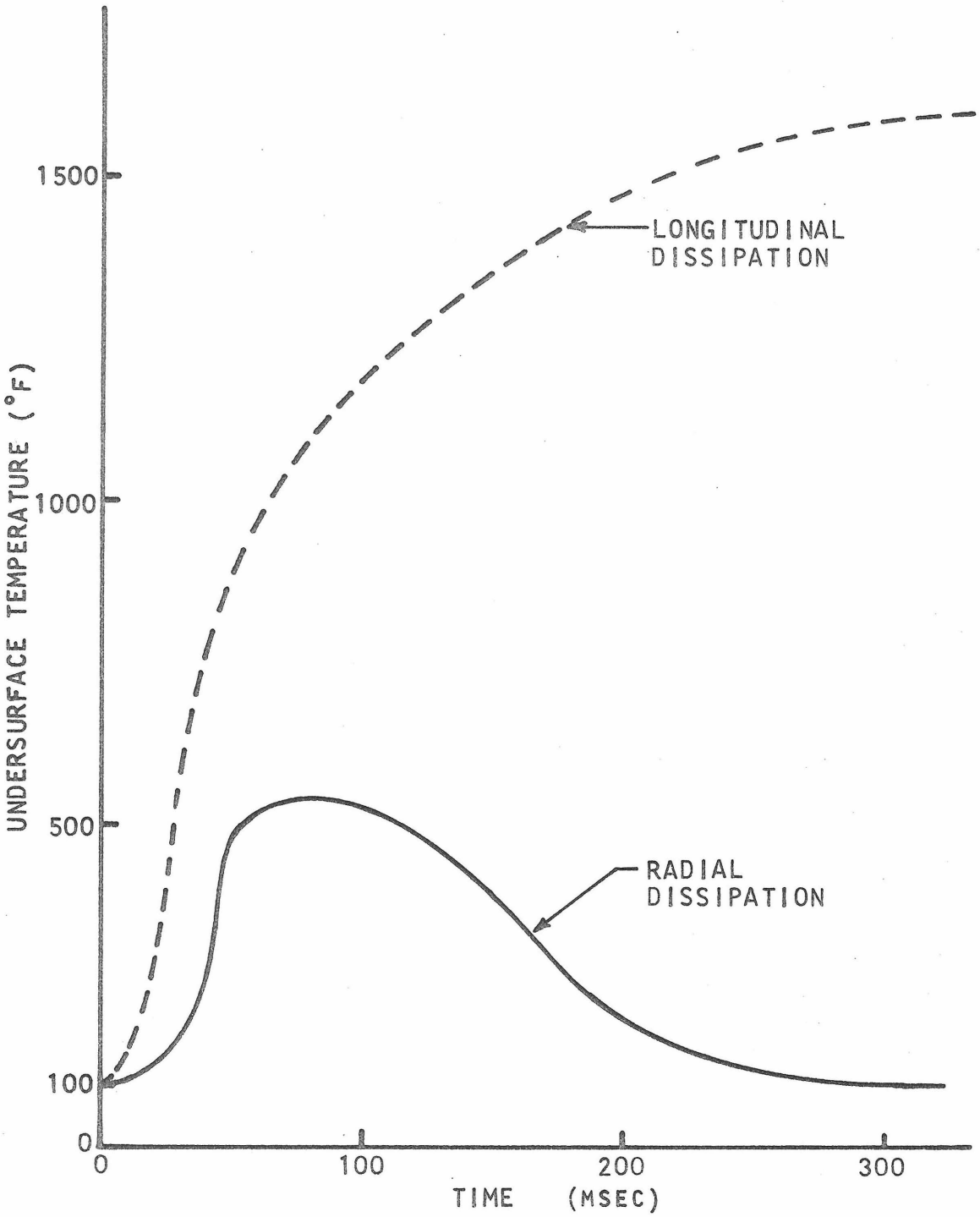

FIGURE 5. EFFECT OF RADIAL DISSIPATION ON
UNDERSURFACE TEMPERATURE AFTER CURRENT INTERRUPTION

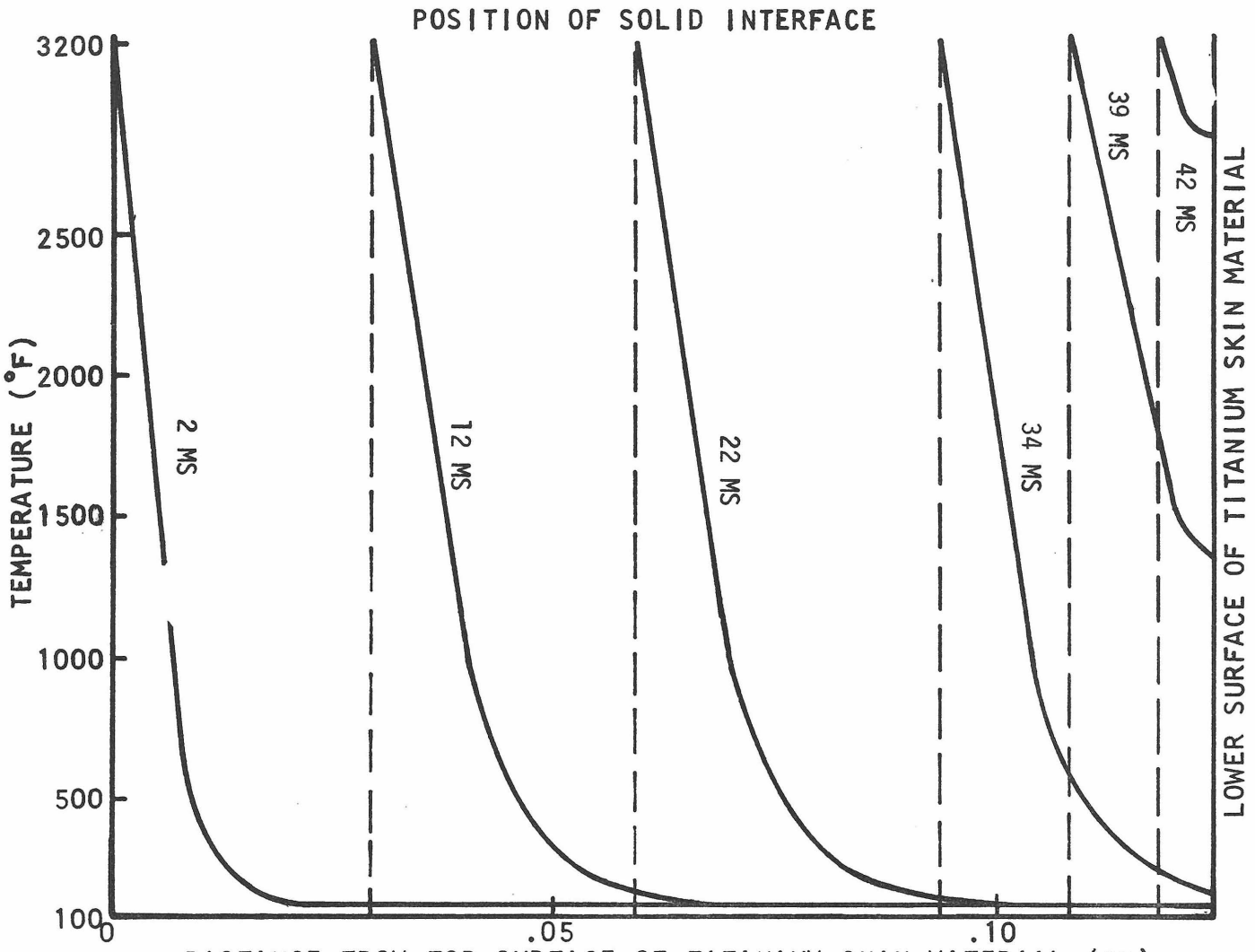

FIGURE 6. CALCULATED TEMPERATURE PROFILES THROUGH .050" (.127 CM) TITANIUM SKIN MATERIAL FOR EROSION RATE (U_S) OF 3 CM/SEC

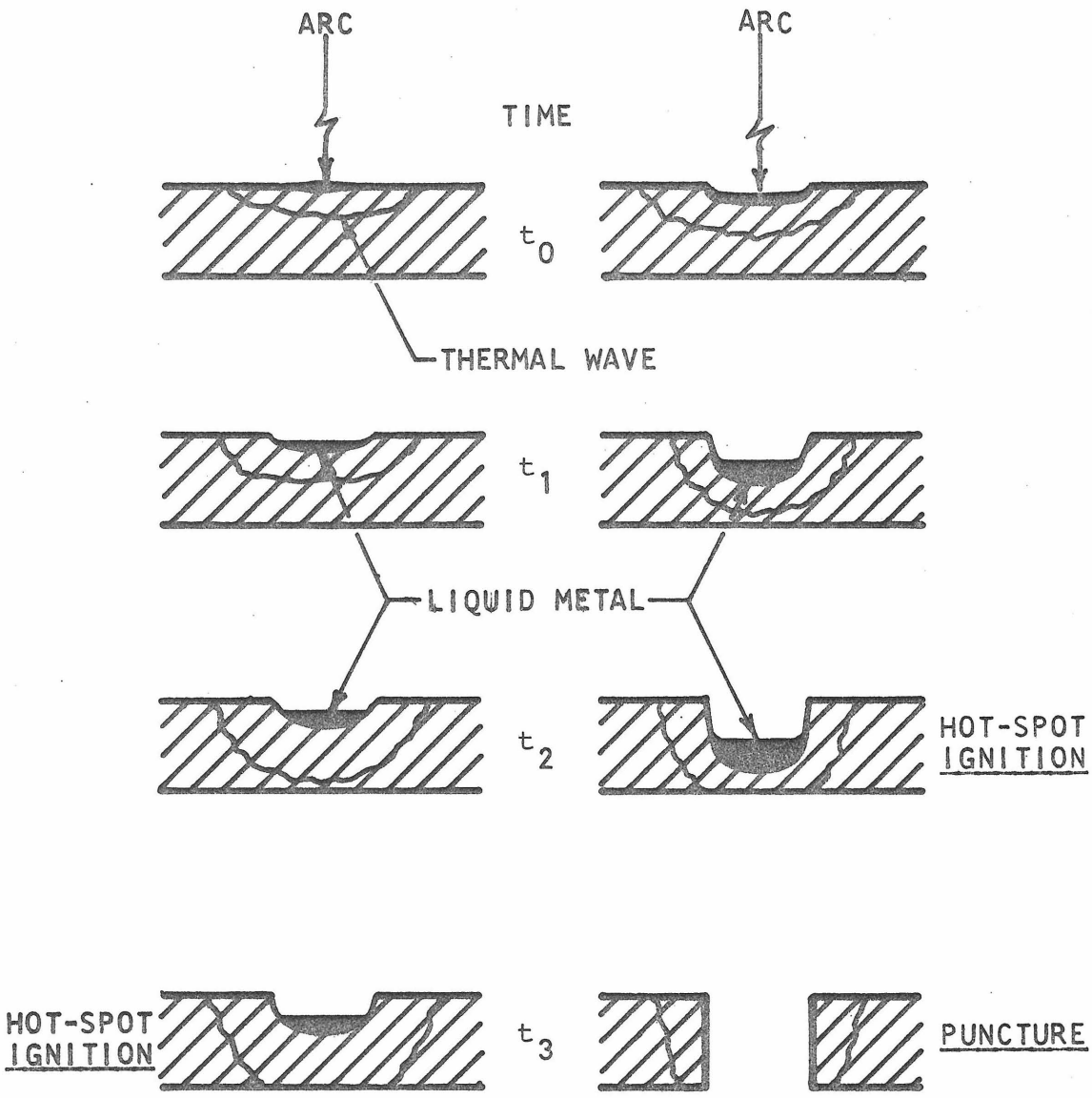

FIGURE 7. CONCEPTUAL DEVELOPMENT OF HOT-SPOT AND BURN-THROUGH IGNITION MECHANISMS

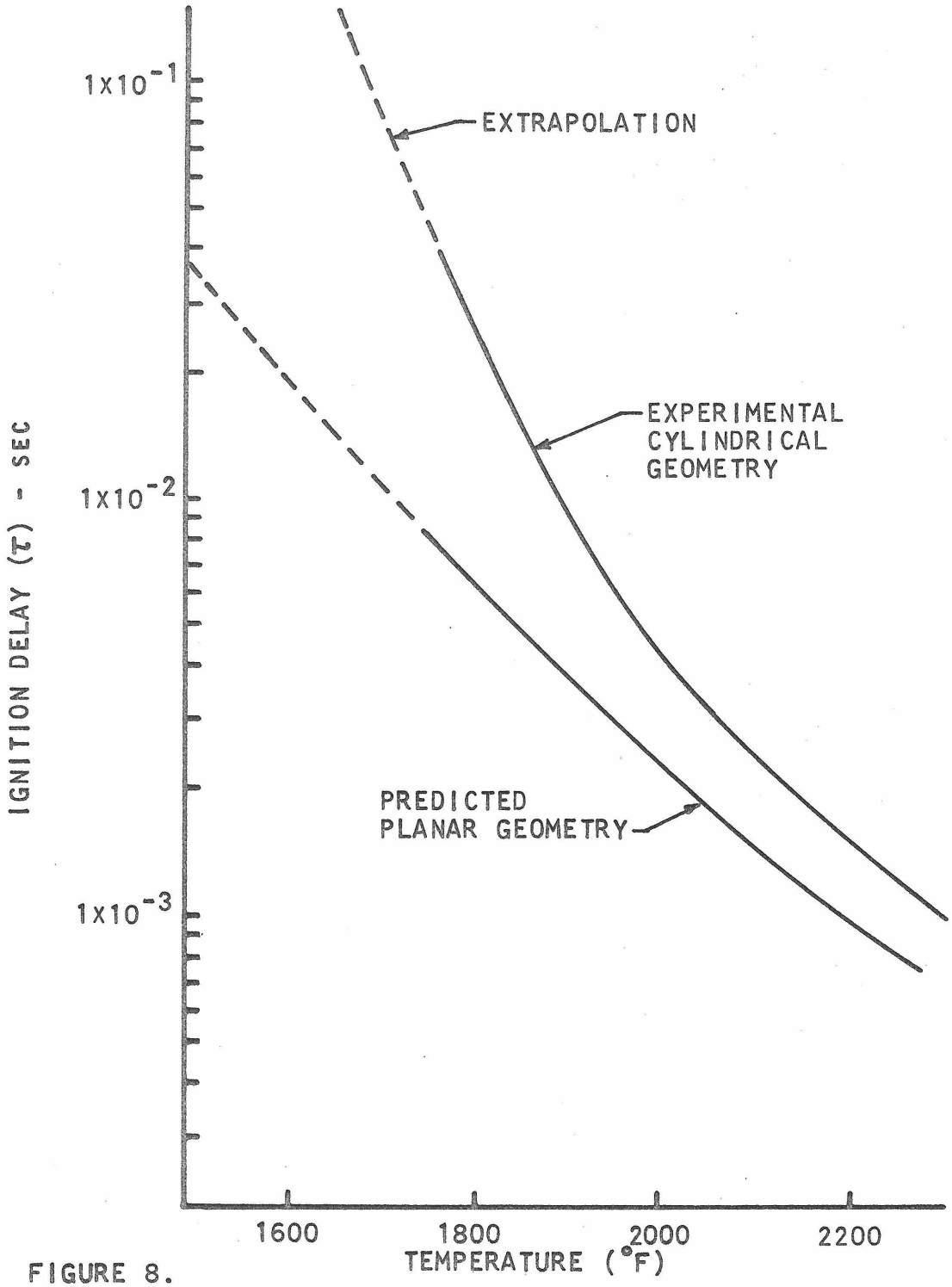

FIGURE 8.
THERMAL IGNITION DELAY AS FUNCTION OF WALL TEMPERATURE

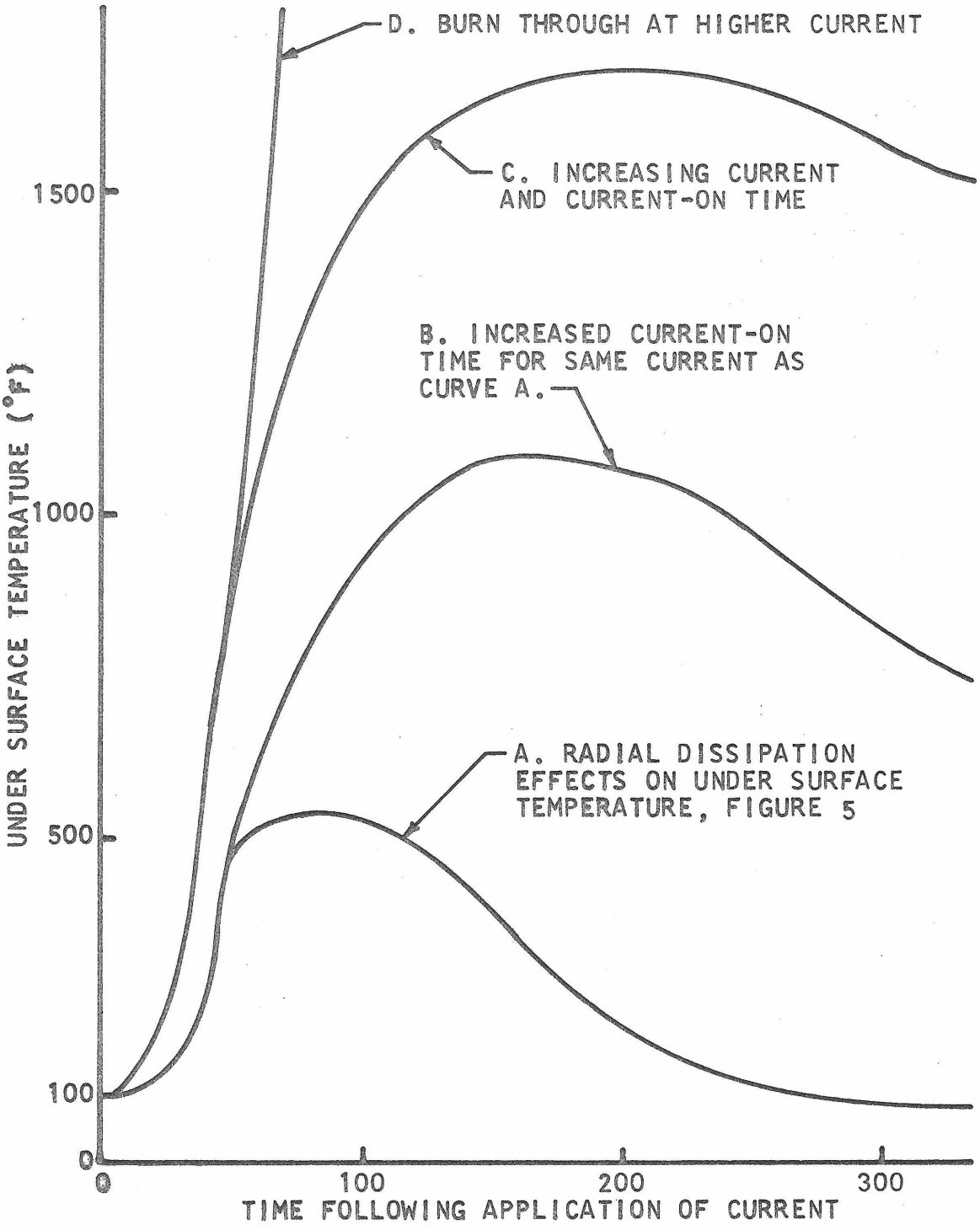

FIGURE 9. ESTIMATED TEMPERATURE HISTORIES OF INNER SURFACE OF FUEL TANK

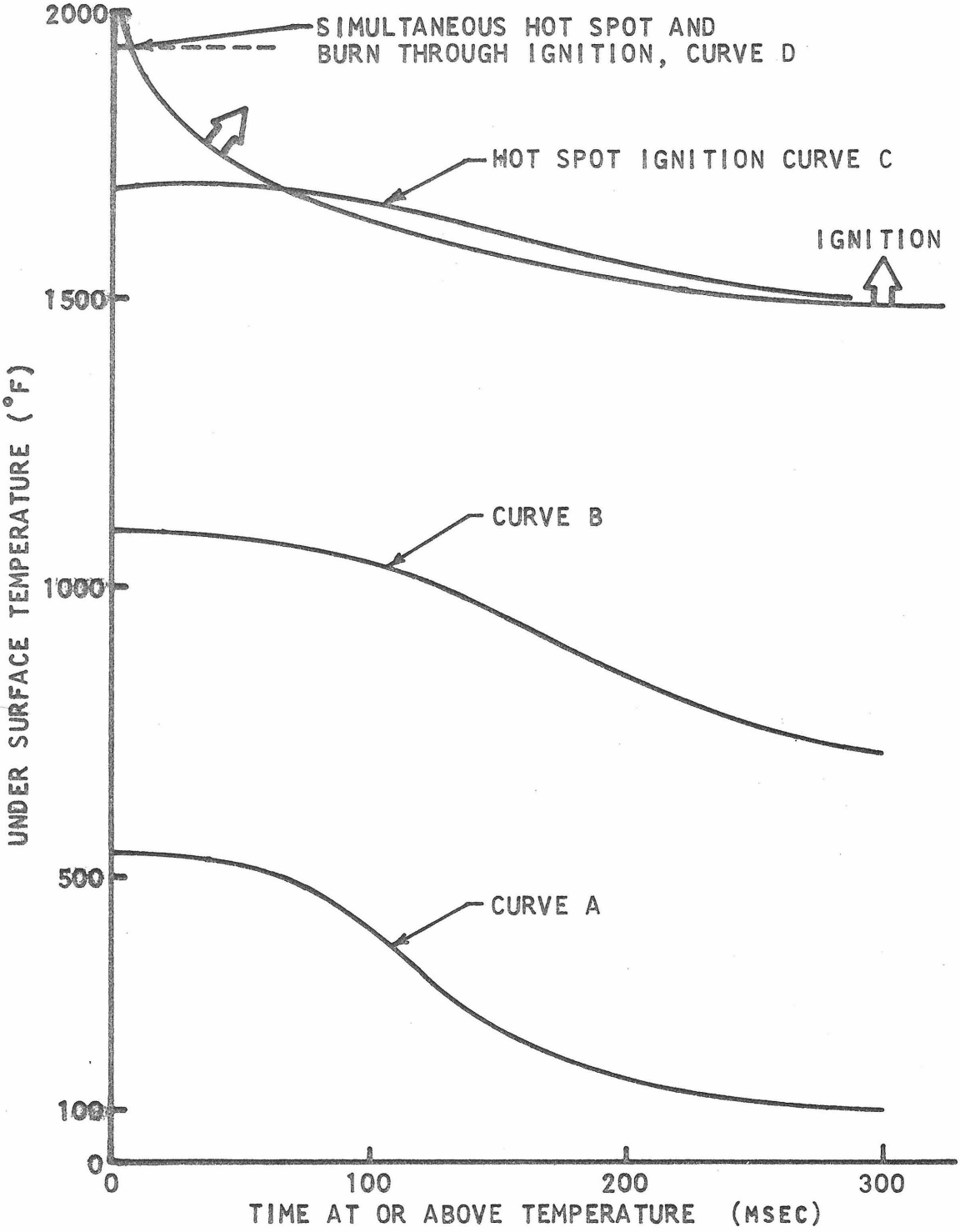

FIGURE 10. ILLUSTRATION OF CONDITIONS FOR NON-IGNITION, HOT-SPOT IGNITION & IGNITION DUE TO BURN-THROUGH

PROPOSITION II

An experimental configuration and procedure is proposed by which the chemical analysis of hydrocarbon-fuel/air mixtures can be rapidly determined for widely varying experimental conditions.

INTRODUCTION

Analytical instruments and experimental procedures for determining the composition of hydrocarbon fuel/air mixtures are discussed in detail in many places (1,2). The problem presented below involves several factors which, individually, may have been resolved, but which do not seem to have been effectively dealt with in a common situation. The problem arose in connection with measurements which were required to help describe the dynamic behavior of the ullage (vapor space) of aircraft fuel tanks. The existence of combustible mixtures in these fuel tanks does, under certain conditions, represent a potentially hazardous situation. But, before action could be taken which would minimize or eliminate the potential hazard it was necessary to quantitatively characterize the behavior of the fuel tank. This required that a large number of chemical analyses of fuel/air mixtures be taken for a wide range of simulated aircraft flight profiles. The object of this proposition is to describe an analytical procedure which was suitable for making these measurements.

THE PROBLEM

Several criteria were involved in evaluating the various analytical instruments and procedures by which the fuel/air ratio of the vapor phase could be determined. These were:

(1) The absolute accuracy was not of primary concern. Rather, a reliable indication of changes in composition was more useful.

(2) Measurements were to be made over a wide composition range (0.01-0.99 mole percent fuel) and several types of molecules (components of aircraft fuel) had to be detected.

(3) Sample temperatures ranged from ambient to 400 ^{o}F.

(4) Total sample pressure ranged from 0.5 to 14.7 psia (simulated sea level to 65,000 feet altitude).

(5) A rapid sampling rate and analysis were required in order to be able to generate time-dependent concentration profiles of the ullage.

(6) A small sample size was required so that the sampling process would not unduly disturb the conditions of the vapor phase.

(7) Because of the large number of samples to be taken the cost-of-analysis/sample was an important consideration.

These requirements, taken together, present rather severe restrictions on any method of analysis which might be proposed, and several analytical instruments were examined and found unsatisfactory for one reason or another. For example, the fact that the thermal conductivity of dilute gases is proportional to the square root of the absolute temperature eliminated the thermal conductivity detector from consideration. Infrared analysis would have required excessively large sample sizes and the temperature limits of the instrument were also too

restrictive. Certain types of small catalytic detectors (3) have been used to monitor unsafe conditions where combustible vapors may be present; however, the composition limits of this type of detector were too low to be useful. An important consideration was that sample temperature and pressure changes be kept to a minimum as condensation of heavy components of the fuel vapors could result in a significant loss of analytical accuracy. Therefore, it was desirable that the sample be injected directly into the analytical instrument with a minimum of handling.

PROBLEM SOLUTION

It is believed that a good compromise of these varied requirements was achieved with the flow sampling system and analysis instrument shown in Figure 1. The analytical instrument is a portable gas chromatograph with flame ionization detector (FID). It was equipped with two columns, either of which could be used by changing the position of a selector lever. One column, that used for the sample analysis, did not separate the components, but merely served to spread the components over a longer time interval. This was necessary to prevent saturation of the detector at high hydrocarbon concentrations. Hold-up time of this spreader column was small, however, so that the samples could be injected and analyzed at intervals of approximately every 40 seconds and not interfere with one another. The second column performed a rough separation of the major hydrocarbon components, and was used to observe major changes in the molecular weight of the fuel vapor.

Sample was drawn through the sampling tube by a vacuum pump at a rate monitored on a small flow meter, and controlled by a needle

valve. The rate was such that the pressure drop in the line between the test tank and the analytical instrument was negligible, but it was also sufficiently fast so that the total flush-out time of the sampling tube was less than 10 seconds. The sample stream passed through a two loop, automatically-operated sampling valve so that a sample was injected into the helium carrier gas and analyzed by the flame ionization detector every 40 seconds. As the chromatograph required only very small ($\sim$ 1 ml) samples, a large number of samples could be removed from the test tank without unduly disturbing the contents. While analysis of one sample was taking place, the sampling line was being flushed out and filled with another. The output of the chromatograph, in millivolts, was fed to a recorder having an automatic integrating circuit, which provided a measure of the fuel vapor in the sample. Total pressure of the sample was measured with a mercury manometer.

The hot (300-400 ^{o}F) vapor samples were heavily fuel-rich and condensation could have been a problem. This was minimized by analyzing the samples as they were taken and by maintaining the sample lines at temperatures greater than 400 ^{o}F. The one sample valve used employed teflon seals and was operable to 400 ^{o}F. The chromatograph, itself, did not impose a practical limit on the temperature of the sample.

In a hydrocarbon fuel/air system the FID responds only to the carbon atoms present. The oxygen, hydrogen, and nitrogen components are not "seen", and the output, therefore, is a measure of the total number of carbon atoms present in a given sample. The fact that the detector response to carbon atoms is almost independent of the molecular source of the atom is helpful in determining the total hydrocarbon content.

Table 1 presents data available from Reference (4) and illustrates the uniformity of response of the ionization detector to carbon atoms derived from various types of molecules. This feature of the FID made it possible to analyze the hydrocarbons as a group so that each sample could be analyzed in a minimum amount of time. Use of the spreader column was essential in analyzing fuel-rich samples which otherwise would have saturated the detector.

Average molecular weights and average hydrogen/carbon ratios were determined for the fuel-vapor molecules, and the measurement for the number of carbon atoms was then converted directly to a weight of hydrocarbon. These latter quantities were estimated with suitable accuracy from knowledge of the chemical make-up of hydrocarbon fuels and also from a physical measurement of the molecular weight of the fuel vapors using standard laboratory procedures. As noted above, for large changes in the molecular weight the gas chromatograph was employed.

The mean molecular weight of the hydrocarbons was used to determine an effective vapor pressure of the fuel vapors. As the total system pressure was measured with a mercury manometer, the weight of air in a sample could be determined by difference and the fuel/air ratio could be calculated.

The sensitivity and accuracy of the FID is well-known. Therefore it may be concluded that inaccuracies in the method described above are probably due to the approximate nature of the measurements and to the assumptions involved in the analysis.

REFERENCES

1. Ettre, Leslie E. and Albert Zlatkis, The Practice of Gas Chromatography, Interscience (1967).

2. Rao, C.N.R., Chemical Applications of Infrared Spectroscopy, Academic Press (1963).

3. Mine Safety Appliances Co. Combustible Gas Detectors.

4. Paciorek, K., Personal Communication (1971).

TABLE 1

SENSITIVITY OF FLAME IONIZATION DETECTOR
TO SEVERAL HYDROCARBON SPECIES

Specie	Integral Output/ Sample Weight	Integral Output/ Carbon Atom
C_2H_6	10,200	5,100
C_2H_4	10,200	5,100
C_3H_8	16,000	5,330
C_3H_6	15,500	5,170
C_2H_2	9,050	4,520
C_4H	21,500	5,370
C_5H_{12}	32,000	6,400
C_6H_{14}	37,000	6,170
C_7H_{16}	42,000	6,000
C_8H_{18}	47,000	5,880

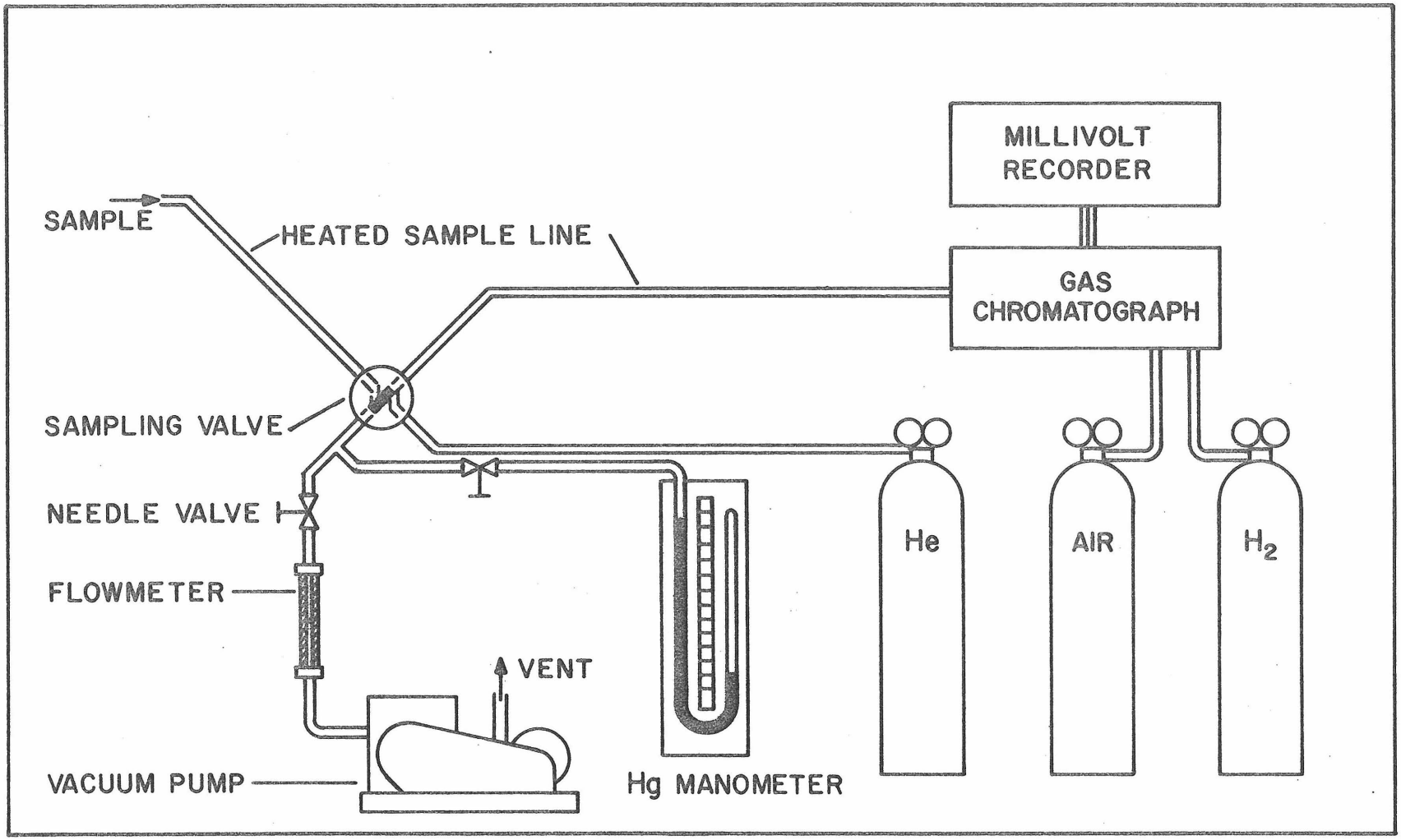

FIGURE 1. FLOW SCHEMATIC OF SAMPLING AND ANALYSIS SYSTEM

PROPOSITION III *

A physical and an analytical model is developed which describes the time-dependent fuel/air composition profiles of the ullage (vapor space) of an aircraft fuel tank during simulated flight.

INTRODUCTION

Aircraft become increasingly vulnerable to ballistic hits in fuel tank areas when the vapor space above the fuel contains flammable fuel/air mixtures. Although the equilibrium fuel/air ratio (calculated from vapor pressure at fuel temperature and total pressure) is often too fuel-rich to support an ignition, transient fuel/air gradients often exist in which the composition may lie within the combustible range. These regions may be brought about by air entering the vent due to fuel consumption, center-of-gravity adjustments or changes in altitude. As the layer becomes larger (involves a larger quantity of the ullage gas), the aircraft becomes more vulnerable to ground fire or accident. Penetration of the fuel tank by an incendiary projectile under these conditions could result in a catastrophic loss of the aircraft. As little is known about the composition gradients which may exist within aircraft fuel tanks, an experimental program was conducted in which fuel/air composition profiles were measured. The purpose of this proposition is to describe the analytical efforts which supported that experimental program (1).

* Major portions of this proposition were extracted from a previously published report "Flight Vibration and Experimental Effects On Formation of Combustible Mixtures Within Aircraft Fuel Tanks," T.C. Kosvic, N.L. Helgeson, B.P. Breen, USAAVLABS Technical Report 70-43.

TEST DESCRIPTION

The general test procedure of a simulated flight profile began with the fuel tank full of fuel to within 6 or 7 inches from the top. The tank pressure was brought to a level which corresponded to a selected altitude and was held there throughout the test. As the test proceeded fuel was withdrawn at a nominal rate which caused the fuel level to change at a steady rate of 1/4 inch per minute. This withdrawal rate was representative of actual aircraft flight requirements. As the fuel was withdrawn, the space which the liquid previously occupied was filled with a fuel vapor and air mixture.

As the vent air and fuel-vapors were withdrawn into the vapor space (ullage), a mixing/diffusion process was initiated to eliminate the concentration gradients that had developed (see Figure 1 (a)). This mixing could have involved several modes of transport: molecular diffusion, turbulent diffusion, free convection, interphase mass transfer, or a combination of any of these. Depending upon the modes of transport involved in any particular case the mixing process could have taken place rapidly (minutes) or slowly (hours). As a result, large fuel/air concentration gradients developed in the ullage space for some conditions and nearly uniform mixtures existed for others.

PHYSICAL MODEL

The process of replacing the consumed fuel with a fuel/air mixture is shown schematically in Figure 1(b). The top of the tank remains stationary and the liquid fuel surface recedes from it at a velocity (v_s). It is assumed that the entire top of the tank is a vent.

Therefore, as the liquid recedes, fuel-free air enters the top of the tank in a uniform stream at a velocity (v_t). The air entered the top of the fuel tank at the same velocity that the fuel was receding ($v_t=v_s$) if there was no supply of fuel vapors from the liquid. It was assumed that the air entered in a uniform stream. The air actually entered at a single point, the vent opening, and then spread out by diffusion and convection into approximately horizontal layers. Experimental results showed this to be a reasonable representation of the process.

Fuel vapor cannot escape from the tank unless its transport (diffusion & bulk) velocity becomes higher than the vent air velocity. Therefore it is possible to make one additional approximation which will help in understanding the experimental results: that the tank top is a semipermeable membrane. That is, air can flow through in one way, but the fuel vapors cannot diffuse through it in the opposite direction (see Figure 1.b).

A third velocity (v_f)characterizes the bulk flow of fuel vapors that emerge from the fuel. Here

$$v_f = \frac{N_{f,o}}{c}$$

where $N_{f,o}$ is the molar flux (moles/area-time) of fuel vapors emerging from the surface of the fuel. It is measured relative to the fuel surface. Whenever there is diffusion of fuel vapors away from the liquid surface into the ullage $N_{f,o}>0$. This quantity becomes increasingly significant as the composition at the surface of the liquid gets richer (high fuel temperature, low ambient pressure) (2). (c) is the total molar density (moles/volume) of the vapor phase.

An equation may be written relating the three velocities:

$$v_t = v_s - v_f$$

If v_f is zero (or small), $v_t \sim v_s$ as mentioned previously. Any increase in the value of v_f retards the rate at which air will enter the top of the fuel tank. As v_f gets larger, v_t eventually becomes negative. That is, there could be bulk flow of material out of the top of the tank in spite of the fact that fuel is being consumed by the aircraft engine. This result accounts for evaporative loss from aircraft at high altitude.

The effect of the relative values of these velocities (v_t, v_s, and v_f) on the composition profile within the ullage is illustrated in Figure 2. The time, t_o, indicates the initial conditions of the test where the vapor space is essentially at equilibrium (i.e., flat composition profile). Times t_1, t_2, and t_3 are progressions of time during the test which show the development of composition profile with time.

In part (a) of Figure 2, $v_f/v_s \ll 1$, so that $v_t \sim v_s$. Here a completely diffusive transport mechanism for transport of fuel vapors from the liquid surface to the top of the ullage may be anticipated. As time progresses from t_o to t_3, the surface of the liquid fuel recedes from the top of the fuel tank. The concentration at the surface of the fuel is constant and is determined by the vapor pressure of the fuel and the tank pressure. The fuel vapors are supplied to the top of the tank by diffusion from the surface of the fuel but do not diffuse out of the tank. As additional air enters the top of the tank, the

concentration of fuel vapors at the top of the tank continues to decrease.

Figure 2 (b) illustrates the case for $v_f/v_s \leq 1$. As v_f increases, transport of fuel vapors to the top of the ullage becomes convective controlled rather than diffusive. The composition profile tends to flatten out as the flow of fuel vapor passing into the ullage at the liquid surface becomes important.

If v_f becomes greater than v_s, a convective motion of the mixture is set up so that material is now flushed out of the ullage through the vent (Figure 2 (c)) and no fresh air is permitted to enter the ullage. Considered in this manner, the ratio v_f/v_s becomes a qualitative measure of the effect of a convective motion generated by interphase mass transfer (evaporation of fuel) on composition profiles within the vapor space. This classification of the controlling phenomena (diffusion/convection) will help in presenting an analysis descriptive of fuel tank behavior.

MODEL FOR DIFFUSION TRANSPORT

Assuming that the fuel/air mixture is of two components, one fuel species and one air species, the equation of continuity for fuel species may be written as (3)

$$N_f = \underbrace{X_f (N_f + N_a)}_{\text{convection}} - \underbrace{c\, D_{fa}\, \nabla X_f}_{\text{diffusion}} \qquad (1)$$

where N_f = molar flux of fuel vapor relative to liquid surface

N_a = molar flux of air relative to liquid surface

X_f = mole fraction components

c = total molar concentration/volume

D_{fa} = binary diffusion coefficient for fuel vapors in air

The quantity $(N_A + N_B)$ represents a bulk convective flow and is measured relative to the liquid surface. For an open system some bulk flow will exist. In the present case (diffusion controlled), it will be considered negligible and Equation (1) becomes

$$N_f = c\, D_{fa}\, \nabla X_f \tag{2}$$

Using the continuity relation

$$\frac{\partial c_f}{\partial t} = c\, \frac{\partial X_f}{\partial t} = -\nabla N_f$$

and differentiating and substituting in equation (2)

$$\frac{\partial X_f}{\partial t} = D_{fa}\, \nabla^2 X_f \tag{3}$$

At this point we are interested in the situation illustrated in Figure 2 (a) $(v_f/v_s \ll 1)$. For this case, the initial and boundary conditions are (see Figure 3 for coordinate system):

$$\begin{aligned} t = 0 \qquad & X_f(z,0) = X_{f,o} = X_{f,e} \\ t > 0 \qquad & \frac{\partial X_f}{\partial z}(L,t) = f(t) \\ & X_f(o,t) = X_{f,o} = X_{f,e} \end{aligned} \tag{4}$$

where $L = L(t) = A + V_s t$.

The subscript o refers to the condition at the liquid surface, L

refers to the top of the tank, and e signifies an equilibrium concentration. The feature that makes these conditions unique is that one of the boundaries (L) is moving at a steady rate to simulate the receding liquid surface. It should also be noted that the boundary condition at L(t) is an unspecified function of time f(t). The gradient at this position (the semipermeable membrane) is not zero, as a steady supply of fuel vapors is required to mix with the incoming air and is subsequently swept back into the tank. This gradient is estimated from experimental data. Using this data a generating function for this boundary condition as a function of time was established.

Analytical solutions for equation (3) for the conditions (4) are not available. However, the moving boundary was accounted for by using the Landau transformation (4) and a numerical integration routine was used to calculate composition-time profiles.

Three calculated experimental curves are compared in Figure 3 for a test time of one hour. The experimental results are below the calculated profile for the two low-temperature tests. Molecular diffusivities were used in the calculations, however, and if any turbulent diffusion did occur this could account for the indicated differences. The fact that the experimentally measured profile is greater than the calculated profile for the high-temperature test indicates that a new mechanism of transport is becoming important. That is, the bulk velocity of the fuel vapors must now be accounted for (see Figure 2.6) but this feature has not been included in the calculational scheme.

REFERENCES

1. Kosvic, T. C., N. L. Helgeson, and B. P. Breen, "Flight Vibration and Experimental Effects on Formation of Combustible Mixtures Within Aircraft Fuel Tanks," USAVLABS Technical Report 70-43.

2. Bird,R. B., W. E. Stewart, and E. N. Lightfoot, Transport Phenomena, Wiley and Sons(1960), 594.

3. Bird,R. B., op.cit., 520.

4. Drew, T. B., Ed., Advances in Chemical Engineering, V, Academic Press(1964), 94.

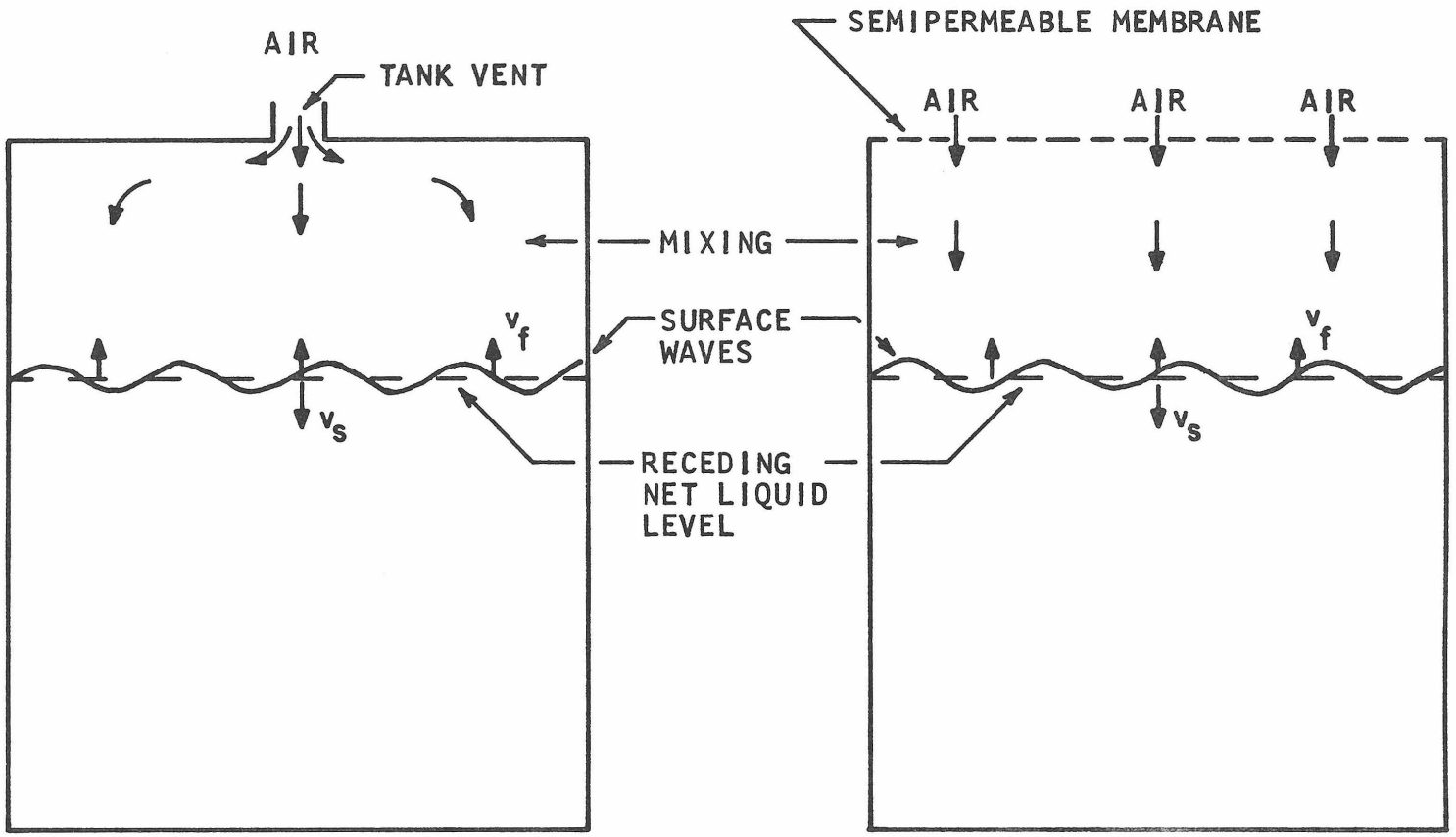

FIGURE 1. COMPARISON OF ACTUAL AND MODEL FUEL TANK VENTING

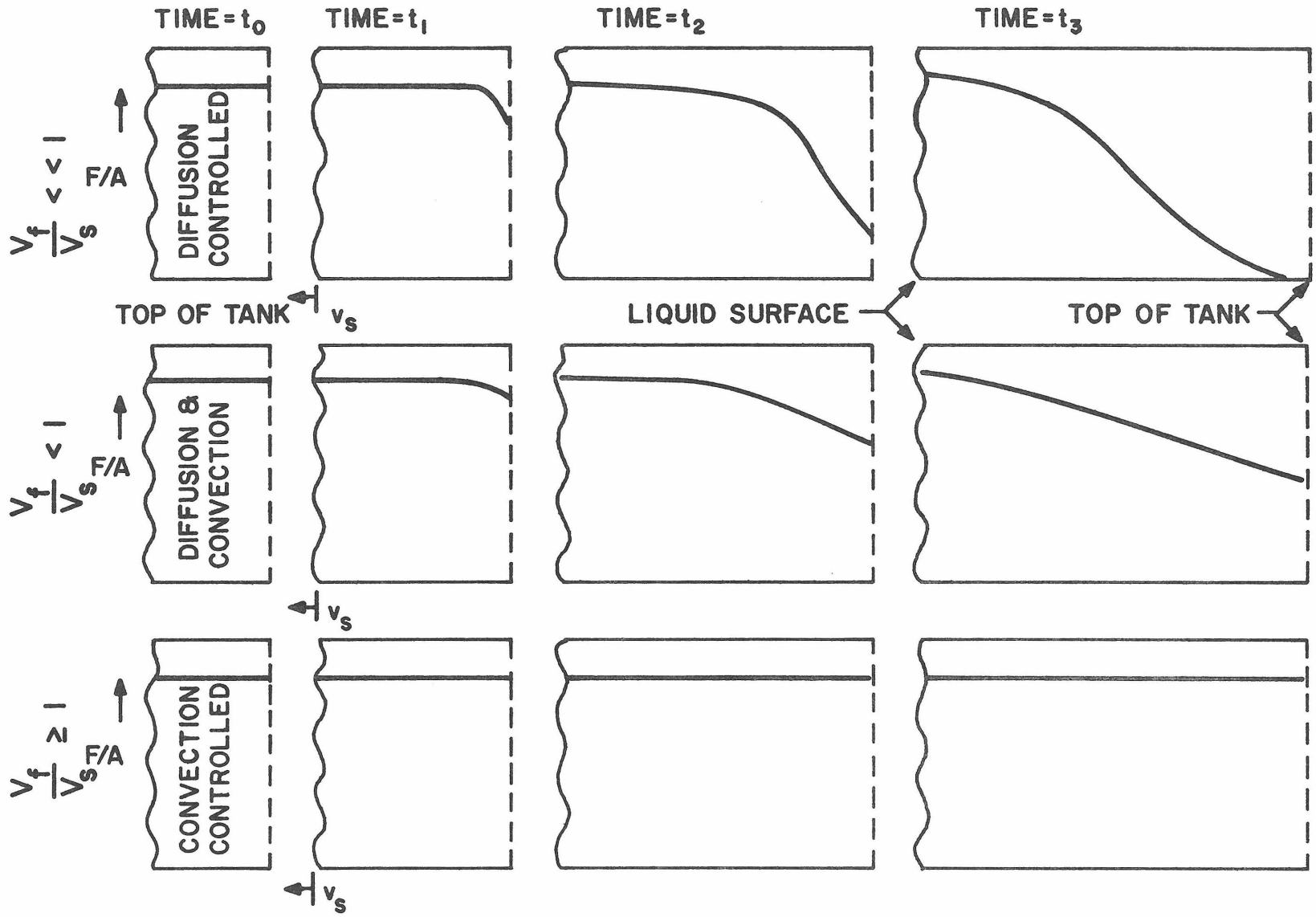

FIGURE 2. ILLUSTRATIVE (FUEL/AIR) COMPOSITION PROFILES IN ULLAGE VOLUME AS A FUNCTION OF TIME FOR VARIABLE v_f/v_s.

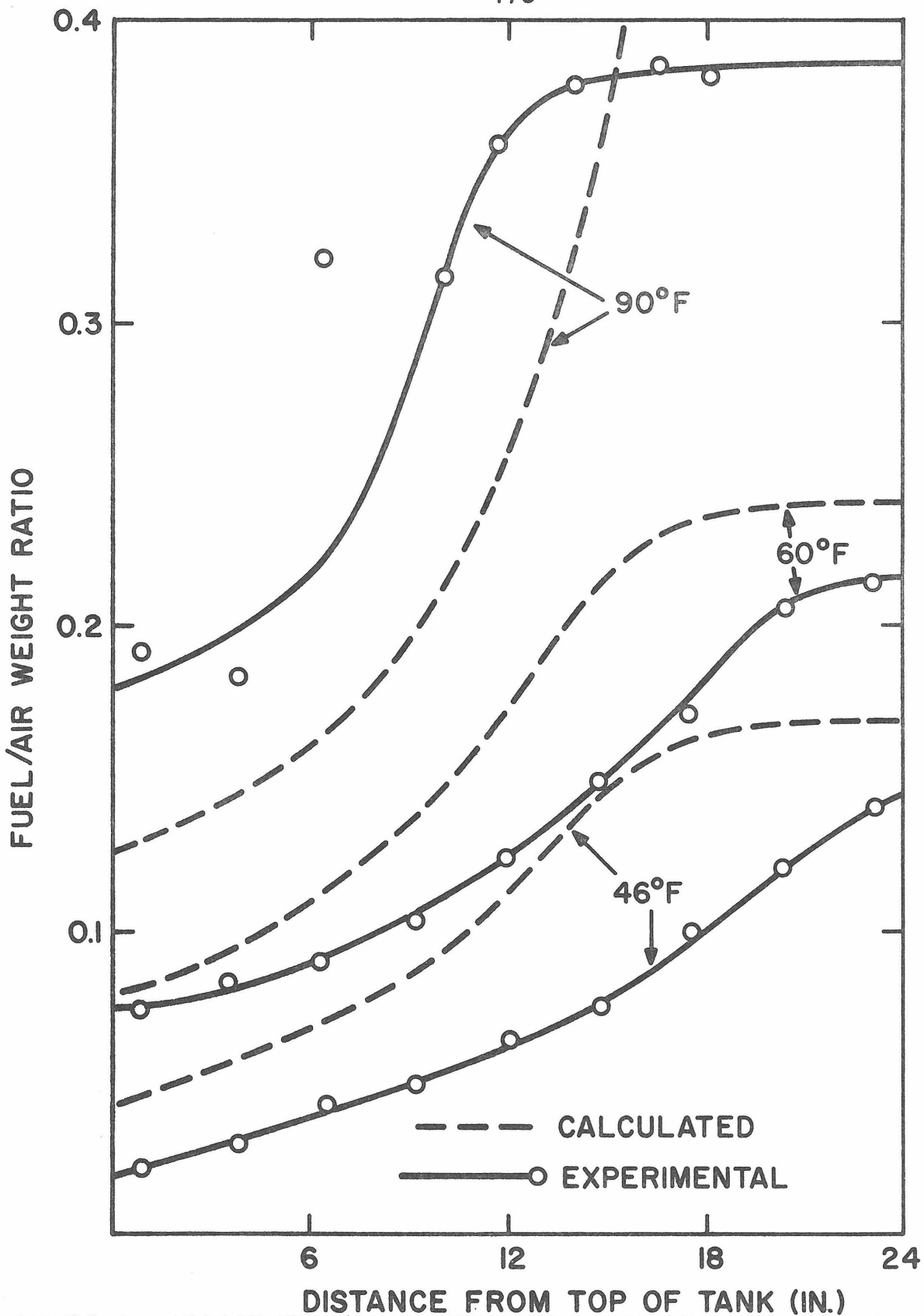

FIGURE 3. ULLAGE FUEL/AIR COMPOSITION PROFILES FOR SEVERAL FUEL TEMPERATURES (TEST TIME 1 HOUR).